Title
Synthesis and Characterization of Iridium- and Cobalt-based Skutterudites for Thermoelectric Power Generation

Author
King, Daniel Jay

Publication Date
2014

Peer reviewed|Thesis/dissertation

UNIVERSITY OF CALIFORNIA

Los Angeles

Synthesis and Characterization of Iridium- and Cobalt-based Skutterudites for Thermoelectric Power Generation

A dissertation submitted in partial satisfaction of the

Requirements for the degree of Doctor of Philosophy

in Chemistry

by

Daniel Jay King, Jr.

2014

ABSTRACT OF THE DISSERTATION

Synthesis and Characterization of Iridium- and Cobalt-based Skutterudites for Thermoelectric Power Generation

by

Daniel Jay King, Jr.

Doctor of Philosophy in Chemistry

University of California, Los Angeles, 2014

Professor Richard B. Kaner, Chair

There are several possible approaches to enhancing the thermoelectric properties of skutterudite materials, most of which strive to reduce the total thermal conductivity of the structure in some way. Formulations of $CoSb_3$ skutterudite that incorporate alkali metals, alkaline-earth elements, or rare-earth elements as void fillers have achieved the highest reported thermoelectric figure of merit (ZT) values for n-type $CoSb_3$. For thermoelectric applications, devices that use $IrSb_3$-based materials as full legs or segments of legs could enable the utilization of a greater maximum temperature, as compared to $CoSb_3$-based devices. A series of n-type $Ba_yIr_4Sb_{12}$ compositions have been synthesized. Phase purity and elemental compositions are analyzed by X-ray diffraction (XRD), scanning electron microscopy (SEM), and electron probe microanalysis (EPMA). Room temperature and high temperature thermoelectric properties are reported with a maximum ZT of about 0.8 at 750 ^oC (1023 K) and EPMA results suggest the maximum filling fraction for barium in $Ba_yIr_4Sb_{12}$ is around $y = 0.3$.

In light of the success of single-element filling of iridium-based skutterudite, double-element filling of the structure was investigated. The high temperature thermoelectric properties for the double-filled $Ba_xYb_yIr_4Sb_{12}$ and $Ba_xEu_zIr_4Sb_{12}$ skutterudites were compared to $Ba_xIr_4Sb_{12}$ single-filled skutterudites. Maximum ZT values for double-filled skutterudites increased as much as 25% over that of single-filled compositions. Phase purity and elemental compositions were analyzed by X-ray diffraction (XRD), scanning electron microscopy (SEM), and electron probe microanalysis (EPMA). Room temperature and high temperature thermoelectric properties are reported with a maximum ZT of 1.0 at 750 ^oC (1023 K) for the $Ba_{0.15}Eu_{0.15}Ir_4Sb_{12}$ nominal composition, but EPMA results show that these skutterudites exhibit preferential filling for certain elements in the case of double-filling, such that Ba > Eu > Yb.

Skutterudite materials were processed by high energy ball milling to produce nanostructured powders. $CoSb_3$ was used as a proof-of-principle material along with $Co_{0.955}Pd_{0.045}Sb_{2.955}Te_{0.045}$, $Ba_{0.05}Yb_{0.15}Co_4Sb_{12}$, and $Ce_{0.9}Fe_{3.5}Co_{0.5}Sb_{12}$. Each skutterudite was milled to a fine powder containing crystallites as small as 1 nm, with sample averages as low as ~20 nm. The powders were characterized by XRD, SEM, and TEM, then hot-pressed and measured for their high temperature thermoelectric properties. Hot-pressing conditions necessary for densification led to significant grain growth. Improvements in reduced thermal conductivity in each of the skutterudites examined were off-set by changes in the electrical properties of the samples. All observed increases in ZT over bulk materials were within the error of the measurement. Nanostructured skutterudite materials often behaved inconsistently and a majority of ball milled samples undergo reactions or phase transformations during high temperature measurements. Improving the ZT of skutterudite materials by ball milling to create nanostructures remains a challenge.

In addition to further studies of new filler atoms in $IrSb_3$ skutterudites, composites and alloys offer promise of reduced thermal conductivities for enhancement of ZT. Preliminary results of alloying small amounts of cobalt in iridium-based skutterudite indicate that with optimization, these alloys have the potential to reduce thermal conductivity by the introduction of point defects in the structure. With more accurate band modeling, it could be possible to incorporate multiple approaches to reducing thermal conductivity into one sample, taking advantages of several different modes of phonon scattering.

The dissertation of Daniel Jay King, Jr. is approved.

Xiangfeng Duan

Yunfeng Lu

Richard B. Kaner, Chair

University of California, Los Angeles

2014

This work is dedicated to my father, my inspiration, Daniel Jay King, Sr.

Table of Contents

Acknowledgements

One of the beautiful things in life is that people help one another to succeed. I feel truly fortunate to have benefitted from the guidance, help, and inspiration of those around me. Coach John Wooden, who has, and always will be a role model for me once famously said, "Although it is often used without true feeling, when it is used with sincerity, no collection of words can be more meaningful or expressive than the very simple word – Thanks." To each and every one of you, my sincere thanks.

First, I thank my advisor, Professor Richard (Ric) Kaner, for his unwavering support and encouragement over the years. It was his Chemistry 171 undergraduate course that convinced me that I wanted to study inorganic chemistry in graduate school. At my most desperate hour, when I was considering giving up on graduate school, Ric stepped in and made it possible for me to continue studying science that I was excited about. I have learned a great deal from Ric, especially as his teaching assistant and I hope I can one day be as good a teacher as he has become. Over the years, he has been both a mentor and a friend, and I look forward to our continuing friendship in the years to come. From the bottom of my heart, thank you.

I was fortunate to also have an additional advisor at the Jet Propulsion Laboratory (JPL) in Pasadena. Dr. Jean-Pierre Fleurial was instrumental in my transition to this field of research and I thank him for agreeing to take me on as a graduate student after my brief internship in his group. His knowledge in the field is amazing and at times difficult to keep up with, but he has always been patient with me as I learn in the space that he has mastered. The research he has included me in has always been exciting, unique, and at the forefront of the thermoelectric's field. I feel very fortunate to have been a part of his group whose work is quite literally, out of this world. I also owe a great deal of thanks to Dr. Thierry Caillat, who does not get any official

credit for being my research advisor; however, his knowledge and experience, especially with skutterudite materials, has been indispensable. I thank him for always making time for me, even when I know he does not have any time to spare and always having a positive attitude and constructive comments about my projects.

At JPL, I thank the Thermal Energy Conversion Technologies (TECT) group for supporting this work. Dr. Sabah Bux was instrumental in my transition to the field of thermoelectrics. Her guidance and support over the years has meant a lot to me. She is a colleague and a good friend and I am fortunate to work with her. Dr. James Ma and Dr. Kurt Star also deserve recognition for their assistance and many helpful discussions during my time at JPL. James and Kurt are two brilliant minds in two very different ways. I love them both and I hope they understand how grateful I am to have had them as colleagues. Many times when I was stuck, it was advice from James or Kurt that helped me move on more quickly. Additionally at JPL, I, and the entire TECT group, all owe huge debts of gratitude to George Nakatsukasa and L. Danny Zoltan for building and maintaining the equipment in the group, in spite of many forces that were seemingly working against them. George always has a positive attitude about resolving problems and the quality of his work is surpassed by none. George inspires me to better my interpersonal skills and to never complain or get upset because it's just not worth it. If I ever start a company, I will offer George a job because he is exactly the kind of person that you want on your team. George, I thank you for opening my eyes to the many wonders of our national parks. Without your urging and your suggestions, I would not have taken the extra steps to research and explore those places, and instead would have let them remain as places I have seen on the internet. Because of this, I have made the effort and seen some of the most remarkable places on earth, right here in the States.

I thank all past members of the Kaner group for leaving behind so much for us current members. I am fairly certain they have no idea what a legacy they have left in our lab, but I assure them that it still persists. Thank you to all current members of the Kaner lab for being my comrades in this academic adventure of graduate school and keeping such unpredictable hours. It was always nice to see smiling faces when I, myself was coming and going at odd hours of the night. Extra thanks are due to Chris Turner and Andrew Lech for helping maintain the legacy equipment in the lab so that we can all get work done. Thanks to Michael Yeung for always being a resource for knowledge and other assistance in the lab. I appreciate that you are always willing to talk about science when I needed a different perspective and you were always more than willing to help. Thanks to Yue (Jessica) Wang for always being supportive and having a positive attitude. Jessica is an inspiration to all in the lab and many would benefit from her example of how to conduct quality research, skillfully and efficiently. Jessica has always inspired me better my presentations, as hers are always well thought-out and skillfully presented with helpful animations, graphics, and informative transitions. Jessica will make an outstanding professor one day if she chooses that career path. I thank good students that I had a chance to work alongside as undergraduate mentees: Ngog-Diep Thi Nguyen (Zoelle), Rebekah Tolopilo, Jonathan Shaw, Adam Makhluf, Crystal Yang, and Lan Huong Nguyen Lai. There were many other graduate student peers in my time at UCLA, that I will always remember, but I must single out Dr. Zach O'Brien, for his always calm brilliance and for teaching me that the pen is truly mightier.

Professor Robin Garrell was the very first professor I ever had for a class at UCLA. I will never forget that first day of class, complete with music and pyrotechnics, as it was also the first day of this remarkable academic journey. Later, Professor Garrell gave me an opportunity

to get involved in undergraduate research in her lab, in spite of very little experience. I was elated and eager to join and I thank Dr. Aaron Wheeler for channeling my enthusiasm into some quality experiments.

In the Garrell Lab, I also benefitted immensely from the knowledge and kindness of Dr. Heather Shepherd, Dr. Debalina Chatterjee, Dr. Sang Uk Son, and Azim Laiwalla. These people were wonderful colleagues and good friends. Azim, beyond the Garrell lab, you have been more than a friend to me, a brother, and I can't even begin to thank you for everything you have done for me. You are the best friend that I never see. I am so impressed by how hard you have worked on so many things. I am always impressed with your diplomacy and your respect for others, even when I feel they may not appreciate your efforts. I have tremendous respect for your desire to help others and for your forgiving nature. I thank you for always inspiring me to be a more patient and forgiving person. I know our friendship is one that will last.

Backtracking somewhat, I must thank Amgen for an amazing summer internship opportunity in the summer of 2003. I learned so much and everyone involved was so helpful. In particular, I thank Jennifer Rattan and Bahram Valamehr for guidance and teaching me the meaning of good experimental controls.

I don't think that I would have ended up in science if it were not for my high school chemistry teacher, Mr. Abrams. He renewed my interest in science in a challenging honors chemistry course at a very difficult time in my life. He was a good teacher and one of my most memorable teachers. I hope I can see him again one day and express my deep gratitude for his profoundly positive influence on my life. Getting a truly inspirational teacher in school appears to be the luck of the draw, but I have been lucky to have had some that I feel changed me for the

better, in ways that I feel others may have not: Mr. Bruce Edwards (JFK High School), Mr. Anthony Scalia (JFK High School), Mr. Richard Acton (Westlake High School), and Mr. Steve Richwood (Blacow Elementary). I also had the good fortune to learn from two outstanding teachers at Moorpark Community College, Dr. Eugene Berg (a UCLA graduate), and Dr. Larry Miller. These two were inspirational science teachers that convinced me without a doubt, that science was exciting interesting. Thank you to Ms. Diana Nguyen and Ms. Debbie Richie for being excellent math teachers, building a strong foundation of math for me.

Dr. Daniel Ezekiel, you are wonderful. I must thank you for who you are. Your incredible, unique, and uncommon warmth as a human being has enriched my life for many years. When I met you, I was young and did not know how to react to your genuine outreach and kindness. I am glad that it only took me about an hour to figure out that you were someone I wanted to be around. You have such an amazing way with others and I love your refusal to quit, your quest for adventure, and your desire to share it all with the world. You inspire me to excel, to be kind, and to enjoy the many parts of life that so many take for granted.

Dr. Micheal C. Wilson has always pushed me to be a better student and a better scientist. A great deal of credit is due to Mike for my decision to change my undergraduate degree to biochemistry from psychology in community college. It was from Mike that I learned how to study more effectively and it was by his example that I became a better student. Without his influence, at a pivotal time in my academic career, I would have ended up in a far different place than I am in now. Mike was my classmate, my coworker, my roommate, and my best friend in college. We didn't always get along, but we were, and remain, great friends. Speaking of Mike, he would want to remind me to thank Dr. Alfred Bacher at UCLA for telling me as a senior undergraduate student that I would never make it in graduate school. His doubt only increased

my drive and determination, so for that, I thank him. I also thank Wendy Fujinami for bearing witness to Dr. Bacher's discouragement and countering with nothing but enthusiastic support and encouragement, even after she moved to another department on campus. From my very first official day on the UCLA campus as an undergraduate student, Wendy has been a great resource, but more importantly, a good friend. Wendy, this campus would be better off if there were more of you here. Additionally, Robin McCallum and Tony Leadholm were wonderful people in the graduate counseling office in the chemistry and biochemistry department that guided me in my first years as a graduate student. Their positive attitudes and warm personalities were always welcoming.

I thank the UCLA Spirit Squad for being my creative outlet and social support group outside of my research setting. I believe it is important to have balance in your life and I was fortunate to have balance from these amazing individuals. Thank you, Alex for always being available for lunch and always listening. Thank you, Mollie for changing my life. There is no better way to say that, and I thank you for amazing things that you have pushed me to do. Thank you, Joe Bruin for always making me happy and always making me laugh. I am so fortunate that we are such close friends. Josie Bruin, you are also due thanks for being an inspiration and making me happy, as well. You are the 8-clap of my heart.

I had amazing mentors in my life with which I unexpectedly crossed paths again, here at UCLA. As a young boy, I had no idea that so many people who had touched my life in such positive ways were UCLA Bruins. Cathleen and Paul Trapani were such wonderful mentors, care takers, and role models for me at EPCC. Cathleen, your after school and summer programs enriched my childhood immeasurably. I loved you and feared you back then, but now I just love you. Thank you for always baking goodies for me even when I shouldn't have had them. Paul,

you were always so much fun and a great role model for leadership and kindness. You are still so much fun and always a great source of wisdom for me. I hope we only grow closer as the years go on. Another UCLA Bruin that I must thank is Todd Katz, and I would be remiss if I did not thank his lovely and equally amazing wife, Dana Katz. You have a big hand in profoundly turning my life around when I was a troubled kid. Todd, Camp Whittle (specifically my silver rag ceremony) changed me for the better, making me the student I am today. I will never forget that turning point in my life and I thank you for helping to make moments like that possible for so many kids.

Finally, and most importantly, I thank my family. I thank them for always believing in me and my abilities, even if they hadn't the foggiest idea of what I was working on. I love your silliness and how when we are together, nothing else seems to matter. To my mother and father, Lorena and Daniel King (Sr.), I hope that I make you proud today and will continue to make you proud forever. I have only reached this point by the accumulation of years of your unwavering support and challenges to better myself. I wish every child in the world could have parents as bright, positive, silly, beautiful, and hard-working as you two. Dad, your work ethic and your willingness to put absolutely everything you can muster, into accomplishing a goal is a constant reminder that I can achieve anything that I truly work for. Mom, your willingness to work extremely hard to better yourself and to follow your dreams has always impressed me. You always find a way to do something, rather than seeing reasons why you can not. I absolutely love that about you and I am so excited for what's next. Mom and dad, together, your drive and determination drives me to excel. Julie and Kristen, I know it has been a rough road at times, but I am proud of you two and who you have become. From the beginning, you have always been my best friends and are always the first ones that I want to talk to when I feel lonely. Krissy,

thank you for having the mustard, always. Jules, thank you for not going in the cave so that I can always remind you that you should have gone in the cave. Jace, you are the brother I always wanted and I am so proud of you. Thank you for being someone I can always trust and confide in. I can't wait to see what you accomplish in life. I hope I can be a part of it and help you achieve great things. Ashlynne, I am so proud of you and how you are excelling in school. You are growing up quickly and your discipline in school has been inspirational for me, especially this year. Visiting you, away at school, was very special for me and I look forward to your success. Yasmine, you have grown up so fast and you have always been a comforting presence as my baby sister when I would take a break from my studies and come home to visit. You'll always be that to me and I am proud to watch you excel at everything you do. Thank you for still letting me flip you over even when you were too big for it. Piggies, it would have been an unthinkably different journey without everything that you've done for me and all that you have sacrificed. Whenever I truly needed something, anything, you were always there to help. Words cannot express my gratitude, so I must simply say thank you. Bear, I thank you for always listening (most of the time). Your presence is always therapeutic and I cherish our friendship. Shadow, Mush, and Wedge, I thank you for your love, even if it is often conditional.

To the University as a whole, I thank you, and everyone at this fine institution, for creating the amazing communities within this university that I have been fortunate enough to be a part of. I remember being driven to and from child-care as a young boy and passing the large grass field and brick buildings on Sunset Boulevard at the intersection of Westwood Boulevard. At the time, I never knew what that place was, but I knew it was a school of some sort. I can't really explain why I was always excited to see that part or our drive in the mornings and in the evenings, but I always looked out the window and wanted to go there. It's strange how a place

can call to you. Being here feels like a childhood dream, renewed as a young man's dream, finally realized, and now passing by. It is both a happy and a sad feeling, but I am thankful for this place and how it has called to me in so many ways. I look forward to being able to give back to this wonderful place in every way that I can. People have asked me if I regretted attending graduate school at the same institution where I received my undergraduate degree, and I have absolutely zero regrets. I would recommend my path to anyone. UCLA has so much to give and I am truly grateful.

Thank you all for this unforgettable journey and I look forward not only to what lies ahead for me, but also to what amazing things will come out of this university, next. Go Bruins.

VITA

2004	B.S., Biochemistry, UCLA, Los Angeles, California B.S., Marine Biology, UCLA, Los Angeles, California
Summer 2004	Intern, Institute for Cell Mimetic Space Exploration, University of California, Los Angeles, California.
Summer 2005	Intern, Perry Institute - Lee Stocking Island, Marine Science Institute, University of California, Santa Barbara.
2004-2005	Research Associate, Amgen, Thousand Oaks, California
2006-2008	NSF-IGERT Fellow, Materials Creation Training Program, University of California, Los Angeles, California.
2005-2007	Graduate Student Researcher, Robin L. Garrell Lab, Department of Chemistry and Biochemistry, University of California, Los Angeles
2007-present	Graduate Student Researcher, Richard B. Kaner Lab, Department of Chemistry and Biochemistry, University of California, Los Angeles

PUBLICATIONS AND PRESENTATIONS

1. Dimitrios Koumoulis, Belinda Leung, Thomas C. Chasapis, Robert Taylor, Daniel King, Mercouri G. Kanatzidis, and Louis-S. Bouchard, "Understanding Bulk Defects in Topological Insulators from Nuclear-Spin Interactions," *Adv. Funct. Mater.*, Dec. 2013.

2. Robert E. Taylor, Fahri Alkan, Dimitrios Koumoulis, Michael P. Lake, Daniel King, Cecil Dybowski, and Louis-S. Bouchard, "A Combined NMR and DFT Study of Narrow Gap Semiconductors: The Case of PbTe," *J. Phys. Chem. C*, vol. 117, no. 17, pp. 8959–8967, May 2013.

3. Dimitrios Koumoulis, Thomas C. Chasapis, Robert E. Taylor, Michael P. Lake, Danny King, Nanette N. Jarenwattananon, Gregory A. Fiete, Mercouri G. Kanatzidis, and Louis-S. Bouchard, "NMR Probe of Metallic States in Nanoscale Topological Insulators," *Phys. Rev. Lett.*, vol. 110, no. 2, p. 026602, Jan. 2013.

4. Daniel J. King, Thierry Caillat, Richard B. Kaner, Sabah K. Bux, Jean-Pierre Fleurial, "Filled n-type $IrSb_3$ Skutterudite," 2012 Materials Research Society Fall Meeting, Boston, MA, United States, Oral presentation, November 26, 2012.

5. Zhongfen Ding, Sabah K. Bux, Daniel J. King, Feng L. Chang, Tai-Hao Chen, Shu-Chuan Huang, and Richard B. Kaner, "Lithium intercalation and exfoliation of layered bismuth selenide and bismuth telluride," *J. Mater. Chem.*, vol. 19, no. 17, p. 2588, 2009.

6. Daniel J. King, Sabah K. Bux, Pawan Gogna, Richard B. Kaner, Jean-Pierre Fleurial, "Bulk nanoskutterudite for thermoelectric power generation," 235th ACS National Meeting, New Orleans, LA, United States, Poster presentation, April 2008.

7. Debalina Chatterjee, Boonta Hetayothin, Aaron R. Wheeler, Daniel J. King, and Robin L. Garrell, "Droplet-based microfluidics with nonaqueous solvents and solutions.," *Lab Chip*, vol. 6, no. 2, pp. 199–206, Feb. 2006.

PUBLICATIONS IN PREPARATION

1. Daniel J. King, Thierry Caillat, Zoelle Nguyen, Richard B. Kaner, Jean-Pierre Fleurial, "Effects of barium filling in $IrSb_3$-based n-type skutterudite: High temperature thermoelectric properties of $Ba_yIr_4Sb_{12}$," (2014).

2. Daniel J. King, Thierry Caillat, Zoelle Nguyen, Richard B. Kaner, Jean-Pierre Fleurial, "Two-element filling in $IrSb_3$-based n-type skutterudite: High temperature thermoelectric properties of $Ba_xYb_yIr_4Sb_{12}$ and $Ba_xEu_zIr_4Sb_{12}$," (2014).

Chapter 1: Effects of barium filling in $IrSb_3$-based n-type skutterudite: High temperature thermoelectric properties of $Ba_yIr_4Sb_{12}$

1.1 Introduction

The skutterudite structure is composed of a cubic lattice with the space group *Im3*. Materials with the skutterudite structure are of particular interest for use as thermoelectric materials. The thermoelectric figure of merit (ZT) is defined by the following equation:

$$ZT = \frac{S^2}{\rho\lambda}T$$

where S is the Seebeck coefficient, ρ is the electrical conductivity, and λ is the total thermal conductivity of the sample. The figure of merit is dimensionless and has a direct relationship to efficiency.[1] Heavily doped $CoSb_3$ –based n-type formulations of skutterudite emerged as viable mid-temperature range thermoelectric materials in the mid-1990's with a ZT around 1.0 at 600 ^oC.[2] Unpublished lifetime testing at the NASA Jet Propulsion Laboratory (JPL) in Pasadena shows that for long-term operation in a thermoelectric device, $CoSb_3$ is sufficiently stable at a maximum temperature of around 600 ^oC (873 K). Thermoelectric properties for n-type $CoSb_3$ with the substitutional dopants Ni, Pd, Pt, or Te[3–6] were subsequently surpassed by employing a new doping method, giving rise to the "filled" skutterudite structures wherein vacancies in the structure are filled with large, electron-donating atoms. This new class of skutterudites produced higher performing $CoSb_3$-based alternatives, mainly due to significant reduction of thermal conductivity that has been attributed to the "rattling" of these filler atoms in the structural voids.[7–11] The "rattling" phenomenon is believed to scatter phonons and lower the thermal conductivities in skutterudite structures. This has led to reports of filled skutterudite structures employing various filler atoms including, but not limited to, Ca[12], Sr[13], In[14,15], Ba[16–18],

La[7–10,19,20], Ce[7,8,11,21–24], Nd[7,25], Sm[26], Eu[7,27], Yb[28–32], and Tl[33,34] for n-type thermoelectric materials.

A thermoelectric device using $IrSb_3$ could have a greater maximum operating temperature than a $CoSb_3$-based device because of the differences in decomposition temperatures of $IrSb_3$ 1414 K (1141^{o}C) and $CoSb_3$ 1146 K (873^{o}C), respectively.[35,36] Formulations of unfilled, n-type $IrSb_3$ with substituted impurity dopants of Pd or Pt have produced low ZT values (less than 0.05) primarily due to poor electrical properties.[37] Overall, $IrSb_3$ skutterudite filling with rare earth elements has been shown to significantly alter the thermoelectric properties as compared to the unfilled structure, particularly in reduced thermal conductivities.[35,38,39] However, the success seen with filled $CoSb_3$ versus unfilled $CoSb_3$ has yet to be realized for $IrSb_3$, as high temperature thermoelectric properties for filled $IrSb_3$ skutterudite are not a significant improvement over the unfilled $IrSb_3$.[20,29] Calculations for the maximum attainable filling fraction in $CoSb_3$ have been made[40] as well as calculations of the reduction in phonon conductivity in Ba-filled $CoSb_3$.[41] The preparation of n-type skutterudites has confirmed the limitations on void-filling in n-type $CoSb_3$-based materials, attaining filling fractions well short of 1.0, with most reports indicating a maximum fraction below 0.4 for atoms considered to be two-electron donors, and even less for atoms expected to be three-electron donors.[15,17,22,27,29,42] In the case of single element filling with barium in the $CoSb_3$-based skutterudite, the upper filling limit was reported to be $Ba_{0.44}Co_4Sb_{12}$ with the optimal thermoelectric properties found in a lesser filled sample in the series, $Ba_{0.24}Co_4Sb_{12}$ with a ZT of 1.1 at 850 K.[17] Addition of excess filler atoms beyond the filling limit can create secondary phases.[43]

The work presented here used a common process for skutterudite synthesis[19,32,44–46] by employing ball milling and hot pressing. The properties of a series of samples at different barium filling fractions, with the general formula $Ba_yIr_4Sb_{12}$, are described.

1.2 Experimental

Baseline, unfilled Ir_4Sb_{12} skutterudite was prepared by sealing stoichiometric amounts of elemental iridium powder (99.99%) and antimony shot (99.999%, Alfa Aesar) in an evacuated quartz tube, and heating that tube in a furnace at 900 ^oC for 48 hours. Barium filled skutterudite compositions were prepared by planetary ball milling of elemental iridium powder (99.99%), antimony shot (99.999%, Alfa Aesar), and barium rod (99+%, Alfa Aesar) in stoichiometric amounts to produce $Ba_yIr_4Sb_{12}$ (y = 0.15, 0.20, 0.25, 0.30, 0.35, 0.40, 0.50, 0.75). The resulting powders from the mechanical alloying were then sealed in evacuated quartz tubes and heated to 900 ^oC in a furnace for 48 hours. After furnace treatment, a small amount of each composition was removed for analysis by powder X-ray diffraction. The powders were then hot-pressed under dynamic vacuum at 880 ^oC in graphite dies, producing cylindrical samples that were geometrically measured to be greater than 98% of their theoretical densities. These hot-pressed samples were then analyzed by X-ray diffraction for phase purity. Room temperature Seebeck coefficient, Hall effect, and electrical resistivity measurements were made for all samples. The high temperature thermal diffusivity, Hall effect, and Seebeck coefficient were measured on samples between room temperature and approximately 750 ^oC (1023 K). The heat capacity and thermal diffusivity were determined using a flash diffusivity technique[47] and the overall error in the thermal conductivity measurements was estimated to be ±10%. The thermal conductivity was calculated from the experimental mass, density, heat capacity, and thermal diffusivity values.

The electrical resistivity (ρ) was measured using the van der Pauw technique with a current of 100 mA and a special high-temperature apparatus.[48] The Hall coefficient was measured in the same apparatus with a forward and reverse magnetic field value of ~9500 G. The carrier density was calculated from the Hall coefficient, assuming a scattering factor of 1 in a single carrier scheme, by $p/n = 1/R_H e$ where p and n are the densities of holes and electrons, respectively, and e is the electron charge. The Hall mobility (μ_H) was calculated from the Hall coefficient and the resistivity values by $\mu_H = R_H / \rho$. The errors were estimated to be ±0.5% and ±2% for the resistivity and Hall coefficient data, respectively. The Seebeck coefficient was measured using a high temperature light pulse technique[49] and it was measured using the same samples used for thermal conductivity, resistivity and Hall coefficient measurements. The error in the Seebeck coefficient measurement was estimated to be less than ±3%.

1.3 Results and Discussions

X-ray diffraction patterns obtained from furnace treated powders and hot-pressed pellets indicated high $IrSb_3$ phase purity, which was confirmed by scanning electron microscopy (SEM) and electron probe microanalysis (EPMA). Table 1.I summarizes the room temperature properties and measured compositions of the barium-filled samples and provides a comparison to the properties of unfilled $IrSb_3$. The volume percent of $IrSb_2$ phase impurity in each of the samples was calculated from SEM images taken at 500x magnification, using a brightness threshold method in ImageJ to calculate the percent area in the image that was covered by the phase identified as $IrSb_2$ by EPMA. The Ir:Sb ratios measured by EPMA in the barium filled sample series are lower than that measured in the unfilled Ir:Sb sample series. Ratios of Sb to the sum of Ir and Ba are similar to the unfilled sample, but begin to decrease as the nominal

filling fraction increases. While this change is expected with increased addition of Ba, there is a significant change observed for samples in which $y > 0.25$ where the Sb:(Ir + Ba) ratio falls more sharply and then levels off. The change in this ratio is a result of the increase in $IrSb_2$ phase impurity with increasing Ba content as well as small percentages of Ba-Sb phases that arise from excess Ba that is not incorporated in the skutterudite structure. EPMA measurements of the percentages of Ba incorporated into the skutterudite structure indicate that the amount of unincorporated Ba available to form Ba-Sb secondary phases would be minimal. Assuming that the unincorporated Ba forms the most antimony-rich of likely Ba-Sb phases,[50] the secondary phase of $BaSb_3$ could account for a maximum of 0.3%, 0.4%, 1.5%, 0.6%, 1.3%, 2.4% by weight, for the y = 0.15, 0.20, 0.25, 0.30, 0.35, 0.40 nominal compositions of $Ba_yIr_4Sb_{12}$, respectively. However, based on the temperature of the furnace annealing process and the hot-press temperature, the Ba-Sb phase is likely less antimony-rich, like BaSb, Ba_2Sb, or Ba_3Sb_2.[50] In these cases, the percentage of Ba-Sb phase impurity in these samples would be even less than the percentages calculated above. These very small percentages could explain why no Ba-Sb secondary phases were clearly present in SEM images or detected by EPMA.

Figure 1.1 shows the X-ray diffraction (XRD) patterns obtained for each of the samples in the series. The XRD data show high $IrSb_3$ phase purity for most samples and the appearance of $IrSb_2$ and Sb peaks in the pattern as the amount of barium added to the synthesis increases. The increase of $IrSb_2$ inclusions was verified by SEM and EPMA as shown in Figure 1.2. The unfilled $IrSb_3$ control sample was single phase, while samples with increasing nominal barium levels showed increasing amounts of the secondary phase $IrSb_2$. Samples with higher nominal levels of barium were also appeared less sintered after hot-pressing, as observed in SEM images. Figure 1.3 plots the barium filling fraction measured by EPMA against the nominal barium

filling fraction. The EPMA measured barium filling fraction was obtained by normalizing the measured atomic percentage to the atomic percentage of antimony, assuming exactly 12 antimony atoms per formula unit. The measured filling fractions fall short of the nominal fractions and appear to reach a maximum around 30%. However, at the top of the range, the $Ba_{0.75}Ir_4Sb_{12}$ nominal composition did show an average of 36.3% barium filling fraction, but this is less than half of the nominal filling fraction and this relatively large amount of excess, unincorporated barium may have contributed to a higher average.

The measured carrier concentrations at room temperature in the barium-filled samples ranged from 1.48 x 10^{20} cm^{-3} and 1.97 x 10^{20} cm^{-3} for all filling fractions of barium attempted. The small differences in room temperature carrier concentrations relative to barium content in the samples indicate that not all of the expected charge carriers from barium filling in these compositions are activated because if each barium contributed two electrons to the structure, the range of carrier concentrations in the series of samples would be significantly wider. For the smallest barium filling fraction synthesized in this sample series, (y = 0.15), if all of the barium in the nominal composition were incorporated in the structure and all of the expected charge carriers were activated, barium would contribute about 7.6 x 10^{20} cm^{-3} electrons to the total. Undoped $IrSb_3$ is naturally a p-type semiconductor with an experimentally measured hole carrier concentration of 1.6 x 10^{19} cm^{-3} as shown in Table 1.I. As a quick estimate, neglecting any small change in the $IrSb_3$ lattice parameter induced by partial void filling, subtracting the room temperature $IrSb_3$ hole concentration from the contribution of two electrons from each barium gives an approximate expected carrier concentration of 7.4 x 10^{20} cm^{-3} for the y = 0.15 composition. The full complement of carriers from the barium in the structure are not activated at room temperature in this composition nor any of the compositions in this series, as room

temperature carrier concentrations are all below this value and in a relatively narrow range. EPMA measurements showed that the maximum filling fraction for Ba was around 0.30. For a Ba filling fraction of 0.30, the predicted carrier concentration is 1.50×10^{21} cm^{-3}, an order of magnitude greater than what is observed at room temperature for this sample series. As shown in Figure 1.4, the $y = 0.15$ composition achieves a carrier concentration consistent with the approximation for full Ba carrier activation somewhere around 550 ^{o}C (823 K), coinciding with a crash in mobility seen in Figure 1.5. Subsequent compositions with greater levels of barium reach the approximate, full activation concentration at higher temperatures as barium levels increase, with the exception of the $y = 0.40$ composition which does not reach this approximated carrier concentration in the measured temperature range. Although the measured carrier concentrations reach these levels at high temperature, it is possible that the observed increase is the result of minority carrier contributions and not Ba carrier activation.

The mobility as a function of temperature is plotted in Figure 1.5. Unfilled, undoped $IrSb_3$ has a very high mobility that is drastically reduced when the structure is filled. The room temperature mobility of the filled series here is greatest in the $y = 0.25$ composition, followed by the $y = 0.30$ composition. Mobility values decrease as the temperature increases and the values for all of the compositions begin to approach zero cm^2/Vs as the temperature nears 750^{o}C (1023 K). The $y = 0.15$ composition reaches zero between 900 K and 1000 K and then rises once more as minority carriers take over. Electrical resistivity as a function of temperature is presented in Figure 1.6. Resistivity decreases with increasing Ba content, until $y = 0.30$, where the room temperature resistivity is greater than that of the $y = 0.25$ composition. However, this increase in resistivity at room temperature is countered at high temperature where the $y = 0.30$, 0.35, and 0.40 compositions have significantly lower resistivity values around the maximum temperature

of 750°C (1023 K). The resistivity data suggest that the barium filling in $IrSb_3$ is optimized at room temperature in the $y = 0.25$ nominal composition while the higher nominal filling fractions appear to be able to utilize additional carriers from extra barium at high temperatures, driving the resistivity sharply down.

The Seebeck coefficient values were measured at room temperature and are presented in Table 1.I. The room temperature Seebeck coefficient values decrease in magnitude, as expected, with increasing Ba addition. Measurements of Seebeck coefficients as a function of temperature are presented in Figure 1.7. The absence of a clear trend in Seebeck coefficient as a function of barium content is likely a product of multiple factors such as the small amounts of metallic $IrSb_2$ inclusions in the sample, as described earlier, and a perhaps a complicated band structure that is still not well understood in filled $IrSb_3$. Just as with the resistivity measurements, the compositions with lower nominal filling fractions have varying Seebeck coefficient values relative to one another, and as the nominal filling fraction increases, the Seebeck coefficient curves converge and are quite close to one another through the entire temperature range, with one notable exception. Once again, the $y = 0.25$ composition curve does not turn up when all the others appear to turn up at high temperature, and instead the Seebeck coefficient continues to steadily increase in magnitude. This behavior at high temperature by the $y = 0.25$ composition is consistent the resistivity data, suggesting that the $y = 0.25$ nominal composition is a composition around which the electronic structure changes significantly with more or less Ba content.

The temperature dependent, total thermal conductivities of the series of Ba-filled samples is presented in Figure 1.8 and the temperature dependent, lattice thermal conductivities are presented in Figure 1.9. All Ba-filled compositions measured exhibit room temperature thermal conductivities that are an order of magnitude less than that of the unfilled structures. Increased

Ba content produced a decrease in total thermal conductivity with another apparent convergence of measured values with the higher levels of Ba content in the series. The one exception to the trend is between the $y = 0.20$ and $y = 0.25$ compositions, where the total thermal conductivity of the $y = 0.20$ composition is less than that of that $y = 0.25$ composition. This is likely because the significant differences in resistivity while the difference in the lattice thermal conductivity between these two compositions is small. Therefore, the significant difference in the contributions of the electronic terms is the major contributing factor to the vast difference in the total thermal conductivities of the $y = 0.20$ and $y = 0.25$ compositions.

The thermoelectric figure of merit, ZT, as a function of temperature is depicted in Figure 1.10 for compositions $y = 0.15$, 0.20, 0.25, 0.30, 0.35, and 0.40. The overall error in ZT was estimated to be about ±20% as an accumulation of measurement errors for each of the factors to calculate ZT. Peak ZT values for $y = 0.25$, 0.30, and 0.35 compositions are greatest, with $y =$ 0.20 and 0.40 compositions near those peak values, but turning downward before 750^{o}C (1023 K).

1.4 Conclusions

Synthesis of viable n-type, filled $IrSb_3$ skutterudite thermoelectric materials have been demonstrated and characterized by XRD, SEM, EPMA, and thermoelectric properties. The filling method has achieved far more favorable electrical and thermal properties in $IrSb_3$, when compared to previous methods used for substitutional doping in the structure. EPMA data indicate that the barium filling limit in $Ba_yIr_4Sb_{12}$ is $0.2 < y < 0.3$, but further investigations are warranted. To our knowledge, this is the first report detailing a filled n-type, $IrSb_3$ skutterudite with ZT values of this magnitude. Although the peak ZT value appears here to be attainable over

a range of barium levels, more work is needed to determine the true limit of barium filling in the $IrSb_3$ structure, and which other atoms are viable candidates for effectively filling this structure. The results presented here suggest that skutterudite-based thermoelectric devices could be able to efficiently operate over a wider temperature range than ever before.

1.5 Acknowledgements

This research was carried out at the Jet Propulsion Laboratory, California Institute of Technology, under a contract with the National Aeronautics and Space Administration. This work was supported by the NASA Science Mission Directorate's Radioisotope Power Systems Technology Advancement Program, the NSF IGERT: Materials Creation Training Program (MCTP) – DGE-0654431 (DM), and the California NanoSystems Institute. The authors thank Dr. Frank Kyte of the University of California, Los Angeles for SEM and EPMA assistance and helpful discussions. The authors also thank the EPSS department at the University of California, Los Angeles for supporting the SEM and EPMA facility. The authors thank Sabah K. Bux, Kurt Star, James Ma, George Nakatsukasa, Andrew Lech and Michael T. Yeung for helpful discussions. Special thanks to George Nakatsukasa, L. Danny Zoltan, and Gregory Gerig for instrumentation support.

1.6 Tables and Figures

Table 1.I. Composition and Room Temperature Transport Properties for Barium-filled Skutterudites – $Ba_yIr_4Sb_{12}$

Nominal Comp.	Ir_4Sb_{12}	$Ba_{0.15}Ir_4Sb_{12}$	$Ba_{0.20}Ir_4Sb_{12}$	$Ba_{0.25}Ir_4Sb_{12}$	$Ba_{0.30}Ir_4Sb_{12}$	$Ba_{0.35}Ir_4Sb_{12}$	$Ba_{0.40}Ir_4Sb_{12}$	$Ba_{0.50}Ir_4Sb_{12}$
EPMA Comp.	$Ir_{3.84}Sb_{12}$	$Ba_{0.135}Ir_{3.75}Sb_{12}$	$Ba_{0.18}Ir_{3.76}Sb_{12}$	$Ba_{0.184}Ir_{3.79}Sb_{12}$	$Ba_{0..273}Ir_{3.81}Sb_{12}$	$Ba_{0.293}Ir_{3.81}Sb_{12}$	$Ba_{0.292}Ir_{3.84}Sb_{12}$	$Ba_{0.303}Ir_{3.78}Sb_{12}$
Ba fill fraction by EPMA	0.0%	13.5%	18.0%	18.4%	27.3%	29.3%	29.2%	30.3%
Electrical resistivity (mΩ cm)	0.36	1.72	1.48	1.00	1.17	1.24	1.24	1.03
Hall mobility ($cm^2/V\ s$)	1079	24.57	21.36	35.72	30.80	28.67	31.36	32.88
Hall carrier concentration (cm^{-3})	$1.62x10^{19}$	$1.48x10^{20}$	$1.97x10^{20}$	$1.75x10^{20}$	$1.73x10^{20}$	$1.75x10^{20}$	$1.61x10^{20}$	$1.84x10^{20}$
Seebeck coefficient (μV/K)	27.3	-108.5	-99.5	-98.2	-92.5	-91.3	-90.3	-88.5
Thermal conductivity (mW/cm K)	124.3	31.14	24.96	28.91	24.96	24.54	24.83	27.11
Lattice thermal conductivity (mW/cm K)	108.8	27.93	21.22	23.45	20.27	20.18	20.42	22.09
$IrSb_2$ phase (vol%)	0.0	2.9	2.3	1.1	2.6	3.3	3.4	6.6
$IrSb_3$ phase (vol%)	100.0	97.1	97.7	98.9	97.4	96.7	96.6	93.4
Ir:Sb ratio in $IrSb_3$ phase (EPMA)	0.331	0.312	0.314	0.315	0.317	0.318	0.320	0.315
Sb:Ir ratio in $IrSb_3$ phase (EPMA)	3.02	3.20	3.19	3.17	3.15	3.15	3.13	3.18
Sb:(Ir + Filler) ratio in $IrSb_3$ phase (EPMA)	3.02	3.09	3.04	3.02	2.94	2.92	2.91	2.94

*Note that all values presented in the table were obtained at room temperature. The $y = 0$ sample is included for comparison. The Ba fill fraction is an average of all measured points in the dominant phase of the sample. The electrical resistivity (ρ) was measured using the van der Pauw technique with a current of 100 mA. The Hall mobility and the carrier density were calculated from the Hall coefficient which was measured with a forward and reverse magnetic field value of ~9500 G. $IrSb_2$ phase impurities were measured using SEM images and ImageJ software to calculate the area of the image occupied by this secondary phase. Elemental ratios were obtained by taking averages of the ratios of the measured atomic percentages of each point in the $IrSb_3$ phase.

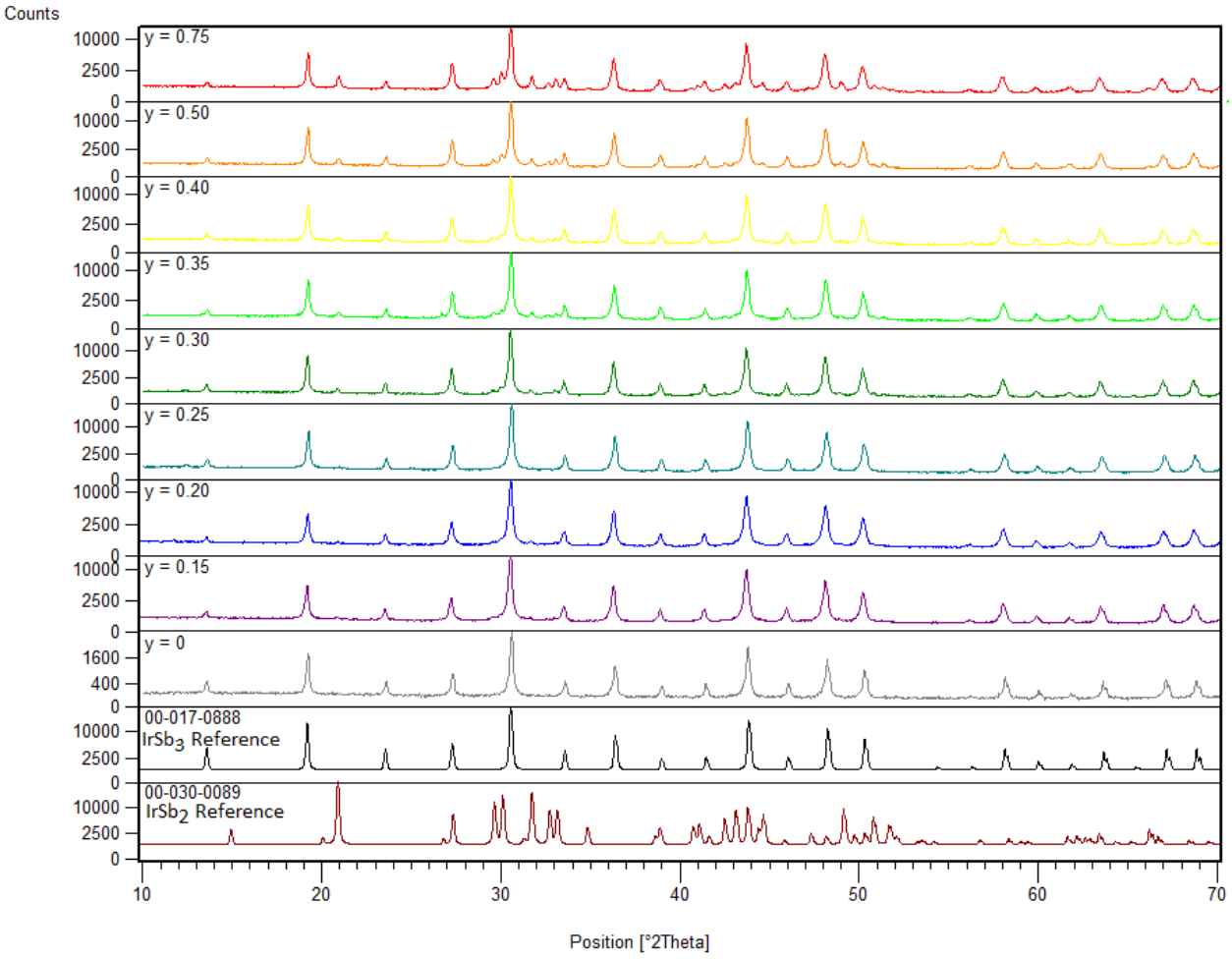

Figure 1.1. X-ray diffraction patterns obtained from the hot-pressed samples. Simulated diffraction patterns generated from JCPDS reference pattern 00-017-0888 for $IrSb_3$ and JCPDS reference pattern 00-030-0089 for $IrSb_2$ are presented here for comparison to the obtained experimental sample patterns.

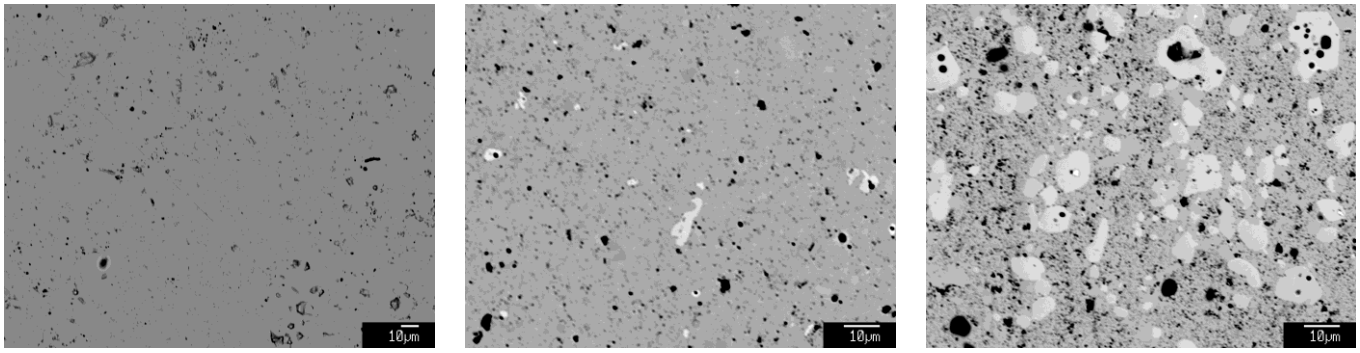

$y = 0$ $y = 0.25$ $y = 0.75$

Figure 1.2. Scanning electron microscope (SEM) images of three $Ba_yIr_4Sb_{12}$ samples. The unfilled, $y = 0$ sample was determined to be single phase by EPMA. The addition of Ba leads to the presence of a secondary phase, $IrSb_2$, which increases with increasing nominal filling fraction.

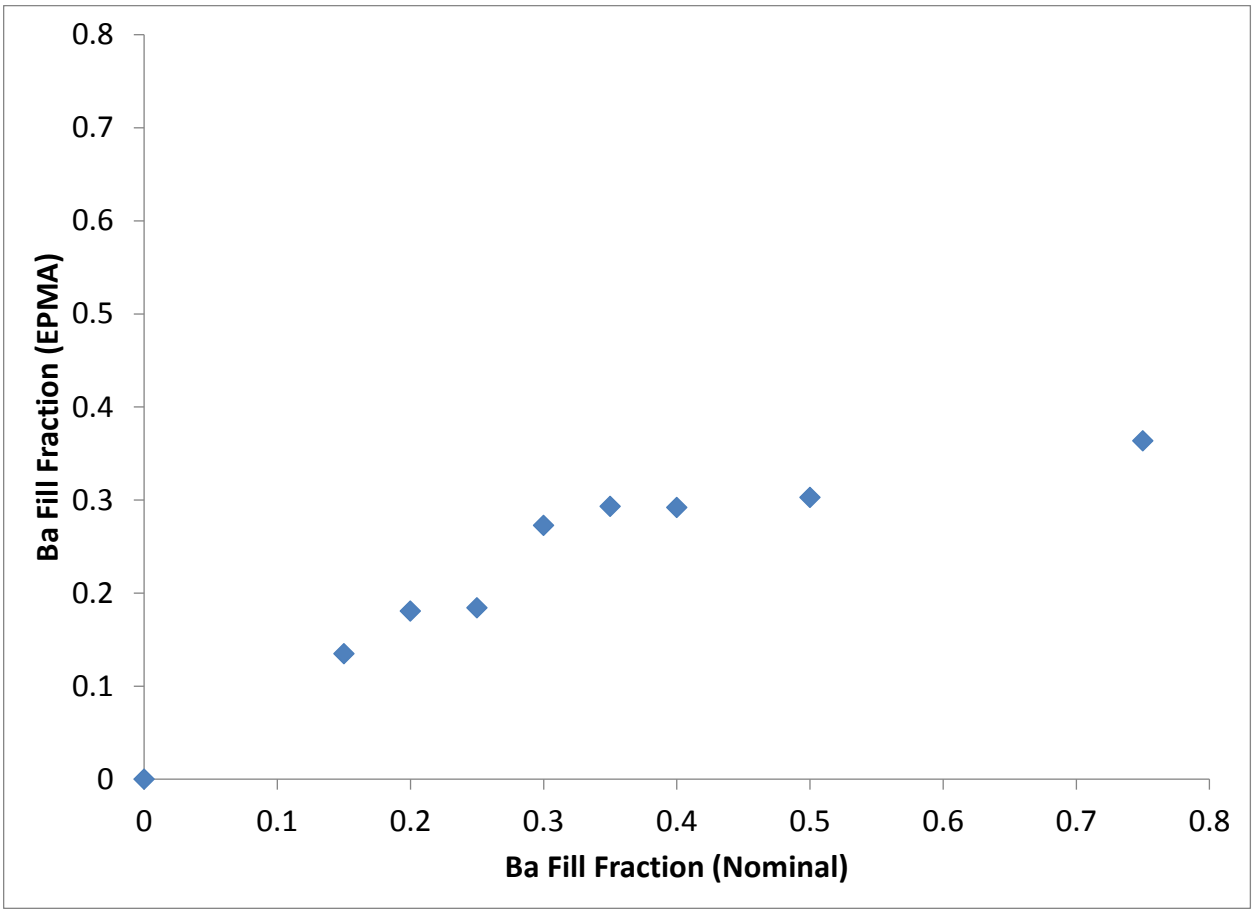

Figure 1.3. Nominal barium fill fraction versus EPMA measured barium fill fraction. Values for EPMA fill fraction are based on atomic percentages measured for barium, normalized by the measured antimony content of the sample.

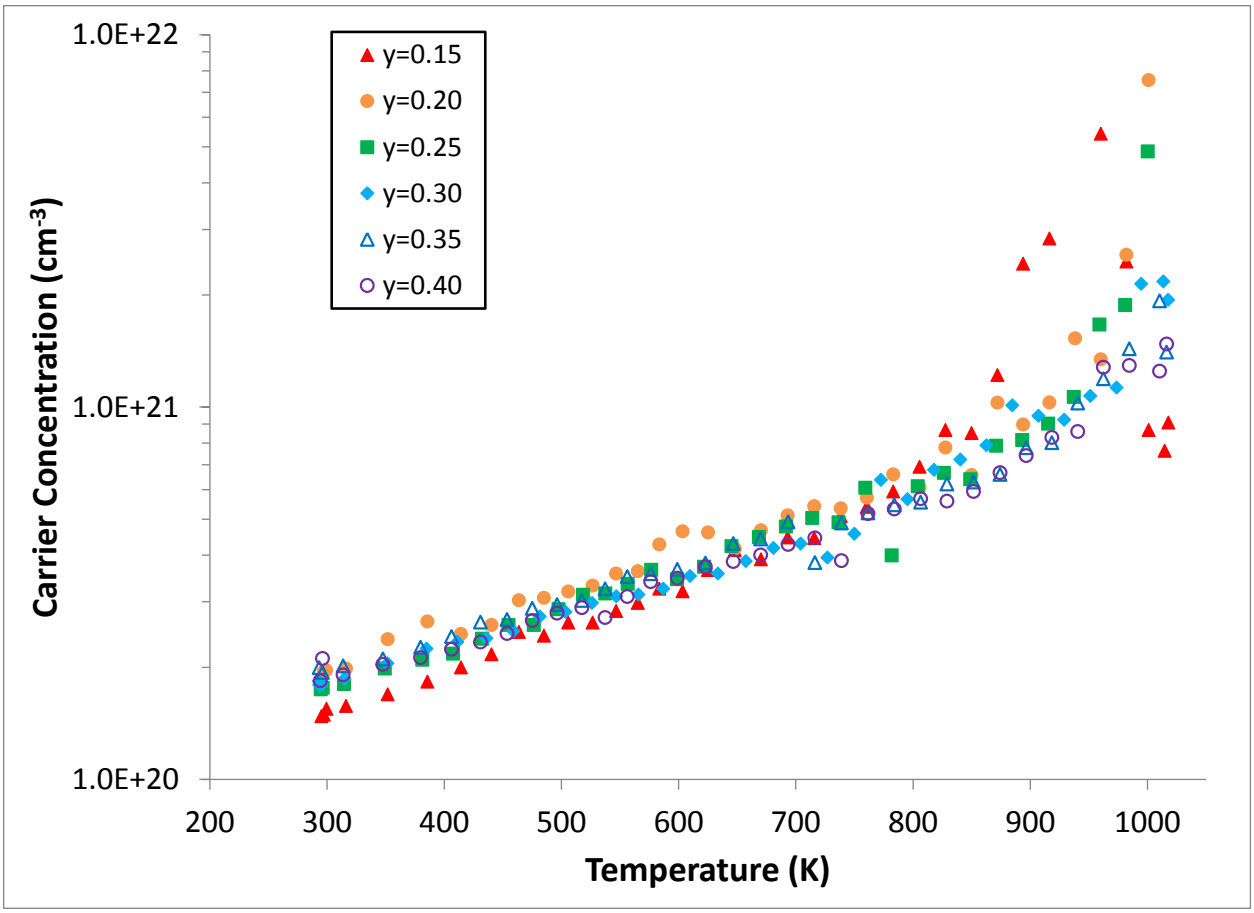

Figure 1.4. Temperature dependence of carrier concentration in $Ba_yIr_4Sb_{12}$ samples. The Hall coefficient was measured with a forward and reverse magnetic field value of ~9500 G. The carrier concentration was calculated from the Hall coefficient, assuming a scattering factor of 1 in a single carrier scheme, by $p/n = 1/R_He$ where p and n are the densities of holes and electrons, respectively, and e is the electron charge. The measurement error was estimated to be ±2% for the Hall coefficient data.

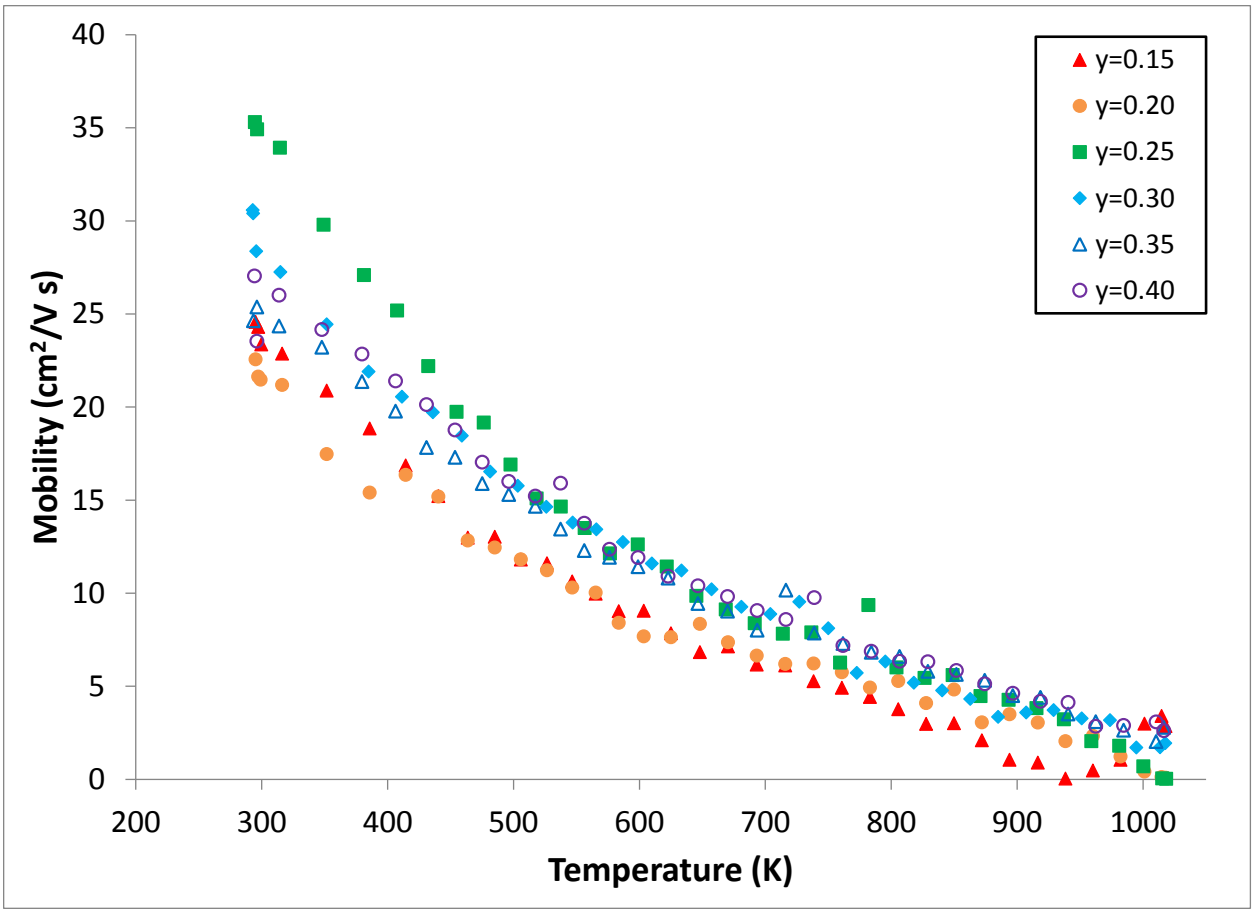

Figure 1.5. Temperature dependence of carrier mobility in $Ba_yIr_4Sb_{12}$ samples. The Hall coefficient was measured with a forward and reverse magnetic field value of ~9500 G and the Hall mobility was calculated from the Hall coefficient. The measurement error was estimated to be ±2% for the Hall coefficient data.

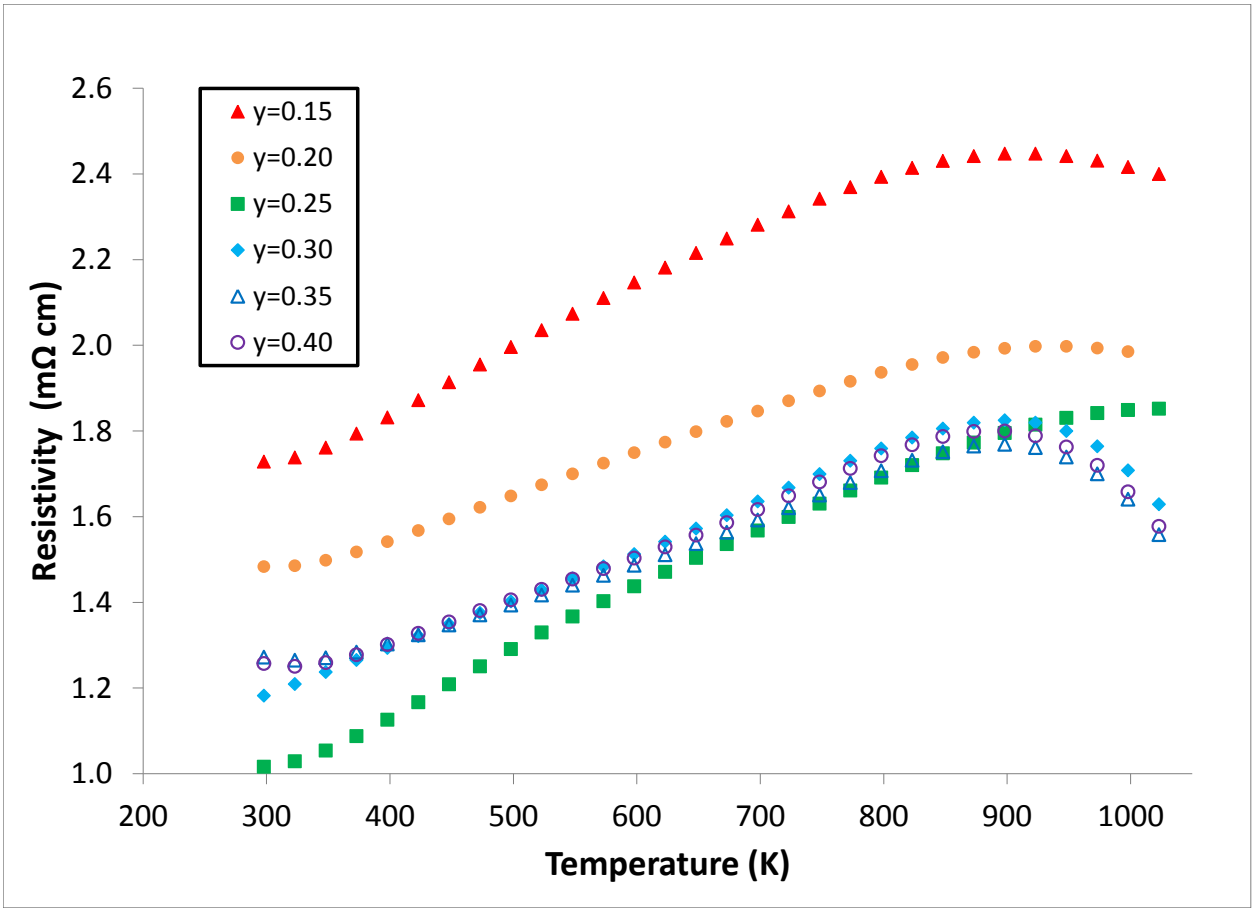

Figure 1.6. Temperature dependence of electrical resistivity in $Ba_yIr_4Sb_{12}$ samples. The electrical resistivity (ρ) was measured using the van der Pauw technique with a current of 100 mA. The measurement error was estimated to be ±0.5% for the resistivity data.

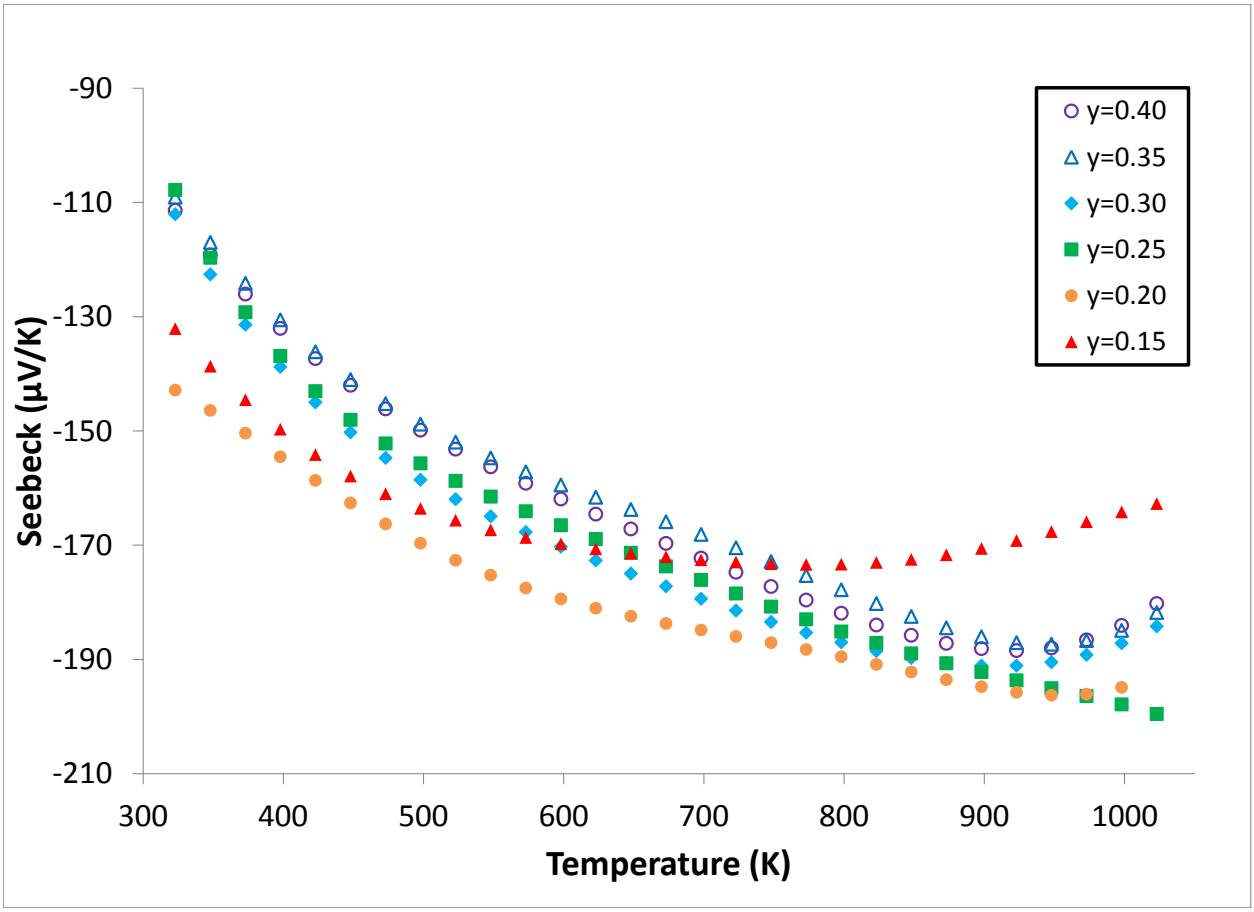

Figure 1.7. Temperature dependence of Seebeck coefficient in $Ba_yIr_4Sb_{12}$ samples. The Seebeck coefficient was measured using a high temperature light pulse technique.[49] The error of the Seebeck coefficient measurement was estimated to be less than ±3%.

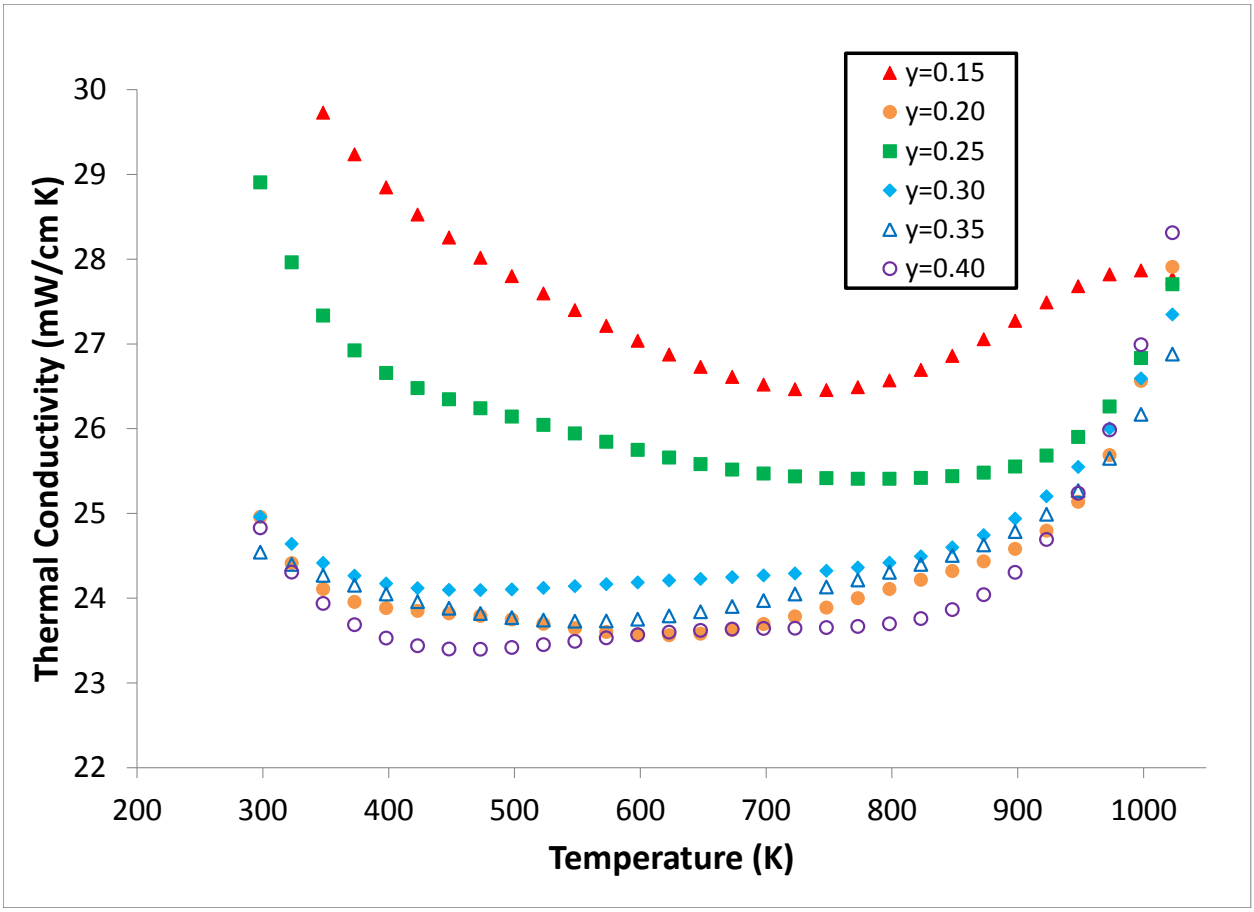

Figure 1.8. Temperature dependence of thermal conductivity (λ) in $Ba_yIr_4Sb_{12}$ samples. The heat capacity and thermal diffusivity were measured using a flash diffusivity technique[47] and the overall error in the thermal conductivity measurements was estimated to be about ±10%. The thermal conductivity was calculated from the experimental mass, density, heat capacity, and thermal diffusivity values.

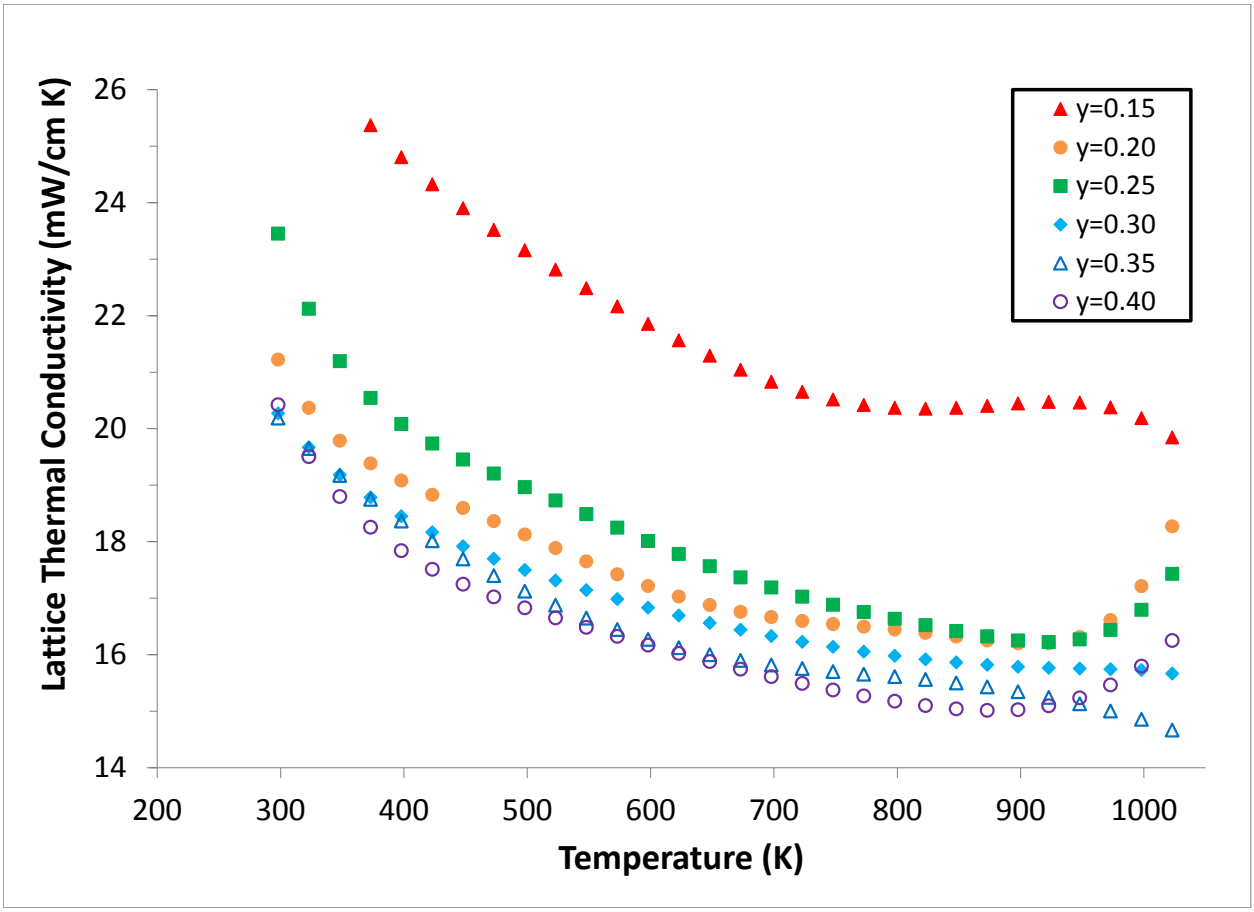

Figure 1.9. Temperature dependence of lattice thermal conductivity ($\lambda_{Lattice}$) in $Ba_yIr_4Sb_{12}$ samples. The lattice thermal conductivity was obtained by subtracting the electronic thermal conductivity contribution from the total thermal conductivity. The electronic contribution was calculated from the resistivity and Lorenz number. The total thermal conductivity was calculated from the experimental mass, density, heat capacity, and thermal diffusivity values. The overall error in the thermal conductivity measurements was estimated to be about ±10%.

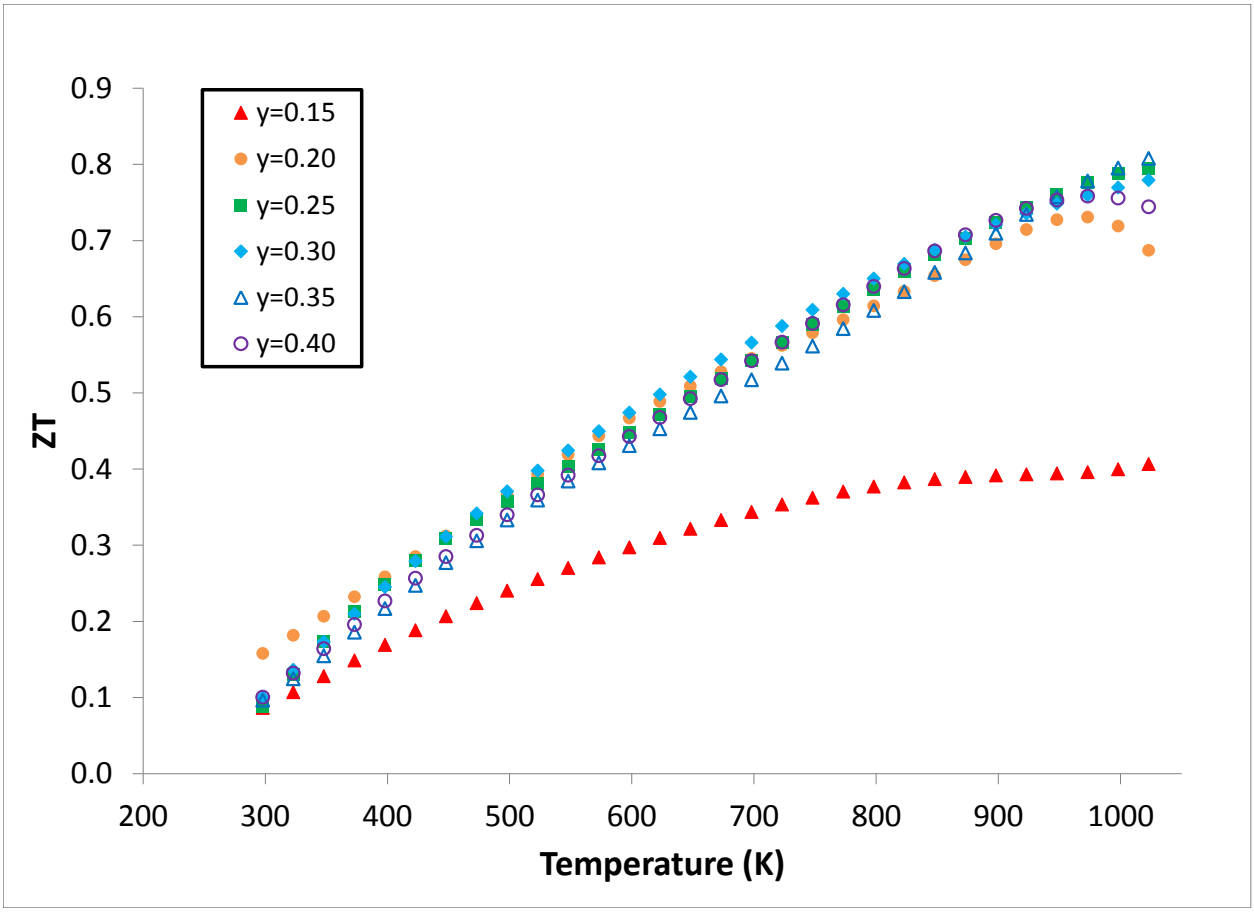

Figure 1.10. Temperature dependence of the thermoelectric figure of merit, ZT in $Ba_yIr_4Sb_{12}$ samples. Combining the Seebeck coefficient, resistivity, and thermal conductivity measurements, the overall error in ZT was estimated to be about ±20%.

1.7 References

(1) Rowe, D. M. *CRC Handbook of Thermoelectrics*; Rowe, D. M., Ed.; CRC Press, 1995.

(2) Fleurial, J.-P.; Caillat, T.; Borshchevsky, A. *Proc. 16th Int. Conf. Thermoelectr.* **1997**, 1.

(3) Liu, W.-S.; Zhang, B.-P.; Li, J.-F.; Zhang, H.-L.; Zhao, L.-D. *J. Appl. Phys.* **2007**, *102*, 103717.

(4) Bertini, L.; Billquist, K.; Christensen, M.; Gatti, C.; Palmqvist, A.; Platzek, D.; Rowe, D. M.; Saramat, A.; Stiewe, C.; Williams, S. G.; Golgi, V. C.; Division, M. C. In *22nd International Conference on Thermoelectrics*; 2003; pp. 48–51.

(5) Chitroub, M.; Besse, F.; Scherrer, H. *J. Alloys Compd.* **2009**, *467*, 31.

(6) Bertini, L.; Stiewe, C.; Toprak, M.; Williams, S.; Platzek, D.; Mrotzek, A.; Zhang, Y.; Gatti, C.; Müller, E.; Muhammed, M.; Rowe, M. *J. Appl. Phys.* **2003**, *93*, 438.

(7) Sales, B. C.; Mandrus, D.; Williams, R. K. *Science (80-.).* **1996**, *272*, 1325.

(8) Sales, B.; Mandrus, D.; Chakoumakos, B.; Keppens, V.; Thompson, J. *Phys. Rev. B* **1997**, *56*, 15081.

(9) Nolas, G.; Cohn, J.; Slack, G. *Phys. Rev. B* **1998**, *58*, 164.

(10) Chakoumakos, B. C.; Sales, B. C.; Mandrus, D.; Keppens, V. *Acta Crystallogr. Sect. B Struct. Sci.* **1999**, *55*, 341.

(11) Meisner, G.; Morelli, D.; Hu, S.; Yang, J.; Uher, C. *Phys. Rev. Lett.* **1998**, *80*, 3551.

(12) Puyet, M.; Lenoir, B.; Dauscher, a.; Pécheur, P.; Bellouard, C.; Tobola, J.; Hejtmanek, J. *Phys. Rev. B* **2006**, *73*, 035126.

(13) Zhao, X. Y.; Shi, X.; Chen, L. D.; Zhang, W. Q.; Zhang, W. B.; Pei, Y. Z. *J. Appl. Phys.* **2006**, *99*, 053711.

(14) Eilertsen, J.; Berthelot, R.; Sleight, A. W.; Subramanian, M. a. *J. Solid State Chem.* **2012**, *190*, 238.

(15) He, T.; Chen, J.; Rosenfeld, H. D.; Subramanian, M. a. *ChemInform* **2006**, *37*, 759.

(16) Chen, L.; Tang, X.; Goto, T.; Hirai, T. *J. Mater. Res.* **2000**, *15*, 2276.

(17) Chen, L. D.; Kawahara, T.; Tang, X. F.; Goto, T.; Hirai, T.; Dyck, J. S.; Chen, W.; Uher, C. *J. Appl. Phys.* **2001**, *90*, 1864.

(18) Zhao, W.; Wei, P.; Zhang, Q.; Dong, C.; Liu, L.; Tang, X. *J. Am. Chem. Soc.* **2009**, *131*, 3713.

(19) Song, X.; Yang, J.; Peng, J.; Chen, Y.; Zhu, W.; Zhang, T. *J. Alloys Compd.* **2005**, *399*, 276.

(20) Kim, S. W.; Kimura, Y.; Mishima, Y. *J. Electron. Mater.* **2004**, *33*, 1.

(21) Fleurial, J.-P.; Borshchevsky, A.; Caillat, T.; Morelli, D. T.; Meisner, G. P. In *15th International Conference on Thermoelectrics*; 1996; Vol. 3, pp. 91–95.

(22) Chen, B.; Xu, J.; Uher, C.; Morelli, D. T.; Meisner, G. P.; Fleurial, J.-P.; Caillat, T.; Borshchevsky, A. *Phys. Rev. B* **1997**, *55*, 1476.

(23) Morelli, D.; Meisner, G.; Chen, B.; Hu, S.; Uher, C. *Phys. Rev. B* **1997**, *56*, 7376.

(24) Xue, Y.; Liu, K.; Li, J.; Chen, N. *Mater. Res. Bull.* **2005**, *40*, 1172.

(25) Kuznetsov, V. L.; Kuznetsova, L. A.; Rowe, D. M. *J. Phys. Condens. Matter* **2003**, *15*, 5033.

(26) Jiang, Y.; Jia, X.; Deng, L.; Ma, H. *J. Rare Earths* **2012**, *30*, 388.

(27) Pei, Y. Z.; Bai, S. Q.; Zhao, X. Y.; Zhang, W.; Chen, L. D. *Solid State Sci.* **2008**, *10*, 1422.

(28) Dilley, N. R.; Bauer, E. D.; Maple, M. B.; Sales, B. C. *J. Appl. Phys.* **2000**, *88*.

(29) Bauer, E.; Galatanu, A.; Michor, H.; Hilscher, G.; Rogl, P.; Boulet, P.; No, H. *Eur. Phys. J. B* **2000**, *14*, 483.

(30) Anno, H.; Nolas, G. S.; Akai, K.; Ashida, K.; Matsuura, M.; Matsubara, K. In *Proceedings of the 20th International Conference on Thermoelectrics*; 2001; Vol. 3, pp. 61–64.

(31) Liu, H.; Zhao, X.; Zhu, T.; GU, Y. *J. Rare Earths* **2012**, *30*, 456.

(32) Yang, J.; Hao, Q.; Wang, H.; Lan, Y.; He, Q.; Minnich, a.; Wang, D.; Harriman, J.; Varki, V.; Dresselhaus, M.; Chen, G.; Ren, Z. *Phys. Rev. B* **2009**, *80*, 115329.

(33) Sales, B.; Chakoumakos, B.; Mandrus, D. *Phys. Rev. B* **2000**, *61*, 2475.

(34) Chakoumakos, B. C.; Sales, B. C. *J. Alloys Compd.* **2006**, *407*, 87.

(35) Slack, G. a.; Tsoukala, V. G. *J. Appl. Phys.* **1994**, *76*, 1665.

(36) Feschotte, P.; Lorin, D. *J. Less Common Met.* **1989**, *155*, 255.

(37) Kim, S. W. N. G.; Kimura, Y.; Mishima, Y. *J. Electron. Mater.* **2003**, *32*, 1141.

(38) Nolas, G. S.; Slack, G. A.; Morelli, D. T.; Tritt, T. M.; Ehrlich, A. C. *J. Appl. Phys.* **1996**, *79*, 4002.

(39) Tritt, T. M.; Cohn, J. L. *J. Appl. Phys.* **1996**, *79*, 8412.

(40) Shi, X.; Zhang, W.; Chen, L. D.; Yang, J.; Uher, C. *Acta Mater.* **2008**, *56*, 1733.

(41) Huang, B.; Kaviany, M. *Acta Mater.* **2010**, *58*, 4516.

(42) Puyet, M.; Lenoir, B.; Dauscher, a.; Weisbecker, P.; Clarke, S. J. *J. Solid State Chem.* **2004**, *177*, 2138.

(43) Mallik, R. C.; Stiewe, C.; Karpinski, G.; Hassdorf, R.; Müller, E. *J. Electron. Mater.* **2009**, *38*, 1337.

(44) Yang, J.; Chen, Y.; Zhu, W.; Peng, J.; Bao, S.; Fan, X.; Duan, X. *J. Solid State Chem.* **2006**, *179*, 212.

(45) Peng, J.; Yang, J.; Zhang, T.; Song, X.; Chen, Y. *J. Alloys Compd.* **2004**, *381*, 313.

(46) Yang, J.; Chen, Y.; Peng, J.; Song, X.; Zhu, W.; Su, J.; Chen, R. *J. Alloys Compd.* **2004**, *375*, 229.

(47) Vandersande, J. W.; Wood, C.; Zoltan, A.; Whittenberger, D. *Therm. Conduct.* **1988**, *19*, 445.

(48) Mccormack, J. A.; Fleurial, J.-P. *MRS Proc.* **1991**, *234*, 135.

(49) Wood, C.; Zoltan, D.; Stapfer, G. *Rev. Sci. Instrum.* **1985**, *56*, 719.

(50) Okamoto, H. *Binary Alloy Phase Diagrams*; Massalski, T. B., Ed.; II.; ASM International, 1990; pp. 3304–3307.

Chapter 2: Two-element filling in $IrSb_3$-based n-type skutterudite: High temperature thermoelectric properties of $Ba_xYb_yIr_4Sb_{12}$ and $Ba_xEu_zIr_4Sb_{12}$

2.1 Introduction

The thermoelectric figure of merit (ZT) is defined by the following equation:

$$ZT = \frac{S^2}{\rho\lambda}T$$

where S is the Seebeck coefficient, ρ is the electrical conductivity, and λ is the total thermal conductivity of the sample. The figure of merit is dimensionless and has a direct relationship to efficiency.[1] The skutterudite structure is described as a cubic lattice with the space group *Im3* and materials with this structure have been studied extensively for thermoelectric applications.[2–7]

Single element void filling in thermoelectric materials with a skutterudite structure has demonstrated significant reductions in thermal conductivities of these materials. Particularly in the case of $CoSb_3$-based n-type skutterudites, this reduction of thermal conductivity is attributed to the "rattling" of the filler atoms in the structural voids.[3,5,8–10] Formulations of n-type $CoSb_3$ skutterudite with single-element filling have been investigated for several elements including Ca[11], Sr[12], In[13,14], Ba[15–17], La[3,5,8,9,18,19], Ce[5,8,10,20–23], Nd[5,24], Sm[25], Eu[5,26], Yb[27–31], and Tl[4,32]. Recent work has demonstrated for the first time that void filling in $IrSb_3$-based skutterudite can reduce the thermal conductivity, achieve necessary doping levels, while at the same time maintaining a large enough Seebeck coefficient to result in a ZT around 0.8 at 750 ^oC (1023 K).[33] A ZT of this magnitude for filled $IrSb_3$ skutterudite makes the material relevant for thermoelectric applications, renewing interest in filler studies for this type of skutterudite.

Barium single-element filling is the only demonstrated filling in $IrSb_3$ skutterudite to have a high ZT. Multiple-element filling in $CoSb_3$ skutterudite has shown that the lower thermal conductivities achieved by single-filled variations can be reduced even further by employing double[17,34–44] or triple-element filling.[45–50] Therefore, multiple-element filling in $IrSb_3$ skutterudite could result in a further decrease in thermal conductivity and an increase in ZT over that obtained recently by barium single-element filling.[33] Calculations for double filling in $CoSb_3$ also suggest that combinations of filler atoms exist whereby the power factor (the product of the electrical conductivity and the square of the Seebeck coefficient) is increased, relative to the analogous single-filled structures.[17,51]

Limitations exist for filling the voids in n-type skutterudite structures, such that the amount of voids that can be occupied by filler atoms is less than 100%, and the filling fraction dependent on which filler elements are used. Filling limits in $CoSb_3$ skutterudite are mostly dependent on the valence electron count in the structure because counter-doping with electron deficient elements on the Co or Sb sites allows for a higher filling fraction than the unsubstituted structure.[15] There is only limited information available on filling limits in unsubstituted $IrSb_3$ skutterudite.[19,33] The goal of multiple-element filling is to scatter phonons of different frequencies as a result of the different vibrational frequencies of each filler element in the structure. Multiple-element filling presents a new and interesting dependent variable to these experiments because with multiple elements competing for the void spaces in the $IrSb_3$ skutterudite structure, it is possible that one element will be more likely to fill than another element and the filling fractions of the individual elements in the same sample will be asymmetric. Excess filler elements that are excluded from the void spaces could influence the formation of secondary phases in filled $CoSb_3$ skutterudite[23,28,52] and filled $IrSb_3$ skutterudite[33]

compositions. Competition for vacancy sites with multiple-element filling may also influence the valence states of some filler elements that are known to have a mixed valence.[29,53,54]

This work describes a common process for skutterudite synthesis[18,31,55–57] by employing ball milling and hot pressing. The $Ba_xYb_yIr_4Sb_{12}$ compositions are reported here for direct comparison to similar Ba + Yb filling in $CoSb_3$. $Ba_xEu_zIr_4Sb_{12}$ is presented as a new, higher performing double-filled variation. Single-element Ba, Yb, and Eu-filled compositions are also characterized to contrast with single and double-filled $IrSb_3$. Values of *x, y,* and *z* were chosen to elucidate differences between the filler elements themselves and how they participate in the $IrSb_3$ skutterudite structure, rather than to explore a wide range in the total filling fraction.

2.2 Experimental

The filled skutterudite compositions were prepared by planetary ball milling of elemental iridium powder (99.99%), antimony shot (99.999%, Alfa Aesar), barium rod (99+%, Alfa Aesar), ytterbium chunk (99.9%, Alfa Aesar), and europium chunk (99.9%, Stanford Materials). The resulting powders from the mechanical alloying were then sealed in evacuated quartz tubes and heated to 900 ^oC in a furnace for 48 hours. After heating, a small amount of each composition was removed for analysis by powder X-ray diffraction. The powders were then hot-pressed under dynamic vacuum at 880 ^oC in graphite dies, producing cylindrical samples that were geometrically measured to be greater than 98% of their theoretical densities. These hot-pressed samples were then analyzed by X-ray diffraction for phase purity. The room temperature Seebeck coefficient, Hall effect, and electrical resistivity measurements were made for all samples. The high temperature thermal diffusivity, Hall effect, and Seebeck coefficient

measurements were carried out between room temperature and approximately 750 ^{o}C (1023 K). The heat capacity and thermal diffusivity were measured using a flash diffusivity technique[58] and the overall error in the thermal conductivity measurements was estimated to be ±10%. The thermal conductivity was calculated from the experimental mass, density, heat capacity, and thermal diffusivity values. The electrical resistivity (ρ) was measured using the van der Pauw technique with a current of 100 mA and a special high-temperature apparatus.[59] The Hall coefficient was measured in the same apparatus with a forward and reverse magnetic field value of ~8000 G. The carrier density was calculated from the Hall coefficient, assuming a scattering factor of 1 in a single carrier scheme, by $p/n = 1/R_H e$ where p and n are the densities of holes and electrons, respectively, and e is the electron charge. The Hall mobility (μ_H) was calculated from the Hall coefficient and the resistivity values by $\mu_H = R_H/\rho$. The errors were estimated to be ±0.5% and ±2% for the resistivity and Hall coefficient data, respectively. The Seebeck coefficient of each composition in the series was measured using a high temperature light pulse technique[60] and was measured on the same samples used for thermal conductivity, resistivity and Hall coefficient measurements. The error of the Seebeck coefficient measurement was estimated to be less than ±3%.

2.3 Results and Discussions

X-ray diffraction (XRD) patterns obtained from hot-pressed pellets of furnace treated powders indicated high $IrSb_3$ phase purity (Figure 2.1). Quantitative analysis of phase purity was confirmed by scanning electron microscopy (SEM) and electron probe microanalysis (EPMA). Table 2.I summarizes the measured compositions and the room temperature transport properties of the three single-filled samples of each filler used in this study at equivalent filling

fractions, along with an unfilled sample for comparison. Table 2.II summarizes the same information at different filling fractions for Ba single-filled, Ba + Yb double-filled, and Ba + Eu double-filled compositions. The volume percent of $IrSb_2$ phase impurity in each sample was calculated from an SEM image taken at 500x magnification, using a brightness threshold method in ImageJ software to calculate the percent area in the image that was covered by the phase identified by EPMA as $IrSb_2$. The Ir:Sb ratios measured by EPMA in the filled samples are lower than that measured in the unfilled Ir:Sb in all filled samples. Comparing the Ir:Sb ratio in the single-filled samples in Table 2.I, the ratio decreases with increasing filling fraction as measured by EPMA. Figure 2.2 shows SEM images for unfilled and select double-filled compositions. These images show the presence of a secondary phase in the filled samples that is not present in the unfilled sample. Figure 2.3 plots the filling fractions measured by EPMA against the nominal filling fractions for each composition. The EPMA measured filling fractions were obtained by normalizing the measured atomic percentage of each filler atom to the atomic percentage of antimony, assuming exactly 12 antimony atoms per formula unit. The measured filling fractions for Yb and Eu fall well short of the nominal fractions in each of the double-filled compositions. Ba filling fractions in the double-filled and the Ba single-filled samples are at least 90% of the nominal value with the exception of the $x = 0.40$ nominal composition where the Ba filling fraction appears to reach a limit around 0.30.

The measured carrier concentrations at room temperature in all of the single and double-filled compositions ranged from 1.07×10^{20} cm^{-3} to 1.73×10^{20} cm^{-3}. The small differences in room temperature carrier concentrations relative to measured barium, ytterbium, and europium content in these compositions indicate that not all of the expected charge carriers from the fillers in these compositions are activated because if each Ba, Yb, and Eu contributed two electrons

each to the structure, the range of carrier concentrations in these samples would be significantly wider. For the smallest barium single-filling fraction synthesized in this sample set ($x = 0.15$), if all of the barium in the nominal composition were incorporated in the structure and all of the expected charge carriers were activated, barium would contribute about 7.6×10^{20} cm^{-3} electrons to the total. Undoped $IrSb_3$ is naturally a p-type semiconductor with an experimentally measured hole carrier concentration of 1.6×10^{19} cm^{-3} as shown in Table 2.I. As a quick estimate, neglecting any small change in the $IrSb_3$ lattice parameter induced by partial void filling, subtracting the room temperature $IrSb_3$ hole concentration from the contribution of two electrons from each barium gives an approximate expected carrier concentration of 7.4×10^{20} cm^{-3} for the $x = 0.15$ composition. EPMA analysis indicates that 90% of the nominal amount of barium is incorporated in the $IrSb_3$ phase of the sample, but the measured carrier concentration at room temperature is only about 20% of the estimated value. Room temperature carrier concentrations for all of the filled compositions in Tables 2.I and 2.II are well below the expected value and these carrier concentrations are in a relatively narrow range. EPMA measurements showed that the maximum filling fraction for Ba in a single-filled sample was around 0.30. For a Ba filling fraction of 0.30, the predicted carrier concentration is 1.50×10^{21} cm^{-3}, an order of magnitude greater than what is observed at room temperature for this sample series.

Carrier concentrations as a function of temperature are presented in Figure 2.4. As the temperature increases, the measured carrier concentrations reach the estimated levels, but it is likely that the observed increase is the result of minority carrier contributions and not carrier activation from filler atoms. Furthermore, comparing the single-filled $Ba_{0.15}Ir_4Sb_{12}$ composition to double-filled compositions with the equivalent amount of Ba filling, $Ba_{0.15}Yb_{0.15}Ir_4Sb_{12}$ and $Ba_{0.15}Eu_{0.15}Ir_4Sb_{12}$, the expected carrier concentration is greater for the double-filled

compositions. However, the opposite is true in that the carrier concentrations are less for these double-filled compositions and the mobility in these compositions increases over that of the Ba single-filled composition. The differences in mobility values at room temperature are an indication that the different fillers are producing significantly different band structures in these compositions.

Mobility as a function of temperature is presented in Figure 2.5. Unfilled, undoped $IrSb_3$ has a high mobility that is drastically reduced when the structure is filled. The room temperature mobility in this set of filled compositions is greatest in the $Ba_{0.15}Eu_{0.15}Ir_4Sb_{12}$ composition and in general, double-filled compositions appear to have greater mobility.

Electrical resistivity as a function of temperature is presented in Figure 2.6. Resistivity differs with different filler combinations and supports the assumption that even at high temperatures, the filler atoms used in this study are not all equivalent in their electronic contributions to the structure.

The Seebeck coefficients were measured at room temperature and are presented in Table 2.I. While room temperature Seebeck coefficient values decrease in magnitude, as expected with increasing Ba single-filling, double-filling appears to provide an overall increase in room temperature Seebeck coefficients. Seebeck coefficients as a function of temperature are presented in Figure 2.7. The double-filled samples outperform the Ba single-filled samples at equivalent total filling fractions.

Each of the filled compositions measured exhibit room temperature thermal conductivities that are an order of magnitude less than that of the unfilled structure, as shown in Tables 2.I and 2.II. The temperature dependent, total thermal conductivities are presented in

Figure 2.8 and the temperature dependent, lattice thermal conductivities are presented in Figure 2.9. In both the total and lattice thermal conductivities, samples with Yb do not achieve the same reductions in thermal conductivity as do the Ba single-filled and Ba + Eu double filled compositions. The large difference between the total and thermal conductivities of the $Ba_{0.15}Yb_{0.15}Ir_4Sb_{12}$ composition and the $Ba_{0.15}Eu_{0.15}Ir_4Sb_{12}$ composition signals a clear difference in how Yb and Eu participate in the Ir_4Sb_{12} structure.

The thermoelectric figure of merit, ZT, as a function of temperature is depicted in Figure 2.10 for single- and double-filled compositions. The $Ba_{0.15}Eu_{0.15}Ir_4Sb_{12}$ composition reaches a maximum ZT of 1.0 at 750^{o}C (1023 K), a 25% increase over barium single-filled compositions. The overall error in ZT was estimated to be about ±20% as an accumulation of measurement error for each of the factors used to calculate ZT.

2.4 Conclusions

Synthesis of double-filled, n-type $IrSb_3$ skutterudite thermoelectric materials have been demonstrated and characterized by XRD, SEM, EPMA, and thermoelectric properties. The double-filling approach has achieved an overall 25% increase in ZT in n-type $IrSb_3$ when compared to previously reported barium single-filling of the structure. EPMA data indicate that the barium filling limit is greater than that of Yb and Eu, and further investigations of the factors influencing filling and preferential filling in double-filled skutterudites are warranted. To our knowledge, this is the highest ZT reported to date for a filled n-type, $IrSb_3$ skutterudite. Improved understanding of filling characteristics for each potential filler atom are necessary before triple-filling can be exploited, but it appears that the triple-filling approach will soon

warrant exploration. The major factor for improving the ZT of these $IrSb_3$ skutterudite materials is an increase in the magnitude of the Seebeck coefficient, while maintaining electrical resistivity and thermal conductivity near that of the barium single-filled samples. With a ZT of 1.0 in n-type $IrSb_3$, this work demonstrates that skutterudite-based thermoelectric devices could be able to operate even more efficiently and at an even higher temperatures than previously possible.

2.5 Acknowledgements

This research was carried out at the Jet Propulsion Laboratory, California Institute of Technology, under a contract with the National Aeronautics and Space Administration. This work was supported by the NASA Science Mission Directorate's Radioisotope Power Systems Technology Advancement Program, the NSF IGERT: Materials Creation Training Program (MCTP) – DGE-0654431 (DM), and the California NanoSystems Institute. The authors thank Dr. Frank Kyte of the University of California, Los Angeles for SEM and EPMA assistance and helpful discussions. The authors also thank the EPSS department at the University of California, Los Angeles for supporting the SEM and EPMA facility. The authors thank Sabah K. Bux, Kurt Star, James Ma, George Nakatsukasa, and Michael T. Yeung for helpful discussions. Special thanks to George Nakatsukasa, L. Danny Zoltan, and Gregory Gerig for instrumentation support.

2.6 Tables and Figures

Table 2.I. Composition and Room Temperature Transport Properties for $M_{0.25}Ir_4Sb_{12}$ Filled Skutterudites

Nominal Composition	Ir_4Sb_{12}	$Yb_{0.25}Ir_4Sb_{12}$	$Eu_{0.25}Ir_4Sb_{12}$	$Ba_{0.25}Ir_4Sb_{12}$
EPMA Composition	$Ir_{3.84}Sb_{12}$	$Yb_{0.073}Ir_4Sb_{12}$	$Eu_{0.171}Ir_{3.73}Sb_{12}$	$Ba_{0.184}Ir_{3.79}Sb_{12}$
Total Fill Fraction (EPMA)	0.0%	7.3%	17.1%	18.4%
Electrical resistivity (mΩ cm)	0.36	329	2.43	1.00
Hall mobility (cm^2/Vs)	1079	1.35	54.05	35.72
Hall carrier concentration (cm^{-3})	1.62×10^{19}	1.40×10^{19}	4.76×10^{19}	1.75×10^{20}
Seebeck coefficient (μV/K)	27.3	-1.6	-139	-98.2
Thermal conductivity (mW/cm K)	124.3	37.32	20.45	28.91
Lattice thermal conductivity (mW/cm K)	108.8	37.31	18.17	23.45
$IrSb_2$ phase (vol%)	0.0	1.6	0.6	1.1
$IrSb_3$ phase (vol%)	100.0	98.4	99.4	98.9
Ir:Sb ratio in $IrSb_3$ phase (EPMA)	0.331	0.313	0.311	0.315
Sb:Ir ratio in $IrSb_3$ phase (EPMA)	3.02	3.20	3.22	3.17
Sb:(Ir + Filler) ratio in $IrSb_3$ phase (EPMA)	3.02	3.14	3.07	3.02

*Note that all values presented in the table were obtained at room temperature. The unfilled Ir_4Sb_{12} sample is included as a baseline for comparison. The Ba fill fraction is an average of all measured points in the dominant phase of the sample. The electrical resistivity (ρ) was measured using the van der Pauw technique with a current of 100 mA. The Hall mobility and the carrier density were calculated from the Hall coefficient which was measured with a forward and reverse magnetic field value of ~8000 G. $IrSb_2$ phase impurities were measured using SEM images and ImageJ software to calculate the area of the image occupied by this secondary phase. Elemental ratios were obtained by taking averages of the ratios of the measured atomic percentages of each point in the $IrSb_3$ phase.

Table 2.II. Composition and Room Temperature Transport Properties for Single- and Double-Filled Skutterudites – $Ba_xYb_yIr_4Sb_{12}$ and $Ba_xEu_zIr_4Sb_{12}$

Nominal Composition	Ir_4Sb_{12}	$Ba_{0.15}Ir_4Sb_{12}$	$Ba_{0.15}Yb_{0.15}Ir_4Sb_{12}$	$Ba_{0.15}Eu_{0.15}Ir_4Sb_{12}$	$Ba_{0.30}Ir_4Sb_{12}$	$Ba_{0.20}Yb_{0.20}Ir_4Sb_{12}$	$Ba_{0.40}Ir_4Sb_{12}$
EPMA Composition	$Ir_{3.84}Sb_{12}$	$Ba_{0.135}Ir_{3.75}Sb_{12}$	$Ba_{0.149}Yb_{0.074}Ir_{3.69}Sb_{12}$	$Ba_{0.135}Eu_{0.078}Ir_{3.75}Sb_{12}$	$Ba_{0.273}Ir_{3.81}Sb_{12}$	$Ba_{0.188}Yb_{0.047}Ir_{3.71}Sb_{12}$	$Ba_{0.292}Ir_{3.84}Sb_{12}$
Total fill fraction (EPMA)	0.0%	13.5%	22.3%	21.3%	27.3%	23.5%	29.2%
Electrical resistivity (mΩ cm)	0.36	1.72	1.65	1.29	1.17	1.26	1.24
Hall mobility (cm^2/Vs)	1079	24.57	32.11	45.23	30.80	37.92	31.36
Hall carrier concentration (cm^{-3})	1.62×10^{19}	1.48×10^{20}	1.18×10^{20}	1.07×10^{20}	1.73×10^{20}	1.30×10^{20}	1.61×10^{20}
Seebeck coefficient (μV/K)	27.3	-108.5	-114.2	-102.9	-92.5	-100.8	-90.3
Thermal conductivity (mW/cm K)	124.3	31.14	30.43	24.86	24.96	27.44	24.83
Lattice thermal conductivity (mW/cm K)	108.8	27.93	27.08	20.47	20.27	22.80	20.42
$IrSb_2$ phase (vol%)	0.0	2.9	4.5	0.5	2.6	1.2	3.4
$IrSb_3$ phase (vol%)	100.0	97.1	95.5	99.5	97.4	98.8	96.6
Ir:Sb ratio in $IrSb_3$ phase (EPMA)	0.331	0.312	0.307	0.313	0.317	0.309	0.320
Sb:Ir ratio in $IrSb_3$ phase (EPMA)	3.02	3.20	3.25	3.20	3.15	3.23	3.13
Sb:(Ir + Filler) ratio in $IrSb_3$ phase (EPMA)	3.02	3.09	3.07	3.03	2.94	3.04	2.91

*Note that all values presented in the table were obtained at room temperature. The unfilled Ir_4Sb_{12} sample and the barium single-filled samples are included for comparison. The fill fraction values presented for each metal in each composition are an average of all measured points in the dominant phase of the sample. The electrical resistivity (ρ) was measured using the van der Pauw technique with a current of 100 mA. The Hall mobility and the carrier density were calculated from the Hall coefficient which was measured with a forward and reverse magnetic field value of ~8000 G. $IrSb_2$ phase impurities were measured using SEM images and ImageJ software to calculate the area of the image occupied by this secondary phase. Elemental ratios were obtained by taking averages of the ratios of the measured atomic percentages of each point in the $IrSb_3$ phase.

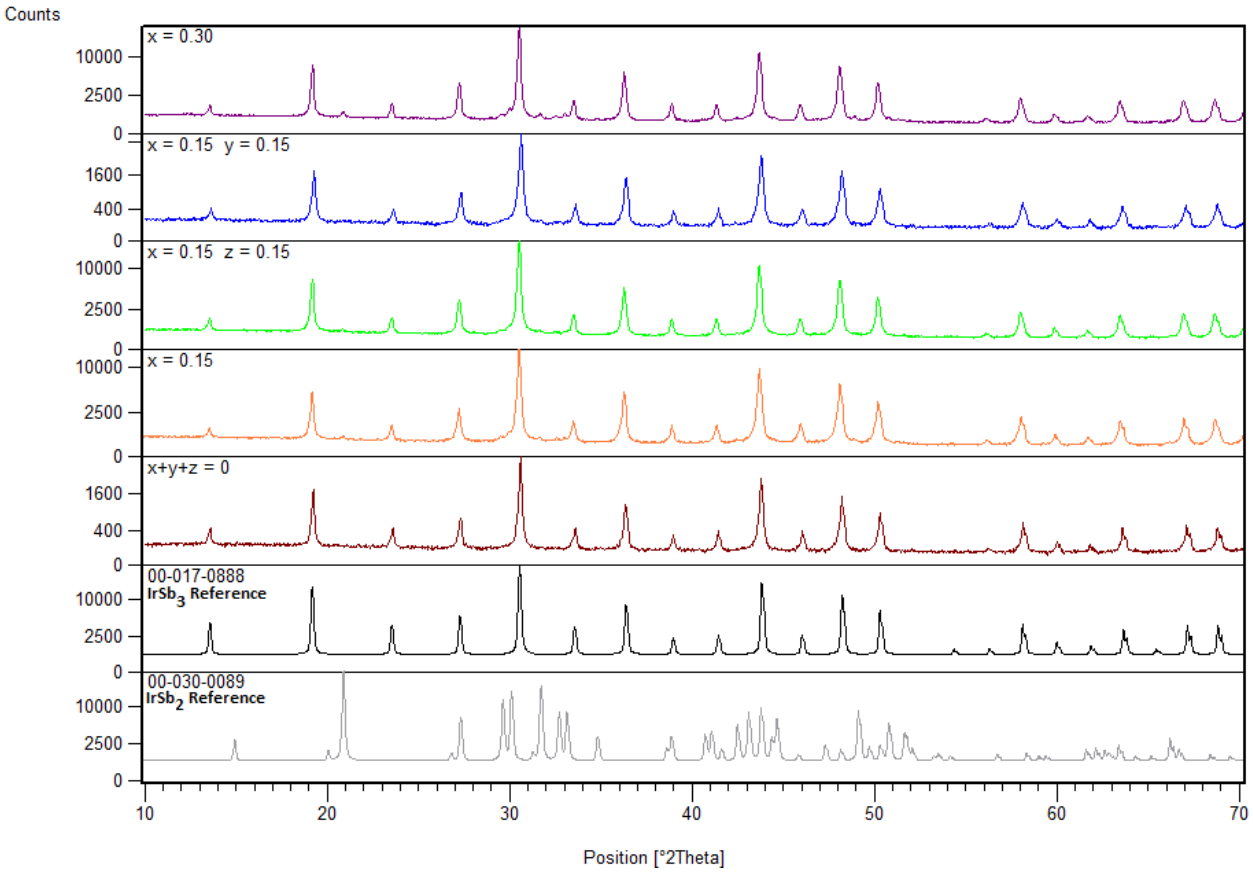

Figure 2.1. X-ray diffraction patterns obtained from hot-pressed samples of selected compositions of $Ba_xYb_yIr_4Sb_{12}$ and $Ba_xEu_zIr_4Sb_{12}$. Simulated diffraction patterns generated from JCPDS reference pattern 00-017-0888 for $IrSb_3$ and JCPDS reference pattern 00-030-0089 for $IrSb_2$ are presented for comparison to the obtained experimental sample patterns.

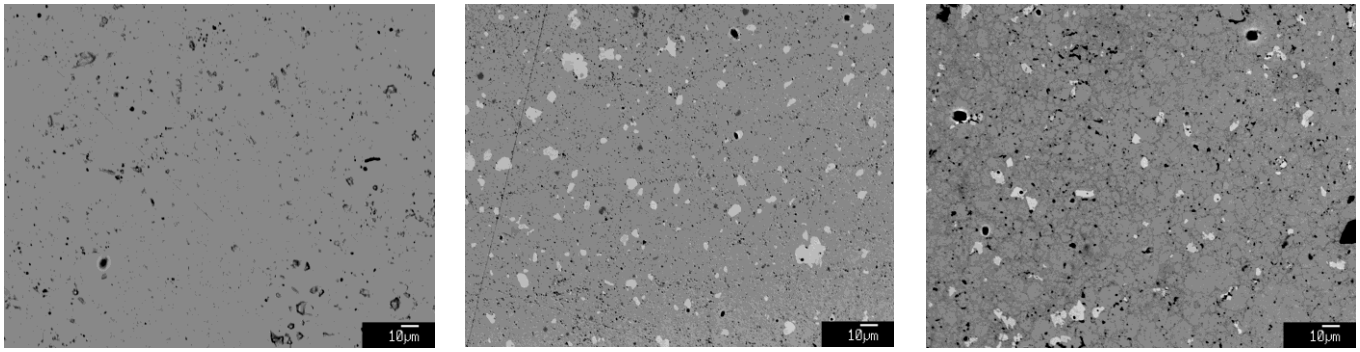

$x, y, z = 0$	$x = 0.15, y = 0.15$	$x = 0.15, z = 0.15$

Figure 2.2. Scanning electron microscope (SEM) images of three representative samples: Ir_4Sb_{12}, $Ba_xYb_yIr_4Sb_{12}$, and $Ba_xEu_zIr_4Sb_{12}$. The unfilled sample was determined to be single phase by EPMA. The addition of Ba, Yb, and Eu lead to the presence of small percentages of a secondary phase, $IrSb_2$.

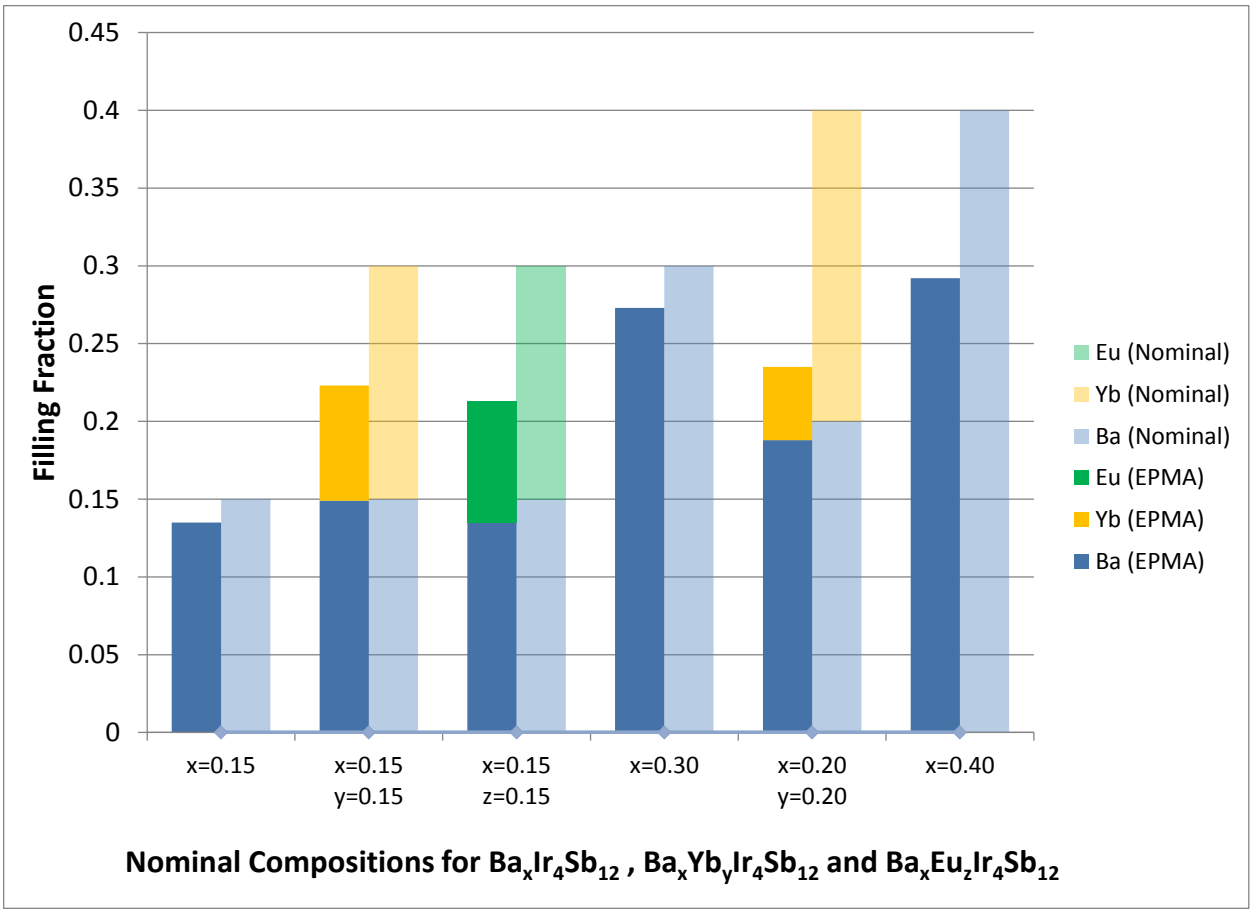

Figure 2.3. Nominal barium fill fraction versus EPMA measured barium fill fraction. Values for EPMA fill fractions are based on atomic percentages measured for barium, normalized by the measured antimony content of the sample.

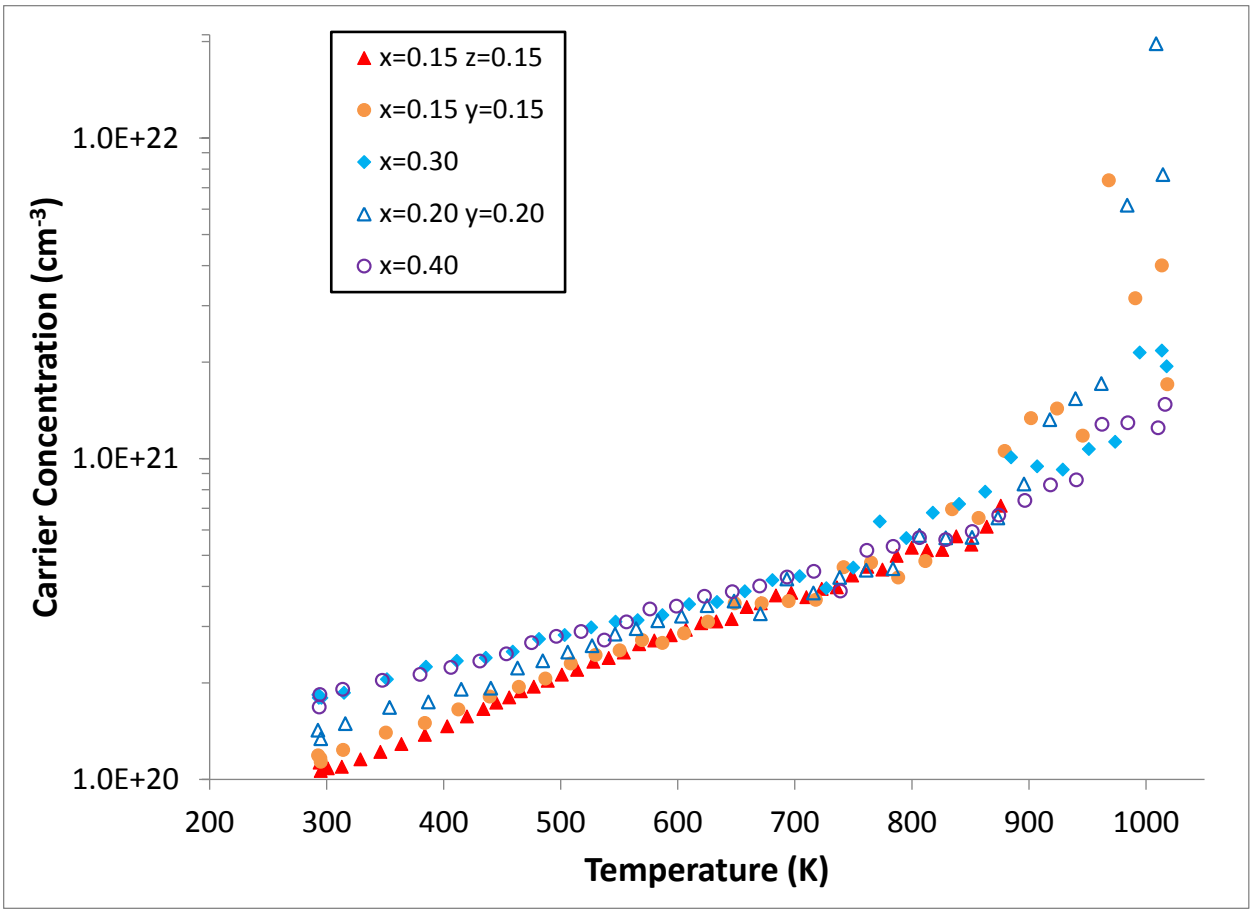

Figure 2.4. Temperature dependence of carrier concentration in $Ba_xYb_yIr_4Sb_{12}$ and $Ba_xEu_zIr_4Sb_{12}$ samples. The Hall coefficient was measured with a forward and reverse magnetic field value of ~8000 G. The carrier concentration was calculated from the Hall coefficient, assuming a scattering factor of 1 in a single carrier scheme, by $p/n = 1/R_He$ where p and n are the densities of holes and electrons, respectively, and e is the electron charge. The measurement error was estimated to be ±2% for the Hall coefficient data.

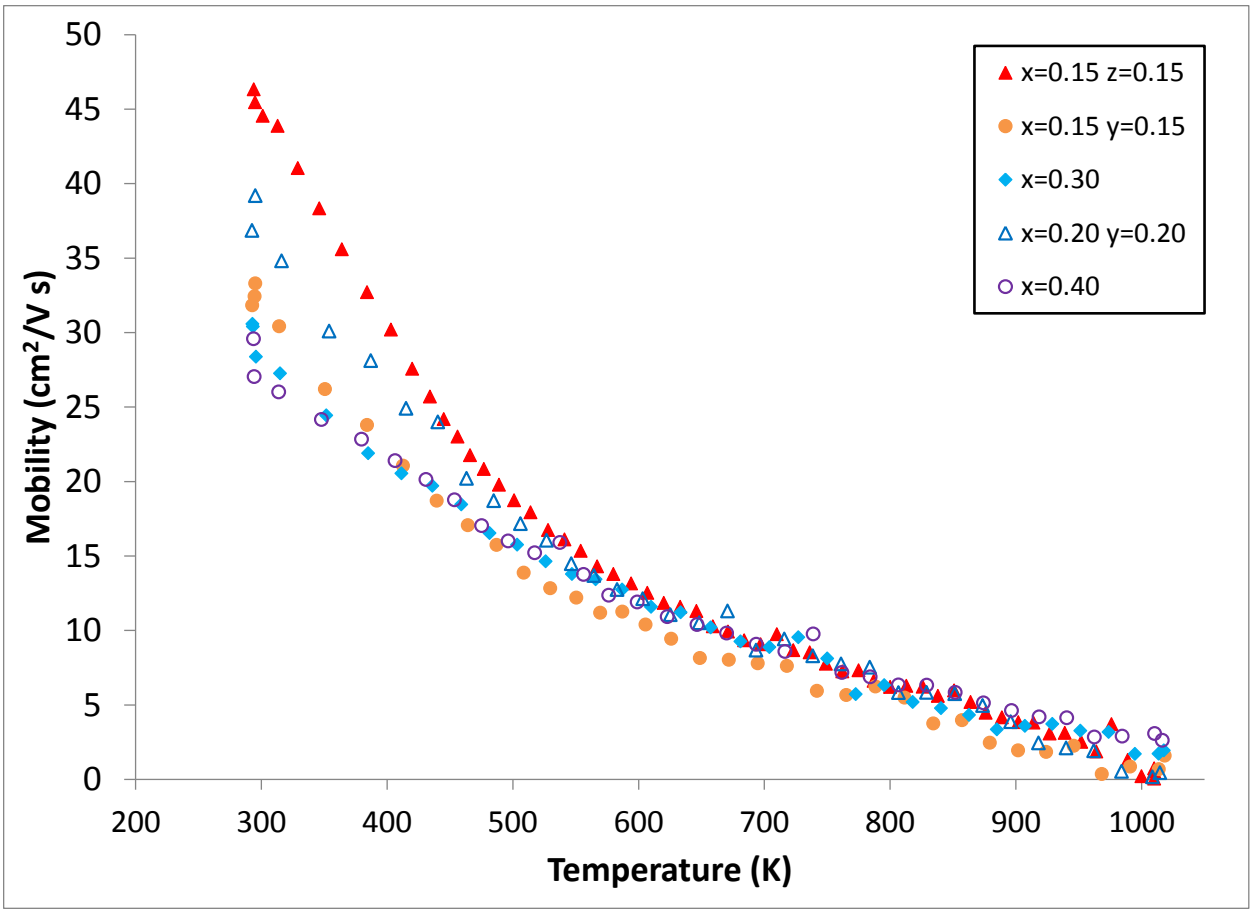

Figure 2.5. Temperature dependence of carrier mobility in $Ba_xYb_yIr_4Sb_{12}$ and $Ba_xEu_zIr_4Sb_{12}$ samples. The Hall coefficient was measured with a forward and reverse magnetic field value of ~8000 G and the Hall mobility was calculated from the Hall coefficient. The measurement error was estimated to be ±2% for the Hall coefficient data.

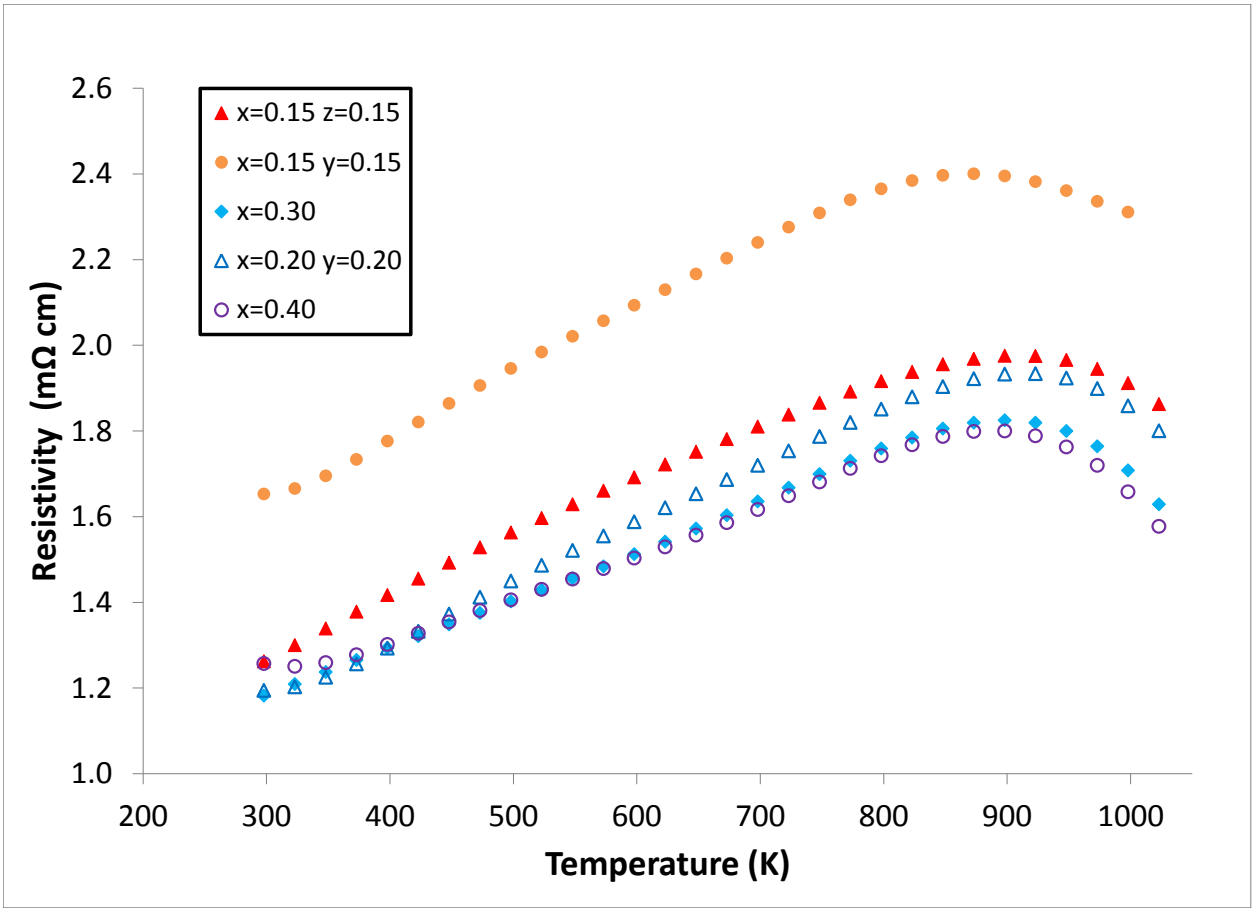

Figure 2.6. Temperature dependence of electrical resistivity in $Ba_xYb_yIr_4Sb_{12}$ and $Ba_xEu_zIr_4Sb_{12}$ samples. The electrical resistivity (ρ) was measured using the van der Pauw technique with a current of 100 mA. The measurement error was estimated to be ±0.5% for the resistivity data.

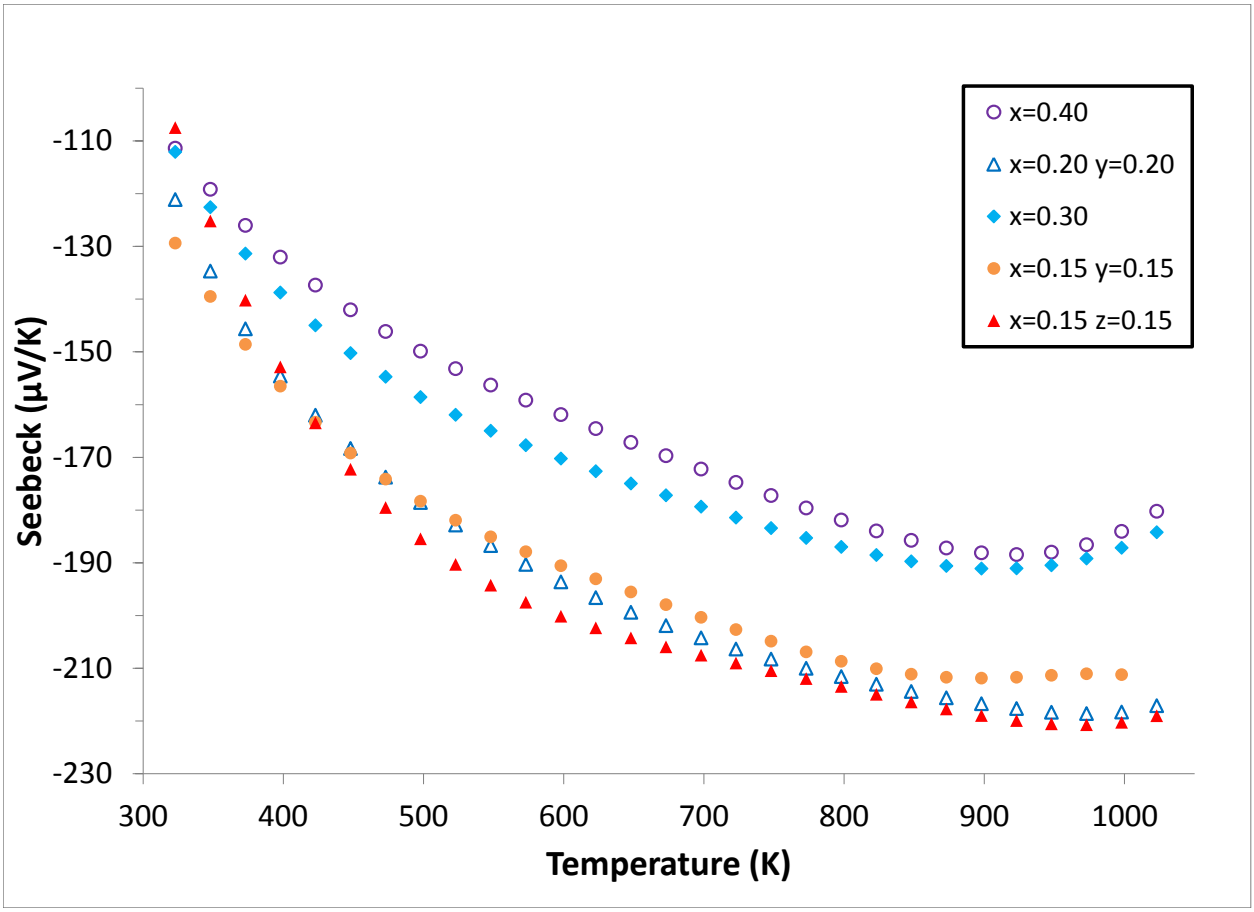

Figure 2.7. Temperature dependence of Seebeck coefficient in $Ba_xYb_yIr_4Sb_{12}$, and $Ba_xEu_zIr_4Sb_{12}$ samples. The Seebeck coefficient was measured using a high temperature light pulse technique.[60] The error of the Seebeck coefficient measurement was estimated to be less than ±3%.

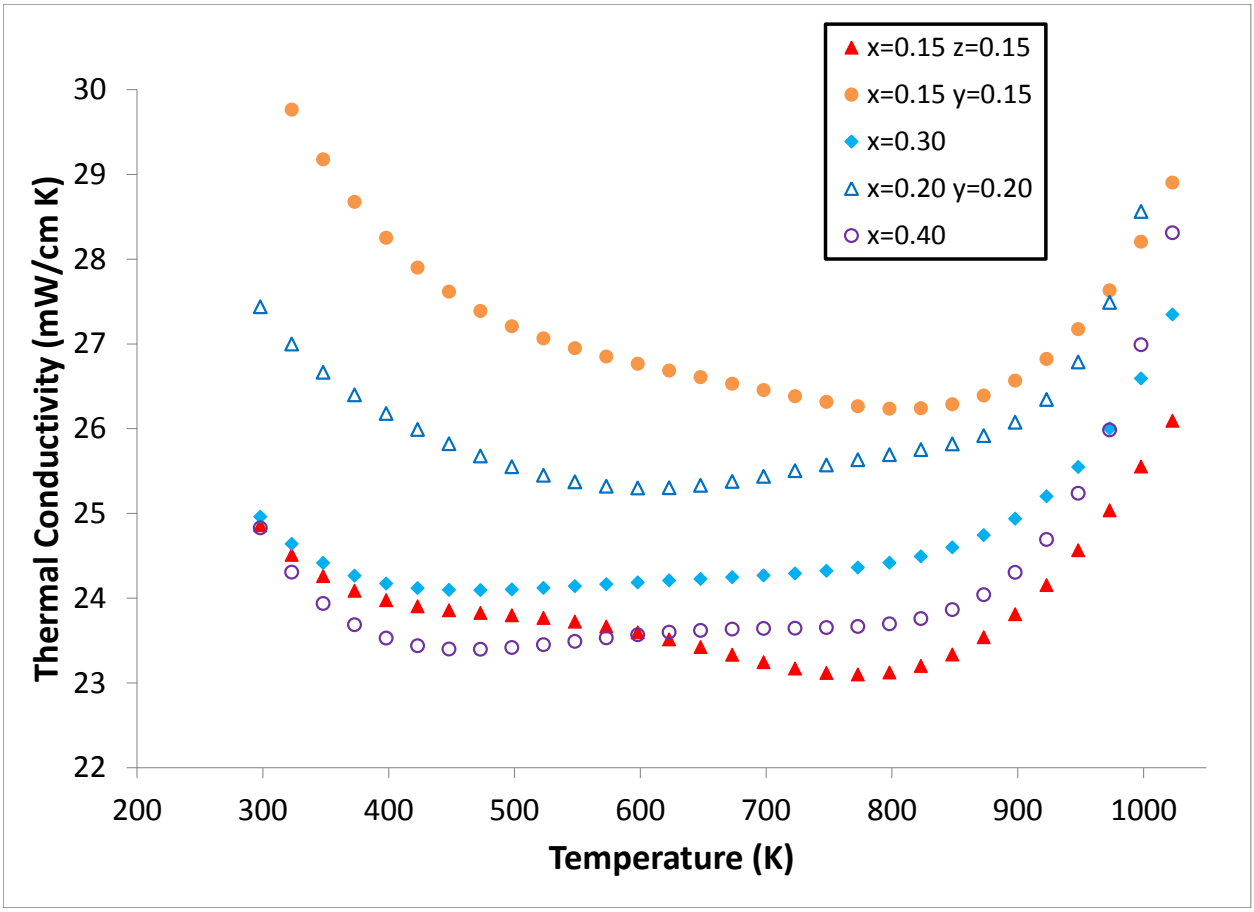

Figure 2.8. Temperature dependence of thermal conductivity (λ) in $Ba_xYb_yIr_4Sb_{12}$ and $Ba_xEu_zIr_4Sb_{12}$ samples. The heat capacity and thermal diffusivity were measured using a flash diffusivity technique[58] and the overall error in the thermal conductivity measurements was estimated to be about ±10%. The thermal conductivity was calculated from the experimental mass, density, heat capacity, and thermal diffusivity values.

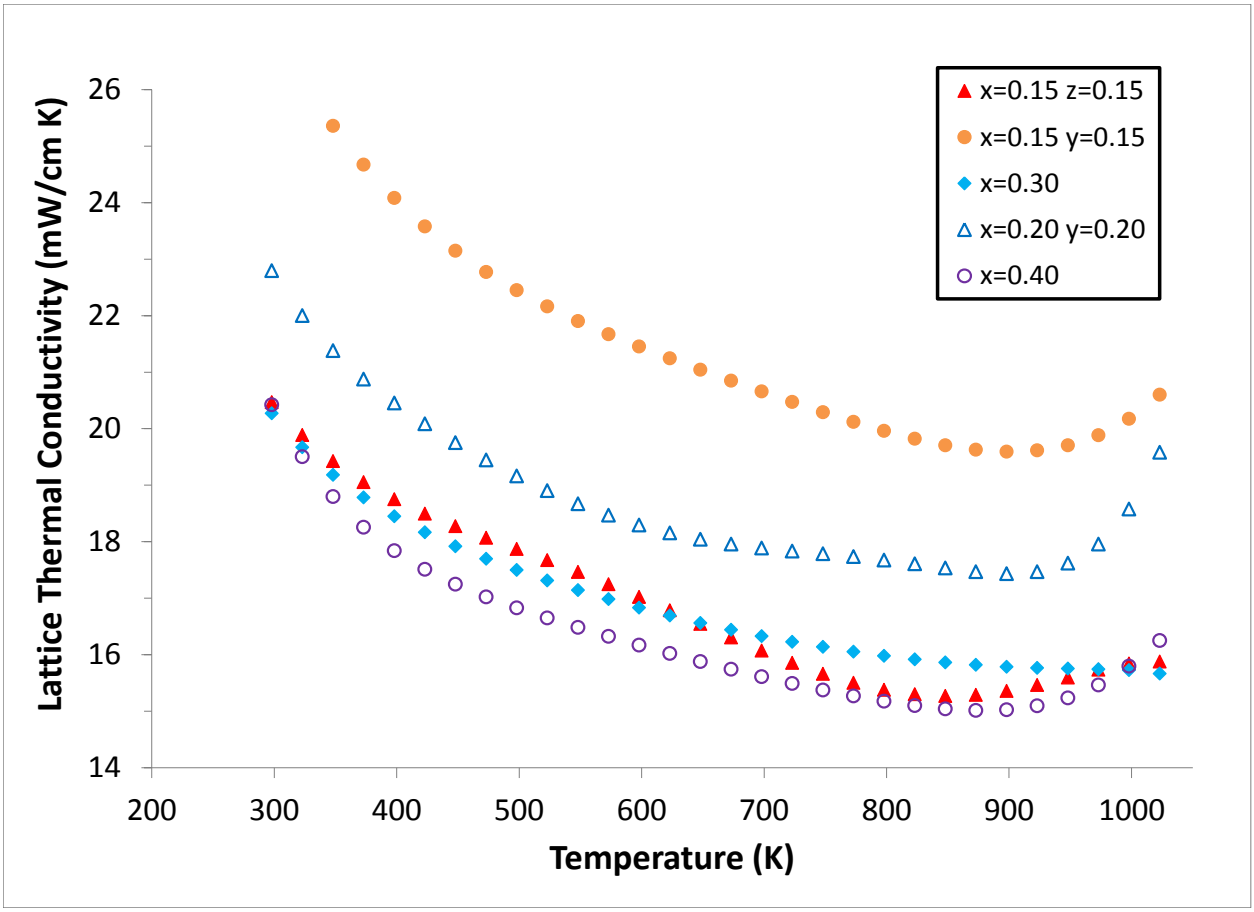

Figure 2.9. Temperature dependence of lattice thermal conductivity ($\lambda_{Lattice}$) in $Ba_xYb_yIr_4Sb_{12}$ and $Ba_xEu_zIr_4Sb_{12}$ samples. The lattice thermal conductivity was obtained by subtracting the electronic thermal conductivity contribution from the total thermal conductivity. The electronic contribution was calculated from the resistivity and Lorenz number. The total thermal conductivity was calculated from the experimental mass, density, heat capacity, and thermal diffusivity values. The overall error in the thermal conductivity measurements was estimated to be about ±10%.

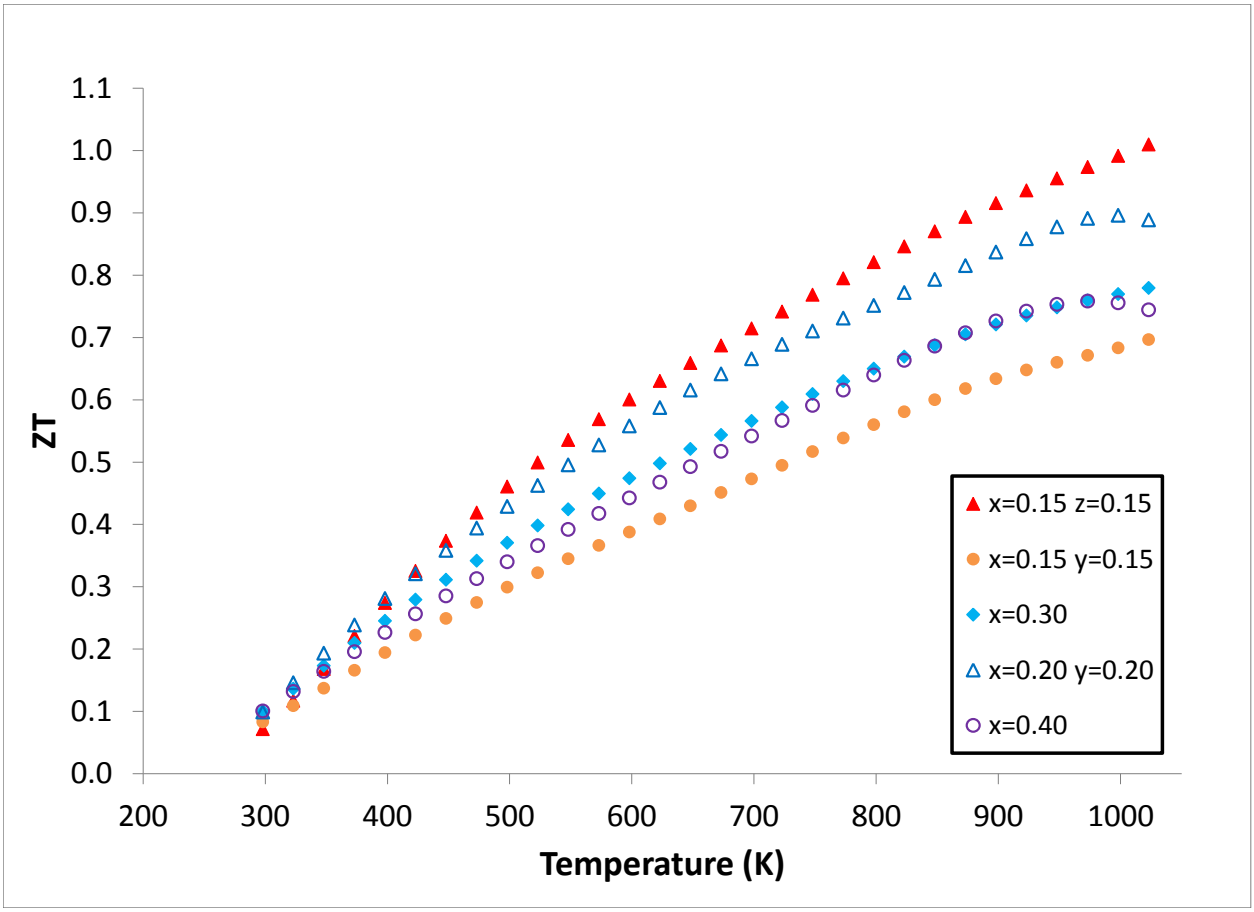

Figure 2.10. Temperature dependence of the thermoelectric figure of merit, ZT in $Ba_xYb_yIr_4Sb_{12}$ and $Ba_xEu_zIr_4Sb_{12}$ samples. Combining the Seebeck coefficient, resistivity, and thermal conductivity measurements, the overall error in ZT was estimated to be about ±20%.

2.7 References

(1) Rowe, D. M. *CRC Handbook of Thermoelectrics*; Rowe, D. M., Ed.; CRC Press, 1995.

(2) Nolas, G. S.; Morelli, D. T.; Tritt, T. M. *Annu. Rev. Mater. Sci.* **1999**, *29*, 89.

(3) Nolas, G.; Cohn, J.; Slack, G. *Phys. Rev. B* **1998**, *58*, 164.

(4) Chakoumakos, B. C.; Sales, B. C. *J. Alloys Compd.* **2006**, *407*, 87.

(5) Sales, B. C.; Mandrus, D.; Williams, R. K. *Science (80-.).* **1996**, *272*, 1325.

(6) Caillat, T. *J. Appl. Phys.* **1996**, *80*, 4442.

(7) Fleurial, J.-P.; Caillat, T.; Borshchevsky, A. *Proc. 16th Int. Conf. Thermoelectr.* **1997**, 1.

(8) Sales, B.; Mandrus, D.; Chakoumakos, B.; Keppens, V.; Thompson, J. *Phys. Rev. B* **1997**, *56*, 15081.

(9) Chakoumakos, B. C.; Sales, B. C.; Mandrus, D.; Keppens, V. *Acta Crystallogr. Sect. B Struct. Sci.* **1999**, *55*, 341.

(10) Meisner, G.; Morelli, D.; Hu, S.; Yang, J.; Uher, C. *Phys. Rev. Lett.* **1998**, *80*, 3551.

(11) Puyet, M.; Lenoir, B.; Dauscher, a.; Pécheur, P.; Bellouard, C.; Tobola, J.; Hejtmanek, J. *Phys. Rev. B* **2006**, *73*, 035126.

(12) Zhao, X. Y.; Shi, X.; Chen, L. D.; Zhang, W. Q.; Zhang, W. B.; Pei, Y. Z. *J. Appl. Phys.* **2006**, *99*, 053711.

(13) Eilertsen, J.; Berthelot, R.; Sleight, A. W.; Subramanian, M. a. *J. Solid State Chem.* **2012**, *190*, 238.

(14) He, T.; Chen, J.; Rosenfeld, H. D.; Subramanian, M. a. *ChemInform* **2006**, *37*, 759.

(15) Chen, L.; Tang, X.; Goto, T.; Hirai, T. *J. Mater. Res.* **2000**, *15*, 2276.

(16) Chen, L. D.; Kawahara, T.; Tang, X. F.; Goto, T.; Hirai, T.; Dyck, J. S.; Chen, W.; Uher, C. *J. Appl. Phys.* **2001**, *90*, 1864.

(17) Zhao, W.; Wei, P.; Zhang, Q.; Dong, C.; Liu, L.; Tang, X. *J. Am. Chem. Soc.* **2009**, *131*, 3713.

(18) Song, X.; Yang, J.; Peng, J.; Chen, Y.; Zhu, W.; Zhang, T. *J. Alloys Compd.* **2005**, *399*, 276.

(19) Kim, S. W.; Kimura, Y.; Mishima, Y. *J. Electron. Mater.* **2004**, *33*, 1.

(20) Fleurial, J.-P.; Borshchevsky, A.; Caillat, T.; Morelli, D. T.; Meisner, G. P. In *15th International Conference on Thermoelectrics*; 1996; Vol. 3, pp. 91–95.

(21) Chen, B.; Xu, J.; Uher, C.; Morelli, D. T.; Meisner, G. P.; Fleurial, J.-P.; Caillat, T.; Borshchevsky, A. *Phys. Rev. B* **1997**, *55*, 1476.

(22) Morelli, D.; Meisner, G.; Chen, B.; Hu, S.; Uher, C. *Phys. Rev. B* **1997**, *56*, 7376.

(23) Xue, Y.; Liu, K.; Li, J.; Chen, N. *Mater. Res. Bull.* **2005**, *40*, 1172.

(24) Kuznetsov, V. L.; Kuznetsova, L. A.; Rowe, D. M. *J. Phys. Condens. Matter* **2003**, *15*, 5033.

(25) Jiang, Y.; Jia, X.; Deng, L.; Ma, H. *J. Rare Earths* **2012**, *30*, 388.

(26) Pei, Y. Z.; Bai, S. Q.; Zhao, X. Y.; Zhang, W.; Chen, L. D. *Solid State Sci.* **2008**, *10*, 1422.

(27) Dilley, N. R.; Bauer, E. D.; Maple, M. B.; Sales, B. C. *J. Appl. Phys.* **2000**, *88*.

(28) Bauer, E.; Galatanu, A.; Michor, H.; Hilscher, G.; Rogl, P.; Boulet, P.; No, H. *Eur. Phys. J. B* **2000**, *14*, 483.

(29) Anno, H.; Nolas, G. S.; Akai, K.; Ashida, K.; Matsuura, M.; Matsubara, K. In *Proceedings of the 20th International Conference on Thermoelectrics*; 2001; Vol. 3, pp. 61–64.

(30) Liu, H.; Zhao, X.; Zhu, T.; GU, Y. *J. Rare Earths* **2012**, *30*, 456.

(31) Yang, J.; Hao, Q.; Wang, H.; Lan, Y.; He, Q.; Minnich, a.; Wang, D.; Harriman, J.; Varki, V.; Dresselhaus, M.; Chen, G.; Ren, Z. *Phys. Rev. B* **2009**, *80*, 115329.

(32) Sales, B.; Chakoumakos, B.; Mandrus, D. *Phys. Rev. B* **2000**, *61*, 2475.

(33) King, D. J.; Caillat, T.; Kaner, R. B.; Fleurial, J.-P. Effects of barium filling in IrSb3-based n-type skutterudite: High temperature thermoelectric properties of BayIr4Sb12, 2014.

(34) Bai, S. Q.; Huang, X. Y.; Chen, L. D.; Zhang, W.; Zhao, X. Y.; Zhou, Y. F. *Appl. Phys. A* **2010**, *100*, 1109.

(35) Xu, W.; Peng, J.; He, J.; Zhou, M.; Yang, J.; Fu, L. *J. Wuhan Univ. Technol. Sci. Ed.* **2013**, *28*, 677.

(36) Ballikaya, S.; Uher, C. *J. Alloys Compd.* **2014**, *585*, 168.

(37) Li, D.; Yang, K.; Hng, H. H.; Yan, Q. Y.; Ma, J.; Zhu, T. J.; Zhao, X. B. *J. Phys. D. Appl. Phys.* **2009**, *42*, 105408.

(38) Bai, S. Q.; Pei, Y. Z.; Chen, L. D.; Zhang, W. Q.; Zhao, X. Y.; Yang, J. *Acta Mater.* **2009**, *57*, 3135.

(39) Yang, J.; Zhang, W.; Bai, S. Q.; Mei, Z.; Chen, L. D. *Appl. Phys. Lett.* **2007**, *90*, 192111.

(40) Yang, K.; Cheng, H.; Hng, H. H.; Ma, J.; Mi, J. L.; Zhao, X. B.; Zhu, T. J.; Zhang, Y. B. *J. Alloys Compd.* **2009**, *467*, 528.

(41) Alleno, E.; Bérardan, D.; Godart, C.; Puyet, M.; Lenoir, B.; Lackner, R.; Bauer, E.; Girard, L.; Ravot, D. *Phys. B Condens. Matter* **2006**, *383*, 103.

(42) Peng, J.; He, J.; Alboni, P. N.; Tritt, T. M. *J. Electron. Mater.* **2009**, *38*, 981.

(43) Tang, G. D.; Wang, Z. H.; Xu, X. N.; He, Y.; Qiu, L.; Du, Y. W. *J. Electron. Mater.* **2011**, *40*, 611.

(44) Shi, X.; Kong, H.; Li, C.-P.; Uher, C.; Yang, J.; Salvador, J. R.; Wang, H.; Chen, L.; Zhang, W. *Appl. Phys. Lett.* **2008**, *92*, 182101.

(45) Ballikaya, S.; Wang, G.; Sun, K.; Uher, C. *J. Electron. Mater.* **2010**, *40*, 570.

(46) Ballikaya, S.; Uzar, N.; Yildirim, S.; Salvador, J. R.; Uher, C. *J. Solid State Chem.* **2012**, *193*, 31.

(47) Shi, X.; Yang, J.; Salvador, J. R.; Chi, M.; Cho, J. Y.; Wang, H.; Bai, S.; Yang, J.; Zhang, W.; Chen, L. *J. Am. Chem. Soc.* **2011**, *133*, 7837.

(48) Zhang, L.; Grytsiv, a; Rogl, P.; Bauer, E.; Zehetbauer, M. *J. Phys. D. Appl. Phys.* **2009**, *42*, 225405.

(49) Rogl, G.; Grytsiv, a; Melnychenko-Koblyuk, N.; Bauer, E.; Laumann, S.; Rogl, P. *J. Phys. Condens. Matter* **2011**, *23*, 275601.

(50) Graff, J.; Zhu, S.; Holgate, T.; Peng, J.; He, J.; Tritt, T. M. *J. Electron. Mater.* **2011**, *40*, 696.

(51) Zhou, A.; Liu, L.; Zhai, P.; Zhao, W.; Zhang, Q. *J. Appl. Phys.* **2011**, *109*, 113723.

(52) Harnwunggmoung, A.; Kurosaki, K.; Kosuga, A.; Ishimaru, M.; Plirdpring, T.; Yimnirun, R.; Jutimoosik, J.; Rujirawat, S.; Ohishi, Y.; Muta, H.; Yamanaka, S. *J. Appl. Phys.* **2012**, *112*, 043509.

(53) Berardan, D.; Godart, C.; Alleno, E.; Bauer, E. *J. Alloys Compd.* **2003**, *351*, 18.

(54) Bérardan, D.; Alleno, E.; Godart, C.; Puyet, M.; Lenoir, B.; Lackner, R.; Bauer, E.; Girard, L.; Ravot, D. *J. Appl. Phys.* **2005**, *98*, 033710.

(55) Yang, J.; Chen, Y.; Zhu, W.; Peng, J.; Bao, S.; Fan, X.; Duan, X. *J. Solid State Chem.* **2006**, *179*, 212.

(56) Peng, J.; Yang, J.; Zhang, T.; Song, X.; Chen, Y. *J. Alloys Compd.* **2004**, *381*, 313.

(57) Yang, J.; Chen, Y.; Peng, J.; Song, X.; Zhu, W.; Su, J.; Chen, R. *J. Alloys Compd.* **2004**, *375*, 229.

(58) Vandersande, J. W.; Wood, C.; Zoltan, A.; Whittenberger, D. *Therm. Conduct.* **1988**, *19*, 445.

(59) Mccormack, J. A.; Fleurial, J.-P. *MRS Proc.* **1991**, *234*, 135.

(60) Wood, C.; Zoltan, D.; Stapfer, G. *Rev. Sci. Instrum.* **1985**, *56*, 719.

Chapter 3: Thermal conductivity reduction in nano-structured $CoSb_3$-based skutterudites: the effects of high energy ball milling on high temperature transport properties in filled and unfilled skutterudite materials

3.1 Introduction

The long lives of deep space probes and orbiters like Voyager 1, Voyager 2, Cassini, and others, have proven that thermoelectric generators are very reliable for power generation. There is a strong desire to realize the potential of thermoelectric materials for terrestrial waste heat recovery, particularly for automobiles.[1–4] The operating temperature of an internal combustion engine is well suited to materials with the skutterudite structure, as they have been identified as suitable materials for mid-temperature applications because of high ZT values in this temperature range.[1,2,5]

The skutterudite structure is composed of a cubic lattice with the space group *Im3*. Materials with the skutterudite structure are of particular interest for use as thermoelectric materials. The thermoelectric figure of merit (ZT) is defined by the following equation:

$$ZT = \frac{S^2}{\rho\lambda}T$$

where S is the Seebeck coefficient, ρ is the electrical conductivity, and λ is the total thermal conductivity of the sample. The figure of merit is dimensionless and has a direct relationship to efficiency.[6]

The search for bulk materials with high ZT has focused on novel complex structure compounds and phases that combine the electrical transport properties of heavily doped semiconductors with the low thermal conductivity of glassy materials. For many years, work

centered around optimization of electrical properties until calculations and experiments showed that synthesizing low dimensional materials was an effective method for significantly reducing the thermal conductivity of a thermoelectric material.[7–11] In spite of fairly large lattice thermal conductivity values,[12] unfilled skutterudite compounds have attractive thermoelectric properties in the 550 K to 950 K temperature range.[5] Filling the skutterudite structure has proven to be an effective method for reducing thermal conductivity values,[13–17] but this approach does not involve the synthesis of low dimensional materials. Minor improvements in ZT have been obtained by introducing point defect scattering through the formation of skutterudite solid solutions, but a new approach that relies on the synthesis of bulk materials with "built-in nano grains" could result in orders of magnitude increases in the density of interfaces, thus more effectively scattering phonons and leading to significant reductions in lattice thermal conductivity values. Synthesis of low dimensional, "nanostructured" skutterudites has been approached via heated aqueous solution processing ("hydro/solvo" or "solvo/thermal" methods),[18–25] while others have used mechanical alloying or ball milling techniques to produce nanostructured skutterudites.[26–29] Thermoelectric materials with higher melting points and less complex structures like silicon can be ball milled under inert atmosphere for long periods of time with little concern for phase degredation[11,30]; however, in the case of $CoSb_3$ skutterudite, extended milling of its complex structure results in the formation of $CoSb_2$.[31]

The work presented here involves high-energy ball milling of bulk polycrystalline $CoSb_3$ as a proof-of-principle for reducing the total thermal conductivity of skutterudite by nanostructuring. Bulk preparations of $Co_{0.955}Pd_{0.045}Sb_{2.955}Te_{0.045}$ and $Ba_{0.05}Yb_{0.15}Co_4Sb_{12}$ skutterudites were also ball milled to determine the cumulative effects of nanostructuring both for unfilled and filled n-type skutterudites. Additionally, a bulk preparation of

$Ce_{0.9}Fe_{3.5}Co_{0.5}Sb_{12}$ was ball milled to determine the cumulative effects of nanostructuring a filled p-type skutterudite. The high temperature thermoelectric properties of the ball milled powders from each of these compositions are described.

3.2 Experimental

Unfilled, undoped $CoSb_3$ skutterudite bulk polycrystalline powder was prepared by sealing stoichiometric amounts of elemental cobalt powder (99.999%, Alfa Aesar) and antimony shot (99.999%, Alfa Aesar) in a glassy carbon crucible in an evacuated quartz tube, and heating that tube in a furnace at 1200 ^{o}C for 10 hours, then immediately removing the tube from the furnace and placing it in a bucket of water at room temperature to quench the reaction. Unfilled, n-type $Co_{0.955}Pd_{0.045}Sb_{2.955}Te_{0.045}$ was prepared in the same 1200 ^{o}C, water quench fashion, except that stoichiometric amounts of palladium powder (99.95%, Alfa Aesar) and tellurium powder (99.99%, Alfa Aesar) were included. Ingots recovered from the quartz tubes after the water quench were subjected to a brief grinding in order to produce powder aliquots from the ingot.

Barium and ytterbium filled n-type skutterudite compositions were prepared by planetary ball milling of elemental cobalt powder (99.999%, Alfa Aesar), antimony shot (99.999%, Alfa Aesar), barium rod (99+%, Alfa Aesar), and ytterbium chunk (99.9%, Alfa Aesar) in stoichiometric amounts to produce $Ba_{0.05}Yb_{0.15}Co_4Sb_{12}$. Cerium filled p-type skutterudite was prepared by high energy planetary ball milling of elemental cerium rod (99.9%, Alfa Aesar), iron powder (99.9%, Alfa Aesar), cobalt powder (99.999%, Alfa Aesar), and antimony shot (99.999%, Alfa Aesar) in stoichiometric amounts to produce $Ce_{0.9}Fe_{3.5}Co_{0.5}Sb_{12}$. The resulting powders from the planetary ball milling processes were then sealed in separate evacuated quartz

tubes and heated to 750 ^{o}C in a furnace for 48 hours. After furnace treatment, the resulting materials were briefly subjected to grinding to produce powders to facilitate division into smaller samples for further processing. A small amount of each of the furnace treated, filled skutterudite compositions were removed for analysis by powder X-ray diffraction (XRD).

The powders obtained from the bulk syntheses described above were then sampled for further processing in high energy ball mills (Spex Sample Prep). Different total milling times were used to produce samples with variations of average crystallite sizes. Small portions of the products of this high energy ball milling step were removed for analysis by XRD for phase purity and average crystallite size calculations. Ball milled powder samples were also characterized by scanning electron microscopy (SEM), and transmission electron microscopy (TEM).

The ball milled powders were then hot-pressed under dynamic vacuum at 620 ^{o}C in graphite dies, producing cylindrical samples that were geometrically measured to be greater than 98% of their theoretical densities. These hot-pressed samples were then analyzed by XRD for phase purity and average crystallite size calculations. Average crystallite sizes were calculated using the method of integral breadths.[32] Room temperature Seebeck coefficient, Hall effect, and electrical resistivity measurements were made for all samples. The high temperature thermal diffusivity, Hall effect, and Seebeck coefficient were measured on samples between room temperature and approximately 600 ^{o}C (873 K). The heat capacity and thermal diffusivity were determined using a flash diffusivity technique[33] and the overall error in the thermal conductivity measurements was estimated to be ±10%. Thermal conductivity was calculated from the experimental mass, density, heat capacity, and thermal diffusivity values. The electrical resistivity (ρ) was measured using the van der Pauw technique with a current of 100 mA and a special high-temperature apparatus.[34] The Hall coefficient was measured in the same apparatus

with a forward and reverse magnetic field value of ~8500 G. The carrier density was calculated from the Hall coefficient, assuming a scattering factor of 1 in a single carrier scheme, by $p/n = 1/R_H e$ where p and n are the densities of holes and electrons, respectively, and e is the electron charge. The Hall mobility (μ_H) was calculated from the Hall coefficient and the resistivity values by $\mu_H = R_H / \rho$. The errors were estimated to be ±0.5% and ±2% for the resistivity and Hall coefficient data, respectively. The Seebeck coefficient was measured by applying a high temperature light pulse technique[35] to the same samples used for thermal conductivity, resistivity and Hall coefficient measurements. The error in the Seebeck coefficient measurement was estimated to be less than ±3%.

3.3 Results and Discussions

3.3.1 Ball Milling

High energy ball milling is intended to rapidly grind a sample such that the average crystallite size of the sample decreases. X-ray diffraction patterns obtained from ball milled powders and hot-pressed pellets allow for comparison of diffraction pattern peak widths and calculation of the average crystallite size in each powder and pressed sample, using the method of integral breadths.[32] Calculated average crystallite sizes along with room temperature thermoelectric properties for a representative set of skutterudite samples is presented in Table 3.I. The trends in Table 3.I agree with several assumptions made for the nanostructuring process, based on the introduction of several orders of magnitude more interfaces in a nanostructured sample versus a bulk sample. Table 3.I shows trends of reduced average crystallite size as a function of milling time, increased electrical resistivity as a result of decreased mobility with smaller crystallites, relatively unchanged carrier concentrations across

all samples, an increase in Seebeck coefficient as a function of milling time, and most importantly, a decrease in the total and lattice thermal conductivities. The ultimate goal of nanostructuring thermoelectric materials is to drastically reduce the thermal conductivity of a material without the negative effects on the electrical properties of that sample outweighing the gains in the thermal properties.

Powder XRD patterns in Figure 3.1 illustrate the increases in diffraction peak widths as a function of milling time. The two most prominent peaks in the pattern are enlarged alongside the full patterns, showing more closely how the peaks broaden as milling time increases. XRD patterns obtained from hot-pressed pellets of the ball milled samples are shown in Figure 3.2, and it is clear from this figure that there is less size variation as a function of milling time observed in the pressed pellets. This is a strong indication that the hot-pressing process causes significant grain growth in the densified samples. Comparisons of calculations of average crystallite sizes before and after hot-pressing the ball milled samples confirms significant grain growth. The $Co_{0.955}Pd_{0.045}Sb_{2.955}Te_{0.045}$ milled sample series is depicted in Figure 3.1 and Figure 3.2, but grain growth during hot-pressing was observed for all four sample sets presented in this work. Efforts to reduce the pressing temperature, pressure, and time resulted in lower density values and poor sintering. Figure 3.3 plots ball milling time versus the calculated average crystallite size in a sample. The limit of ball milling skutterudites to reduce average crystallite size appears to be between 20 and 25 nm, as increases in milling time reach a plateau of crystallite size on the graph.

SEM and TEM images were taken to gain a better understanding of particle size distributions in the ball milled powder samples. $Co_{0.955}Pd_{0.045}Sb_{2.955}Te_{0.045}$ powder milled for 60 minutes is presented as a representative qualitative example of milled powder particle

distributions. SEM images in Figure 3.4 show that particle sizes are quite large, up to several microns, but closer inspection shows that these large particles are agglomerates of smaller crystallites that appear to be as small as tens of nanometers at the higher SEM magnifications. The lower size limit of the distribution of crystallites in milled samples is better depicted in TEM images in Figure 3.5. Lattice fringes that can be seen in the higher magnifications of the TEM images show crystalline domains that are as small as a few nanometers.

The effects of ball milling were apparent in SEM images of hot-pressed samples of bulk and ball milled powders. Figure 3.6 shows SEM images obtained from a bulk sample and two ball milled samples, milled for significantly different amounts of time. In these images, the grain structure in the sample clearly decreases in size as the milling time increases. This set of images also illustrates the decreasing sample integrity with increased milling time, as the milled samples show secondary phases that are not present in the bulk sample, likely phase degradation as a result of milling, as well as rougher surfaces that are the result of poor sintering leading to pull-out during polishing for SEM sample preparation.

3.3.2 $CoSb_3$: Proof-of-Principle

Undoped, unfilled $CoSb_3$ skutterudite provides a proof-of-principle for the reduction of thermal conductivity through nanostructuring of skutterudites, with less contribution to the total thermal conductivity from electron-phonon scattering than in heavily doped skutterudites. Unfilled skutterudite also discounts any reductions in the thermal conductivity that may be achieved through the rattling of filler atoms.[13–17] As expected, ball milled $CoSb_3$ samples show significant reductions in total and lattice thermal conductivities. Thermal conductivities as a function of temperature are presented in Figures 3.7 and 3.8 for a series of $CoSb_3$ samples that were ball milled for varying amounts of time.

Figure 3.9 shows the temperature dependent carrier concentration for $CoSb_3$ bulk and ball milled samples. The large variation in carrier concentrations for these samples was unexpected and is an indication that ball milling could significantly alter electrical properties as well as thermal properties. $CoSb_3$ is a p-type semiconductor and if the 60 and 120 minute milled samples have higher carrier concentrations, then the process must be introducing carriers into the material by contamination or by the introduction of additional defects to the structure. Bulk $CoSb_3$ has a high carrier mobility at room temperature, as seen in Figure 3.10. The drastic differences between milled and bulk samples of $CoSb_3$ indicates that the ball milling process reaches a point at which the structure deteriorates such that the electrical properties begin to change significantly. The increases in resistivity at room temperature for the samples with longer milling times supports this assumption, but Figure 3.11 shows that at high temperature, the resistivity values converge for the bulk and milled samples. This convergence is either the result of significant grain growth at high temperature within the sample, or more likely due to the coincidence that the once high mobility value in the bulk sample is approaching a very low mobility value at high temperature where it meets those of the milled samples. The Seebeck coefficients as a function of temperature follow a trend at room temperature whereby the samples milled for a longer time have a greater Seebeck coefficient. This follows the expectation after observing an increase in room temperature resistivity values, but once again, the values are fairly close to one another for all $CoSb_3$ samples at high temperature, as seen in Figure 3.12.

Although there is a clear reduction in the lattice and total thermal conductivities from bulk to ball milled samples, the sum of the effects of ball milling $CoSb_3$ does not result in an increase in ZT for milled samples over bulk preparations. The ZT as a function of temperature for bulk and milled $CoSb_3$ samples is depicted in Figure 3.13. Although there is no increase, it is worth

noting that ball milling only led to a decrease in ZT for one of the milled samples in this series, so other formulations of skutterudite with more robust electrical properties may benefit from ball milling to reduce thermal conductivity.

3.3.3 Unfilled, n-type Skutterudite

Unfilled, heavily doped $Co_{0.955}Pd_{0.045}Sb_{2.955}Te_{0.045}$ skutterudite is a logical material to next apply a ball milling approach to reducing thermal conductivity. Electron-phonon scattering is more of a factor for this heavily doped composition, but if carrier concentrations and mobilities remain largely unchanged from ball milling, then electron-phonon scattering in all of the samples should be equivalent. Figure 3.14 shows that the carrier concentrations for bulk and milled samples vary only a small amount at room temperature and remain close to one another at higher temperatures. Room temperature carrier mobility does decrease with increasing milling time, but as with the undoped $CoSb_3$, the values converge somewhat at high temperature as the mobilities approach zero. Overall, comparing the mobility as a function of temperature in Figure 3.15, for the bulk sample versus the milled samples, the mobility of the bulk sample reaches zero at a slightly lower temperature and begins to rise again, before any of the milled samples, resulting in the bulk sample beginning and ending with higher mobility across this temperature range. This observation follows the assumption that the introduction of orders of magnitude greater interfaces within the sample will make it more difficult for a charge carrier to move freely throughout the sample. As stated previously, this nanostructuring approach ultimately relies on these detrimental electronic effects being outweighed by the benefits of thermal conductivity decreases.

The measured resistivities of this series of samples indicates that after 30 minutes of milling, the resistivity of a sample will increase more significantly and as shown in Figure 3.16,

unlike the undoped $CoSb_3$, these resistivity values of samples subjected to different milling times do not converge at high temperature. The temperature dependence of the Seebeck coefficient in Figure 3.17 indicates that ball milling this composition of skutterudite decreases the Seebeck coefficient at both room temperature and high temperature and for most ball milled samples in the series, increased milling time appears to accentuate these differences at high and low temperatures.

The total thermal conductivity and lattice thermal conductivity of each of the ball milled samples in relation to the bulk sample and in relation to one another, follow a trend of lower thermal conductivity with increases in milling times. This difference persists throughout most of the temperature range until the samples with higher milling times begin to rise sharply. These unexpected sharp rises are more indicative of physical changes occurring within the sample than they are of actual thermal properties. Furthermore, the 60 minute sample turns sharply near the end of the temperature range and the 120 minute sample turns at a much lower temperature, suggesting that milling beyond 30 minutes leads to this temperature instability that becomes even more unstable with more milling. This would be consistent with $CoSb_3$ decomposing to $CoSb_2$ and Sb, which in a dispersion on the nanometer scale, Sb would have a melting or sublimation temperature depression below that of the bulk Sb solid and could be causing this observed change in the thermal conductivity. Because all ball milled samples tested in this study used the same portion of the pressed sample for each of the three high temperature measurements, in the order of thermal conductivity, Hall effect, and Seebeck coefficient measurements, if Sb were volatilizing from the 60 and 120 minute samples, it would be most apparent in the thermal conductivity measurements, as this was the first high temperature characterization after hot-

pressing. The total thermal conductivity and lattice thermal conductivity as a function of temperature are presented in Figure 3.18 and Figure 3.19, respectively.

The cumulative effect of ball milling $Co_{0.955}Pd_{0.045}Sb_{2.955}Te_{0.045}$ skutterudite is only a small change in ZT that is within the measurement error. Although there is a distinct trend of decreasing thermal conductivity with increasing milling time, the increases in resistivity and the sharpening of the ends of the Seebeck coefficient curves with increased milling times negate the improvements in thermal conductivity. However, Figure 3.20 does clearly show that the effects of ball milling become detrimental by 60 minutes and the properties of samples milled longer than that deteriorate at an even lower temperature.

3.3.4 Filled n-type Skutterudite

Filled n-type skutterudites rely on the contribution of dopant electrons from filler atoms that are not covalently bound to atoms in the lattice. Therefore, the percentage of these filler atoms that are included and thus, electronically participating in the structure, must be more sensitive to a change in the surface to volume ratio of the crystallites that constitute the sample than are dopants that are covalently bound to the structure. The possibility of excluding these dopant fillers from the structure suggests that a more severe change will be apparent when ball milling leads to degradation of the composition of the starting material.

Ball milling of $Ba_{0.05}Yb_{0.15}Co_4Sb_{12}$ n-type skutterudite led to little change in the carrier concentration of the sample up to 60 minutes, but the sample milled for 120 minutes showed a drop in carrier concentration beginning at room temperature and continuing across the temperature range. Figure 3.21 shows the carrier concentration at high temperature for bulk and ball milled samples of $Ba_{0.05}Yb_{0.15}Co_4Sb_{12}$ skutterudite. Figure 3.22 shows the temperature dependence of carrier mobility and once more, the 120 minute sample is remarkably different

from all other samples in the series, which are quite similar to one another. This trend continues with resistivity as a function of temperature in Figure 3.23 where the resistivity of the 120 minute sample is very high, while all other samples trace an almost identical path across the temperature range. The Seebeck coefficients as a function of temperature presented in Figure 3.24 once again show that the Seebeck coefficients of ball milled samples turn more sharply up than do the Seebeck coefficients of bulk samples. The effects of this decrease in the magnitude of the Seebeck coefficient manifest themselves in the ZT values at high temperature where most skutterudite materials would otherwise reach their maximum ZT.

Total and lattice thermal conductivities presented in Figure 3.25 and Figure 3.26 show little change for the milled samples as compared to the bulk sample, with the exception of the 120 minute sample that clearly has a significantly lower electronic contribution to the total thermal conductivity in that its total thermal conductivity is less than the other samples, but its lattice thermal conductivity is markedly higher. This aligns with the significant differences observed in the electrical properties of this sample. Figure 3.27 contains the temperature dependence of ZT in bulk and ball milled $Ba_{0.05}Yb_{0.15}Co_4Sb_{12}$ skutterudite samples. The 120 minute sample has clearly undergone degradation. The other samples, having similar resistivities and thermal conductivities can attribute their drops in ZT at high temperature to a sharper decrease in the magnitude of their Seebeck coefficients at high temperature, as compared to a flatter curve for the bulk material. It is unclear how an increase in the density of interfaces in the material may make the Seebeck coefficient behave in this way, but one possible difference in bulk versus milled samples is the change in surface to volume ratio for milled samples wherein the filler atoms are more likely to leave the structure and instead occupy grain boundaries and be more vulnerable to oxidation as the surface to volume ratio of the powder increases. This change in

surface to volume ratio could also cause a change in how filler atoms just inside the lattice fringes behave at high temperature, leading to this observed difference in Seebeck coefficient, but there is no direct evidence of this in the data.

3.3.5 Filled p-type Skutterudite

The filled p-type $Ce_{0.9}Fe_{3.5}Co_{0.5}Sb_{12}$ skutterudite chosen for this characterization of the effects of nanostructuring has a high filling fraction, such that the effects of changing the surface to volume ratio, as discussed above for filled n-type skutterudite, could be more pronounced because there are more occupied vacancies than empty vacancies in the structure, and with the change in this ratio, Ce filler could be excluded from the structure at a higher rate than the lesser-filled n-type skutterudite discussed above. This is a significant difference from all other structures described in this study and therefore could lead to the greatest variation of electrical properties as a function of milling time for all compositions of skutterudite discussed.

The temperature dependence of carrier concentrations for the bulk and ball milled $Ce_{0.9}Fe_{3.5}Co_{0.5}Sb_{12}$ skutterudite samples are presented in Figure 3.28. Ball milled samples show increases in carrier concentrations as milling times increase and this is consistent with the proposed loss of cerium in the structure, as cerium contributes electrons to the structure. The difference in carrier concentration is small for the 0 minute control and the 60 minute sample, but the difference is very clear for the 120 minute sample. The temperature dependence of carrier mobility depicted in Figure 3.29 indicates that with an increase in hole concentration, the mobility decreases significantly. The bulk sample has a higher overall mobility across the temperature range and the 120 minute sample remains around 1 $cm^2/V•s$ or below throughout the entire temperature range.

Similar to filled n-type skutterudite, the filled p-type samples maintain similar resistivities as a function of temperature with the exception of the 120 minute sample as shown in Figure 3.30. This similarity between samples is also evident in the Seebeck coefficient as a function of temperature, shown in Figure 3.31. The total and lattice thermal conductivities in Figure 3.32 and Figure 3.33 show similar thermal conductivities for bulk and ball milled samples with the 120 minute sample again standing apart. The increase in the total thermal conductivity and the lattice thermal conductivity is once again consistent with a decrease in cerium occupying the vacancies in the skutterudite structure because cerium that occupies vacancies in the skutterudite structure has been shown to scatter phonons.

The ZT as a function of temperature is plotted in Figure 3.34. The 60 minute milled sample shows only a slight increase in ZT at the top of the temperature range, owing mostly to a slightly greater Seebeck coefficient at the maximum temperature measured, but that increase in ZT is well within the experimental error and therefore insignificant.

3.4 Conclusions

Four distinct classes of skutterudite materials were synthesized in bulk and then processed by high energy ball milling in order to create nanostructured materials. The powders were characterized by XRD, SEM, and TEM before being hot-pressed and measured for their thermoelectric properties. Thermal conductivity reductions were most pronounced in the ball milled samples of unfilled skutterudites, whereas the filled samples remained mostly unchanged until milling led to apparent sample decomposition. All reductions in thermal conductivities were matched by deterioration of the electrical properties in the samples. In each case, the overall effect on ZT was more often a decrease than an increase, and all increases in ZT over

bulk materials were within the error of the measurement. The nature of ball milling skutterudite is such that extensive and careful processing to reduce the average crystallite sizes of samples is quickly countered in the hot-press densification step if adequate temperatures and pressures are used to obtain products near full density. Lower temperatures and pressures result in porous samples with unreliable, irreproducible thermal conductivity and transport measurements. Overall, nanostructured skutterudite results have been difficult to consistently reproduce and a majority of samples undergo reactions or phase transformations during high temperature measurements. The approach to improving the ZT of skutterudite materials by ball milling to produce nanostructures and reduce thermal conductivity is a significant challenge because of the complex structure of skutterudites.

3.5 Acknowledgements

This research was carried out at the Jet Propulsion Laboratory, California Institute of Technology, under a contract with the National Aeronautics and Space Administration. This work was supported by the NASA Science Mission Directorate's Radioisotope Power Systems Technology Advancement Program, the NSF IGERT: Materials Creation Training Program (MCTP) – DGE-0654431 (DM), and the California NanoSystems Institute. The authors thank Kurt Star for helpful discussions. The authors thank Dr. Frank Kyte of the University of California, Los Angeles for SEM assistance and helpful discussions. The authors also thank the EPSS department at the University of California, Los Angeles for supporting the SEM/EPMA facility. Special thanks to George Nakatsukasa, L. Danny Zoltan, and Gregory Gerig for instrumentation support.

3.6 Tables and Figures

3.6.1 Milling Characterizations

Table 3.I. Crystallite Size Calculations and Room Temperature Transport Properties for Ball Milled n-type $Co_{0.955}Pd_{0.045}Sb_{2.955}Te_{0.045}$ Skutterudite

Milling time (min)	0 min	15 min	30 min	60 min	120 min
Avg. crystallite size: Powder (nm)	71 nm	66 nm	40 nm	34 nm	33 nm
Avg. crystallite size: Pressed (nm)	71 nm	57 nm	64 nm	51 nm	60 nm
Electrical resistivity (mΩ cm)	0.67	0.68	0.71	0.99	0.76
Hall mobility (cm^2/Vs)	32.7	32.5	33.0	23.8	29.2
Hall carrier concentration (cm^{-3})	2.84×10^{20}	2.81×10^{20}	2.68×10^{20}	2.66×10^{20}	2.82×10^{20}
Seebeck coefficient (μV/K)	-102	-112	-115	-123	-127
Thermal conductivity (mW/cm K)	58.4	42.5	40.5	35.4	34.2
Lattice thermal conductivity (mW/cm K)	50.1	34.6	32.8	29.3	28.6

* Note that all values presented were obtained at room temperature. The 0 minutes sample is included for comparison. The average crystallite sizes for powder and pressed samples were calculated using the method of integral breadths[32] from the obtained XRD patterns. The electrical resistivity (ρ) was measured using the van der Pauw technique with a current of 100 mA. The Hall mobility and the carrier density were calculated from the Hall coefficient which was measured with a forward and reverse magnetic field value of ~8500 G.

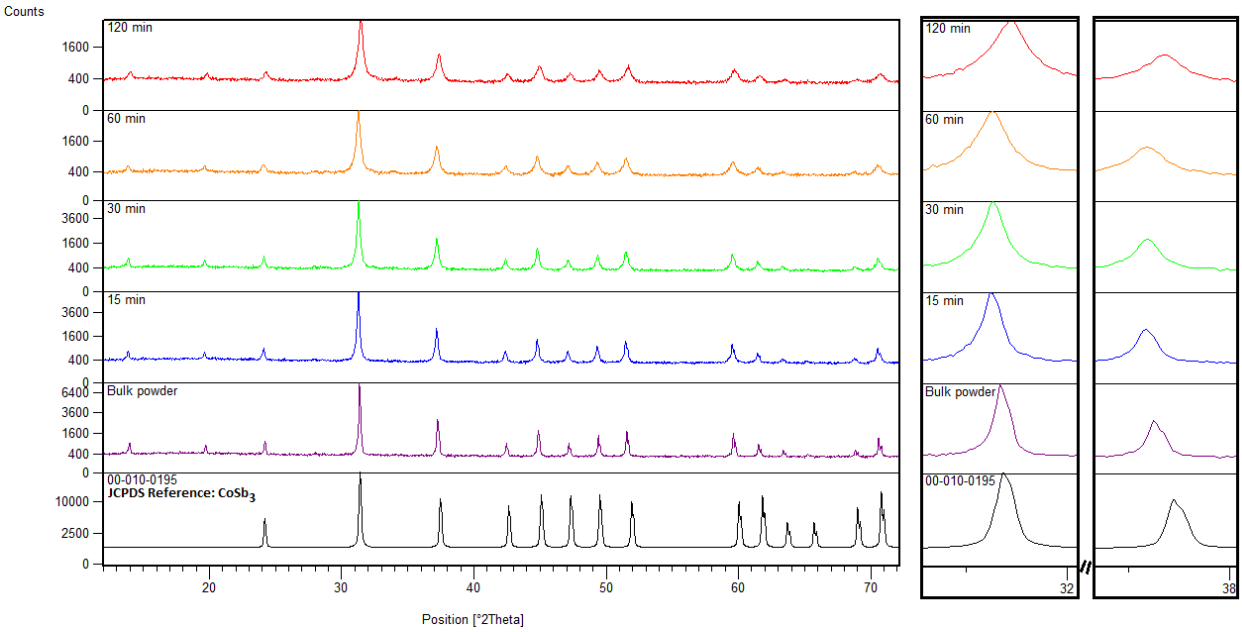

Figure 3.1. X-ray diffraction patterns obtained from bulk and ball milled samples of $Co_{0.955}Pd_{0.045}Sb_{2.955}Te_{0.045}$. Milling times are indicated in the legend and the two enlarged regions on the right show the relative peak widths in relation to milling time. Peak shifts here are the result of measurement error from differences in sample heights in the diffractometer. A simulated pattern from JCPDS reference pattern 00-010-0195 for $CoSb_3$ is presented for comparison to the obtained experimental sample patterns.

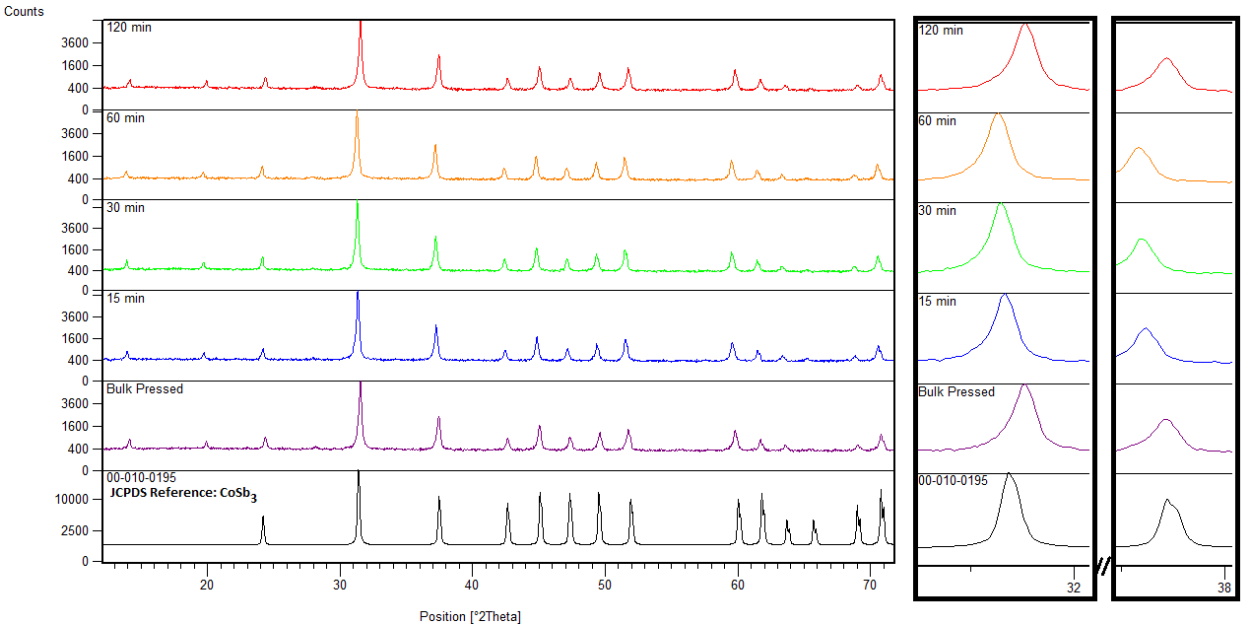

Figure 3.2. X-ray diffraction patterns obtained from hot-pressed pellets of bulk and ball milled samples of $Co_{0.955}Pd_{0.045}Sb_{2.955}Te_{0.045}$. Milling times are indicated in the legend and the two enlarged regions on the right show the relative peak widths of the pressed samples in relation to the original milling time of each sample. Peak shifts here are the result of measurement error from differences in sample heights in the diffractometer. A simulated pattern from JCPDS reference pattern 00-010-0195 for $CoSb_3$ is presented for comparison to the obtained experimental sample patterns.

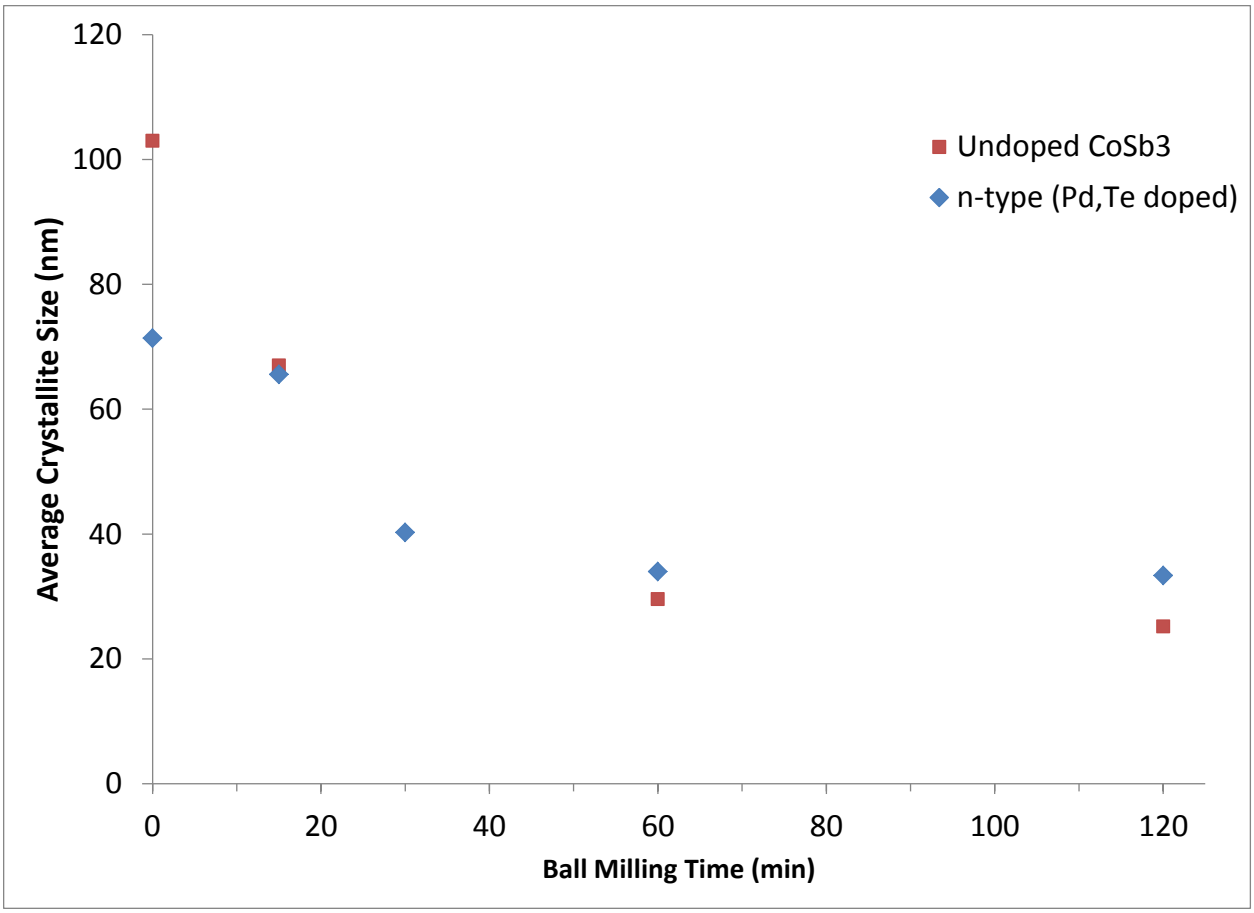

Figure 3.3. **C**alculated average crystallite sizes as a function of ball milling time for undoped and n-type $Co_{0.955}Pd_{0.045}Sb_{2.955}Te_{0.045}$ skutterudite samples. Average crystallite sizes were calculated from XRD data, using the method of integral breadths.[32]

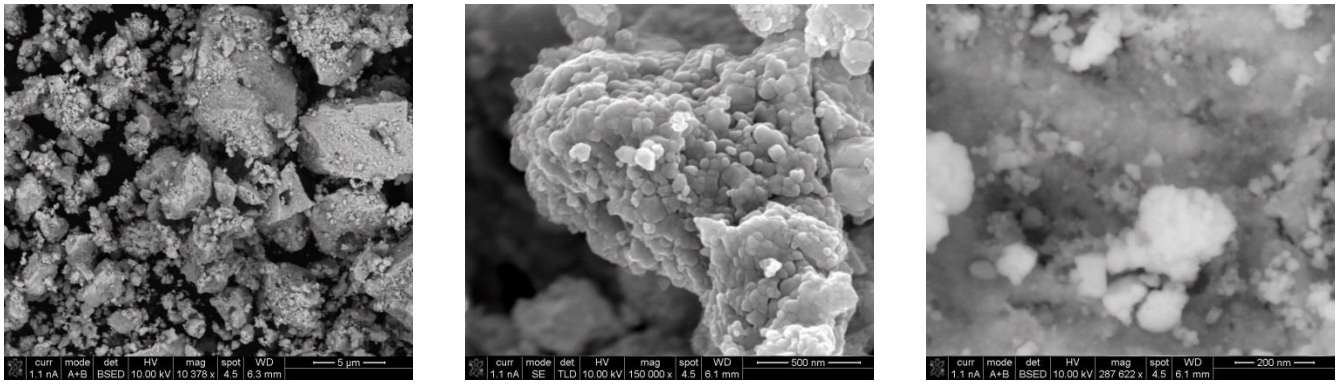

Figure 3.4. Scanning electron microscope (SEM) images at increasing magnifications of $Co_{0.955}Pd_{0.045}Sb_{2.955}Te_{0.045}$ powder, milled for 60 minutes.

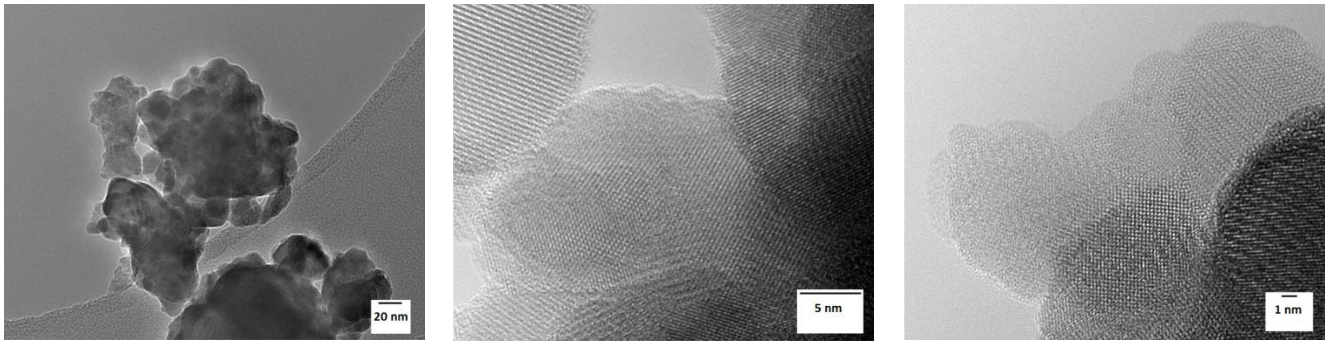

Figure 3.5. Transmission electron microscope (TEM) images at increasing magnifications of $Co_{0.955}Pd_{0.045}Sb_{2.955}Te_{0.045}$ powder, milled for 60 minutes.

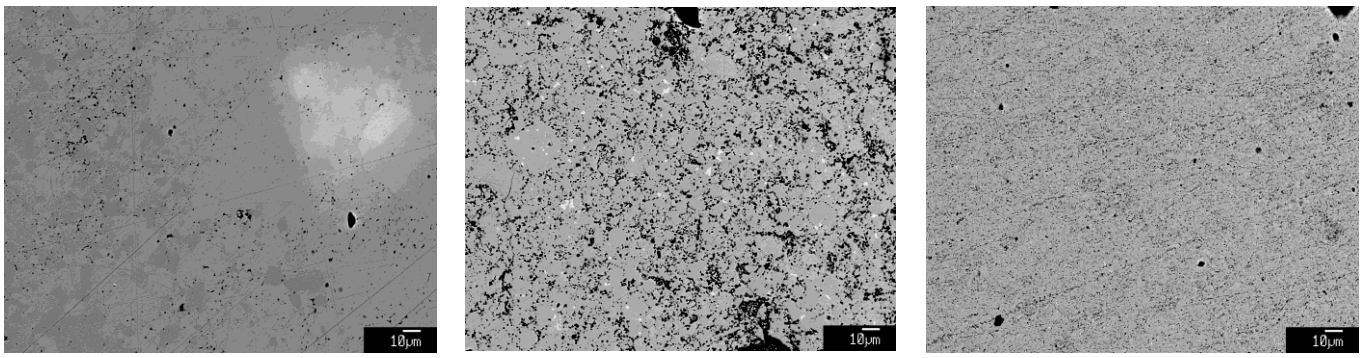

Bulk, 0 min | Milled 15 min | Milled 120 min

Figure 3.6. Scanning electron microscope (SEM) images of three pressed $Co_{0.955}Pd_{0.045}Sb_{2.955}Te_{0.045}$ samples subjected to increasing milling times.

3.6.2 Milled $CoSb_3$

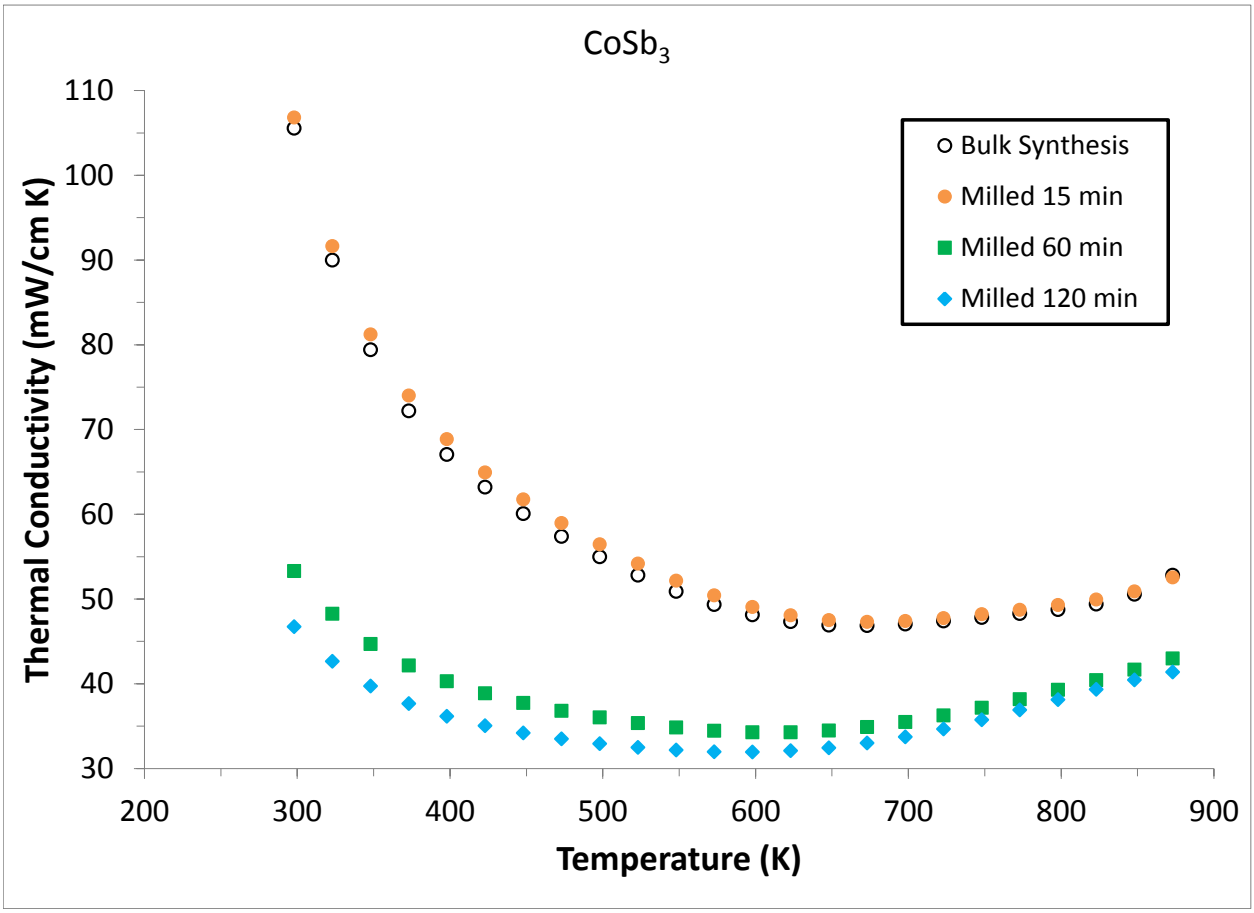

Figure 3.7. Temperature dependence of thermal conductivity (λ) in bulk and ball milled $CoSb_3$ skutterudite samples. The heat capacity and thermal diffusivity were measured using a flash diffusivity technique[33] and the overall error in the thermal conductivity measurements was estimated to be about ±10%. The thermal conductivity was calculated from the experimental mass, density, heat capacity, and thermal diffusivity values.

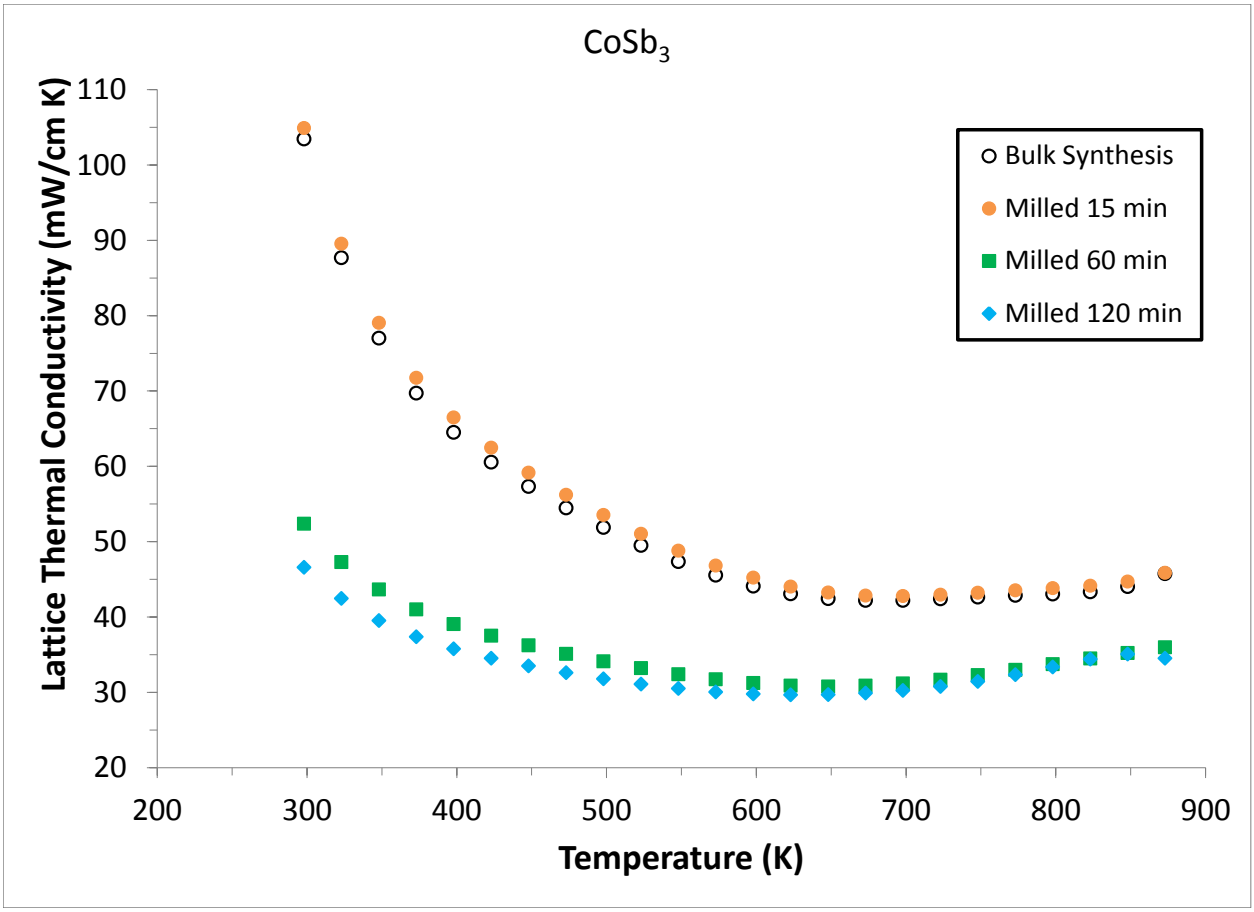

Figure 3.8. Temperature dependence of lattice thermal conductivity ($\lambda_{Lattice}$) in bulk and ball milled $CoSb_3$ skutterudite samples. The lattice thermal conductivity was obtained by subtracting the electronic thermal conductivity contribution from the total thermal conductivity. The electronic contribution was calculated from the resistivity and Lorenz number. The total thermal conductivity was calculated from the experimental mass, density, heat capacity, and thermal diffusivity values. The overall error in the thermal conductivity measurements was estimated to be about ±10%.

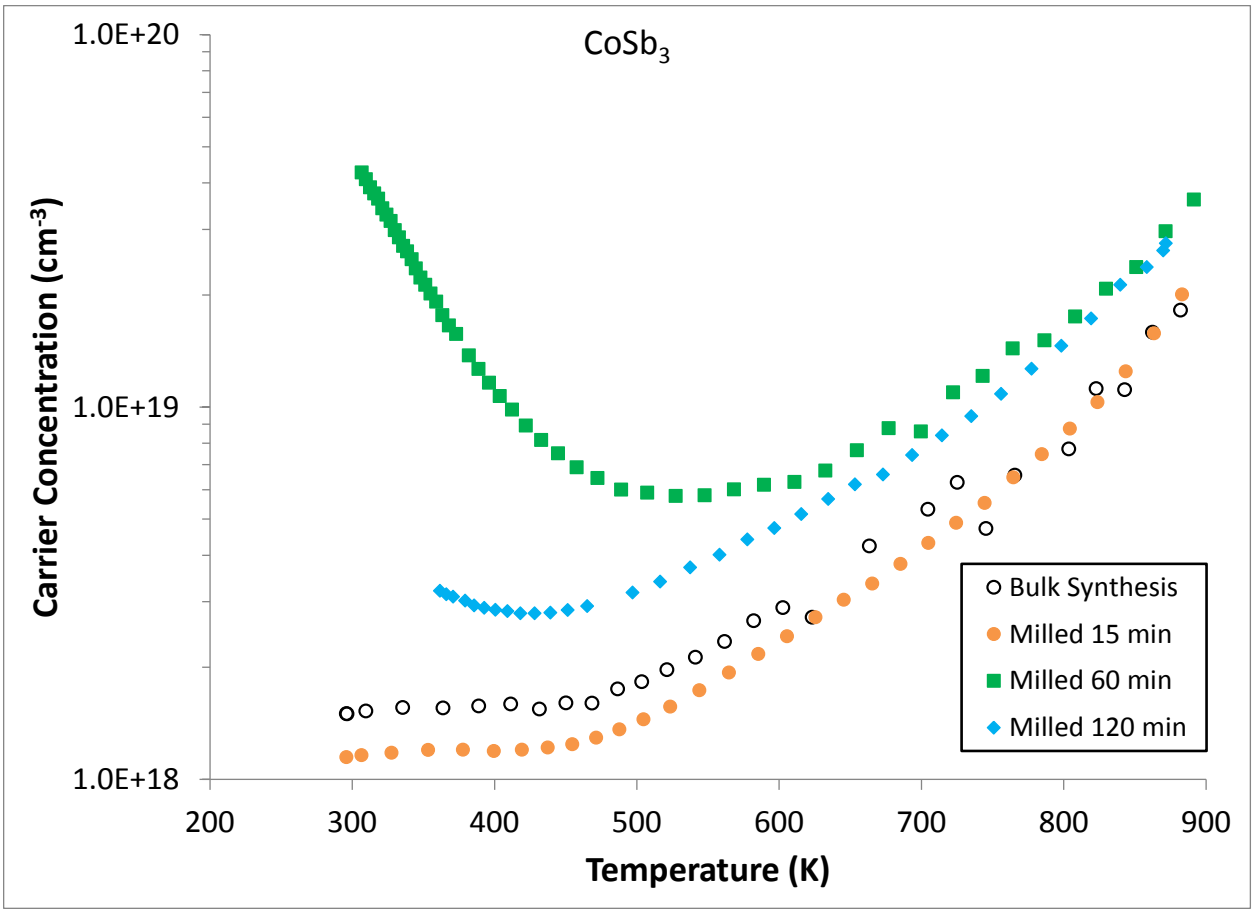

Figure 3.9. Temperature dependence of carrier concentration in bulk and ball milled $CoSb_3$ skutterudite samples. The Hall coefficient was measured with a forward and reverse magnetic field value of ~8500 G. The carrier concentration was calculated from the Hall coefficient, assuming a scattering factor of 1 in a single carrier scheme, by $p/n = 1/R_H e$ where p and n are the densities of holes and electrons, respectively, and e is the electron charge. The measurement error was estimated to be ±2% for the Hall coefficient data.

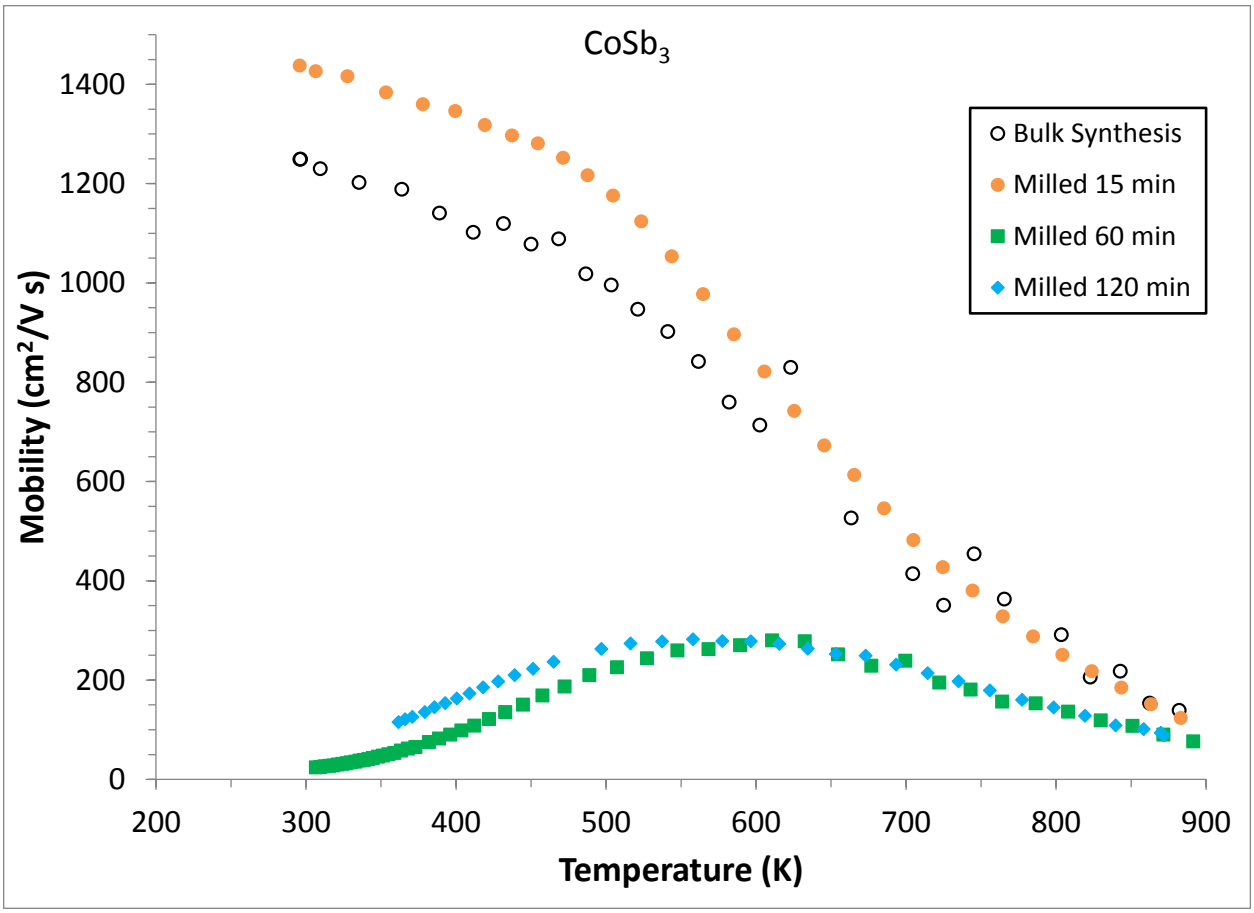

Figure 3.10. Temperature dependence of carrier mobility in bulk and ball milled $CoSb_3$ skutterudite samples. The Hall coefficient was measured with a forward and reverse magnetic field value of ~8500 G and the Hall mobility was calculated from the Hall coefficient. The measurement error was estimated to be ±2% for the Hall coefficient data.

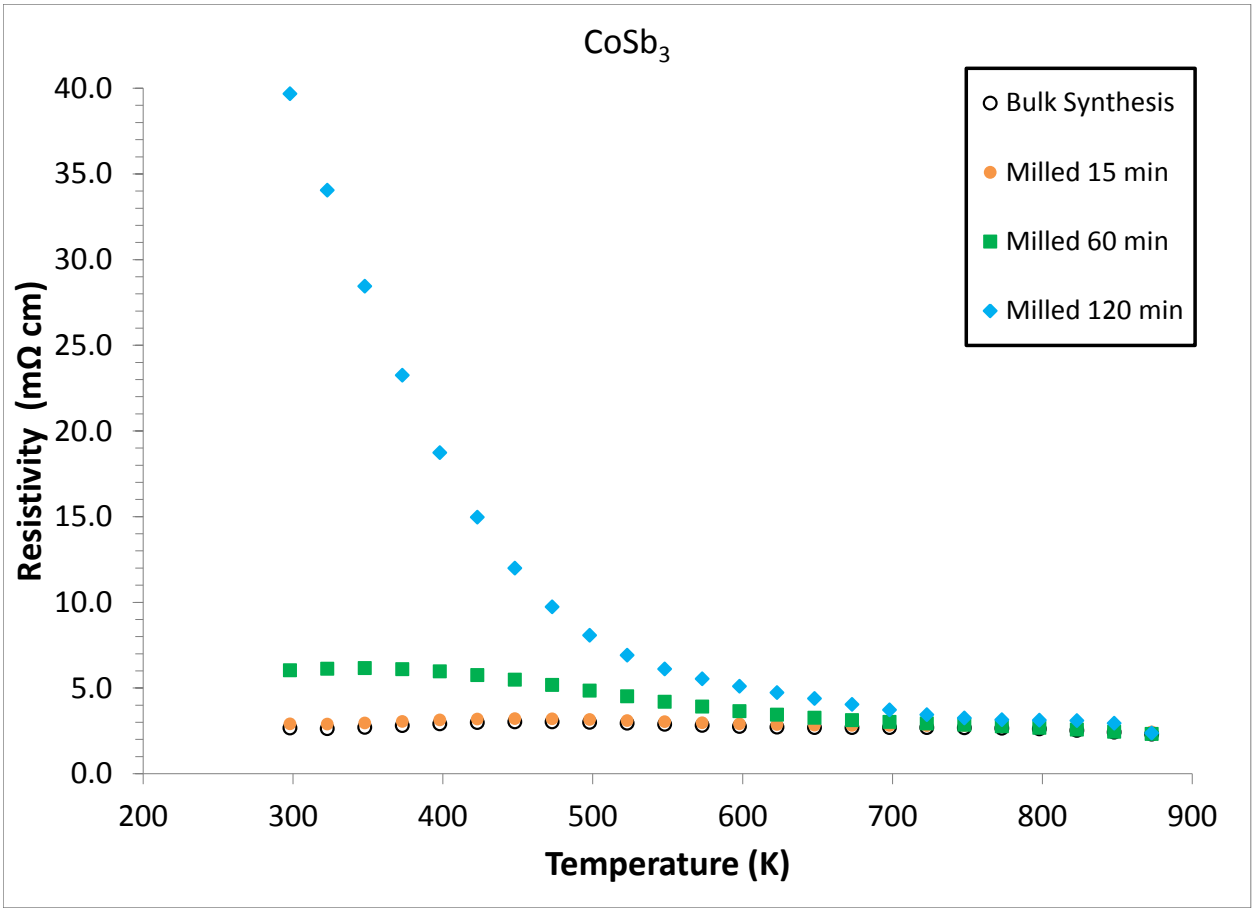

Figure 3.11. Temperature dependence of electrical resistivity in bulk and ball milled $CoSb_3$ skutterudite samples. The electrical resistivity (ρ) was measured using the van der Pauw technique with a current of 100 mA. The measurement error was estimated to be ±0.5% for the resistivity data.

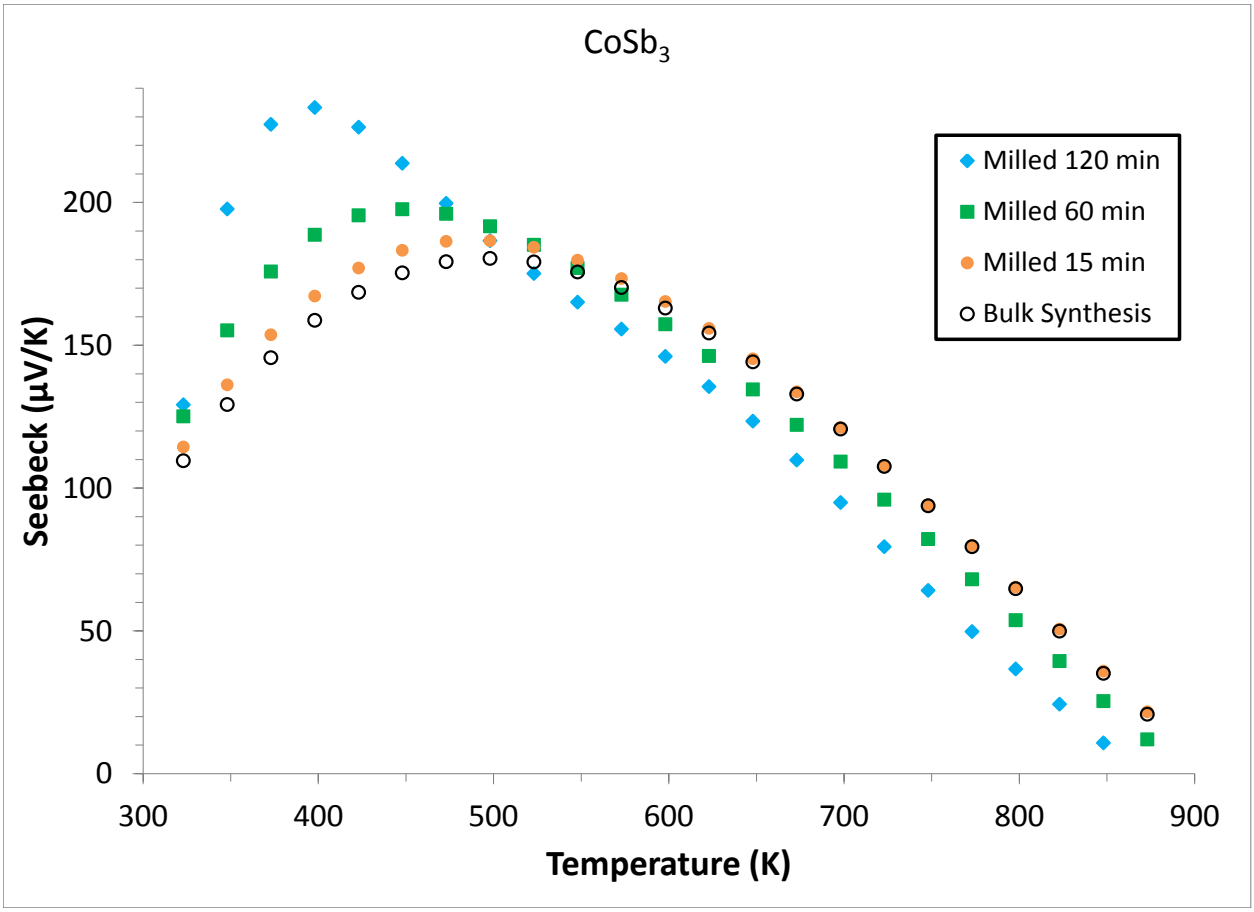

Figure 3.12. Temperature dependence of Seebeck coefficient in bulk and ball milled $CoSb_3$ skutterudite samples. The Seebeck coefficient was measured using a high temperature light pulse technique.[35] The error of the Seebeck coefficient measurement was estimated to be less than ±3%.

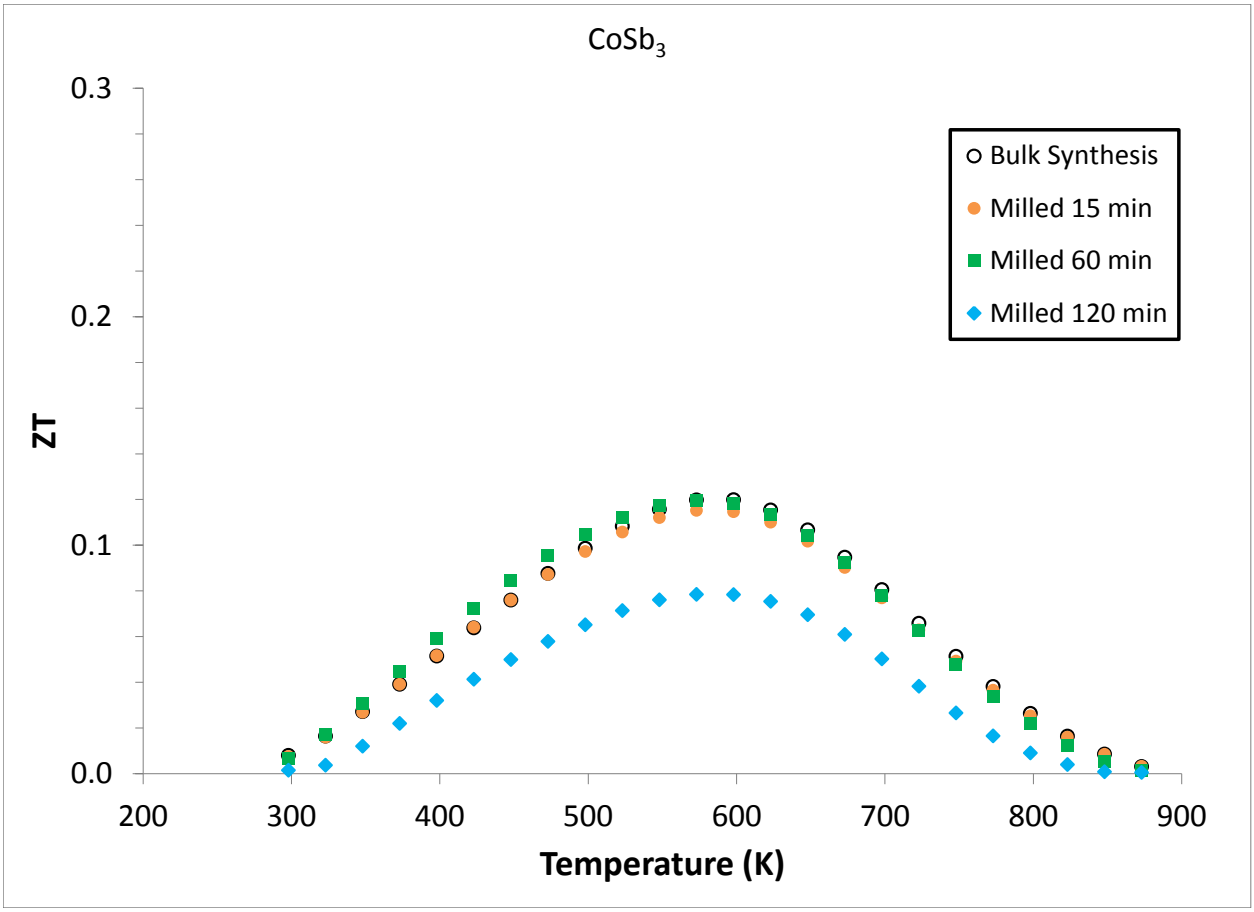

Figure 3.13. Temperature dependence of the thermoelectric figure of merit, ZT in bulk and ball milled $CoSb_3$ skutterudite samples. Combining the Seebeck coefficient, resistivity, and thermal conductivity measurements, the overall error in ZT was estimated to be about ±20%.

3.6.3 Milled, unfilled n-type $Co_{0.955}Pd_{0.045}Sb_{2.955}Te_{0.045}$

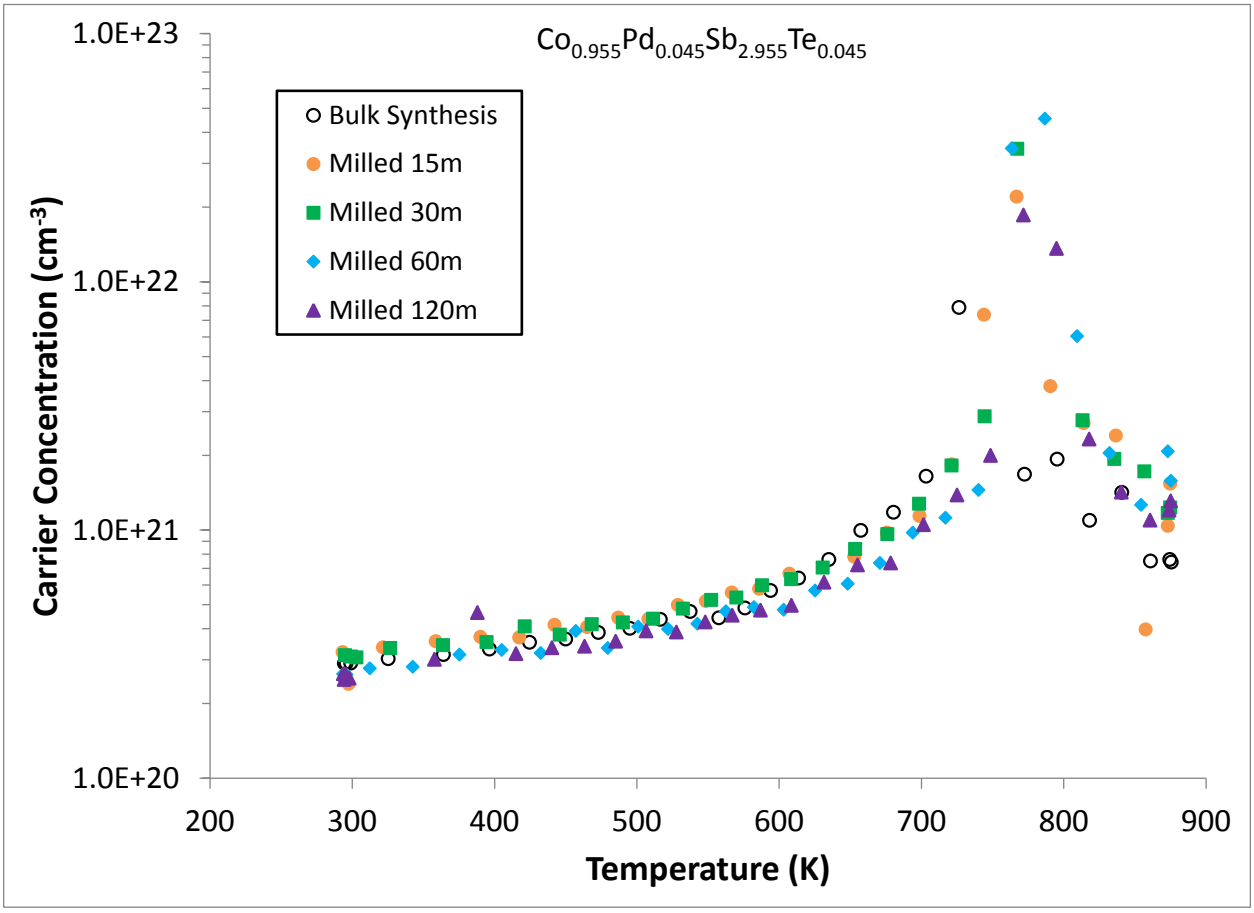

Figure 3.14. Temperature dependence of carrier concentration in bulk and ball milled $Co_{0.955}Pd_{0.045}Sb_{2.955}Te_{0.045}$ skutterudite samples. The Hall coefficient was measured with a forward and reverse magnetic field value of ~8500 G. The carrier concentration was calculated from the Hall coefficient, assuming a scattering factor of 1 in a single carrier scheme, by $p/n = 1/R_H e$ where p and n are the densities of holes and electrons, respectively, and e is the electron charge. The measurement error was estimated to be ±2% for the Hall coefficient data.

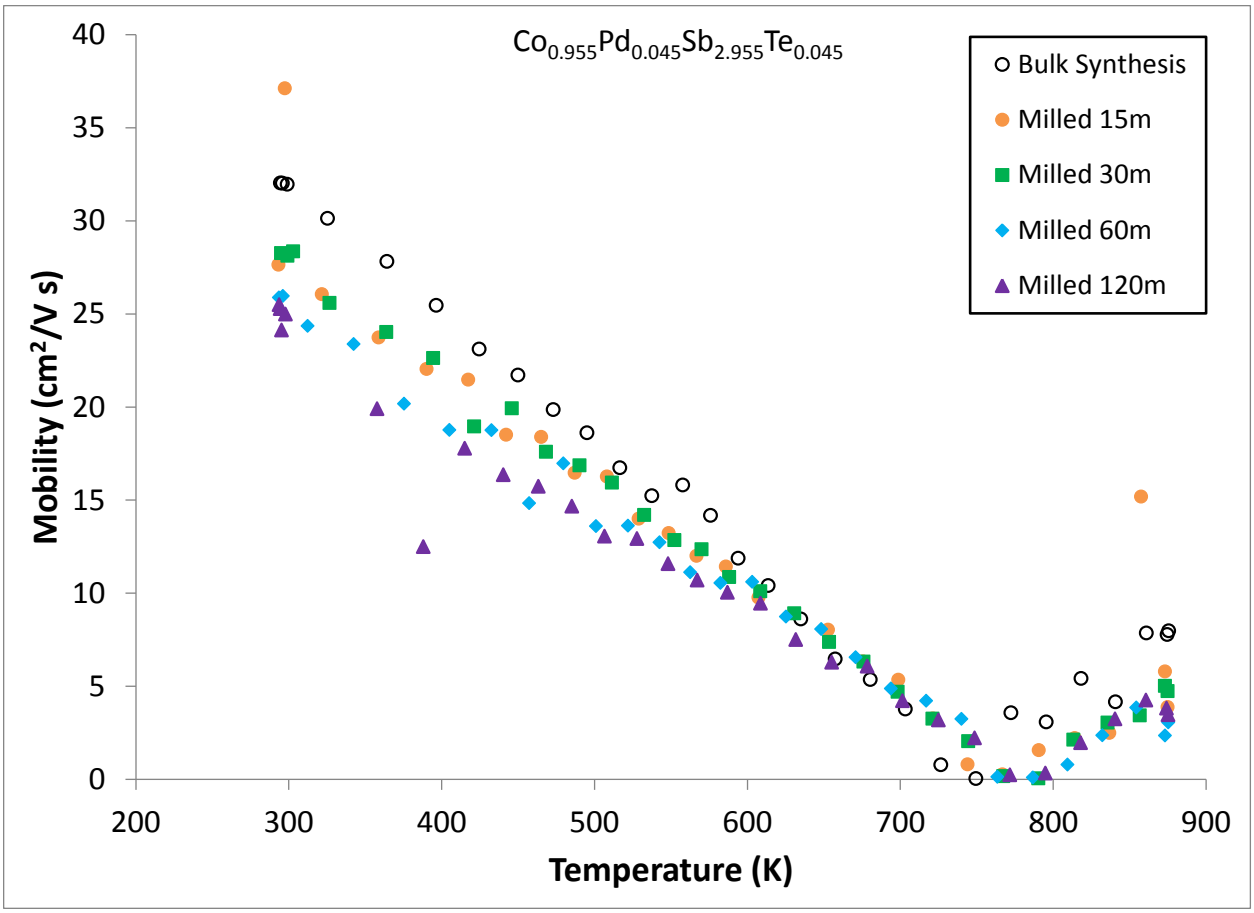

Figure 3.15. Temperature dependence of carrier mobility in bulk and ball milled $Co_{0.955}Pd_{0.045}Sb_{2.955}Te_{0.045}$ skutterudite samples. The Hall coefficient was measured with a forward and reverse magnetic field value of ~8500 G and the Hall mobility was calculated from the Hall coefficient. The measurement error was estimated to be ±2% for the Hall coefficient data.

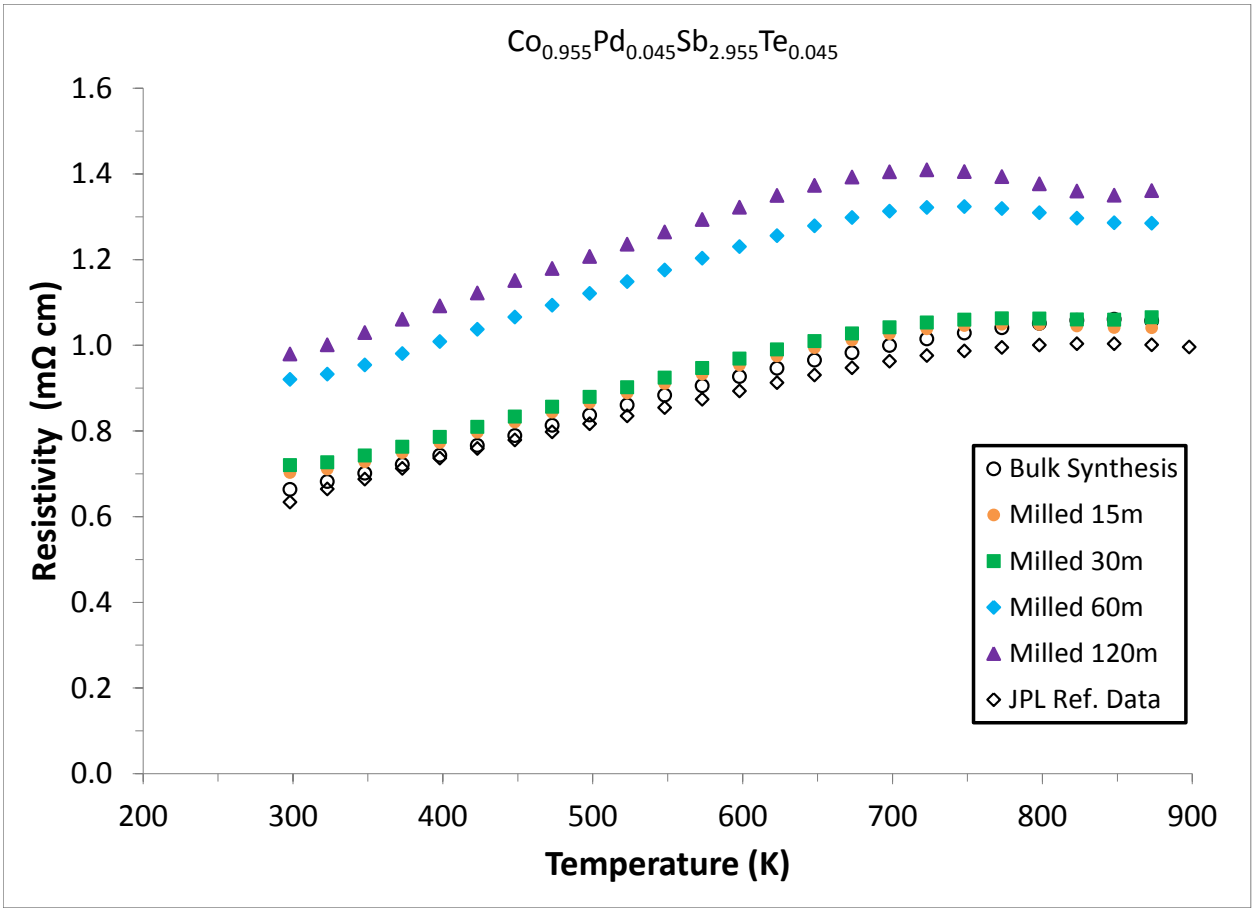

Figure 3.16. Temperature dependence of electrical resistivity in bulk and ball milled $Co_{0.955}Pd_{0.045}Sb_{2.955}Te_{0.045}$ skutterudite samples. The electrical resistivity (ρ) was measured using the van der Pauw technique with a current of 100 mA. The measurement error was estimated to be ±0.5% for the resistivity data.

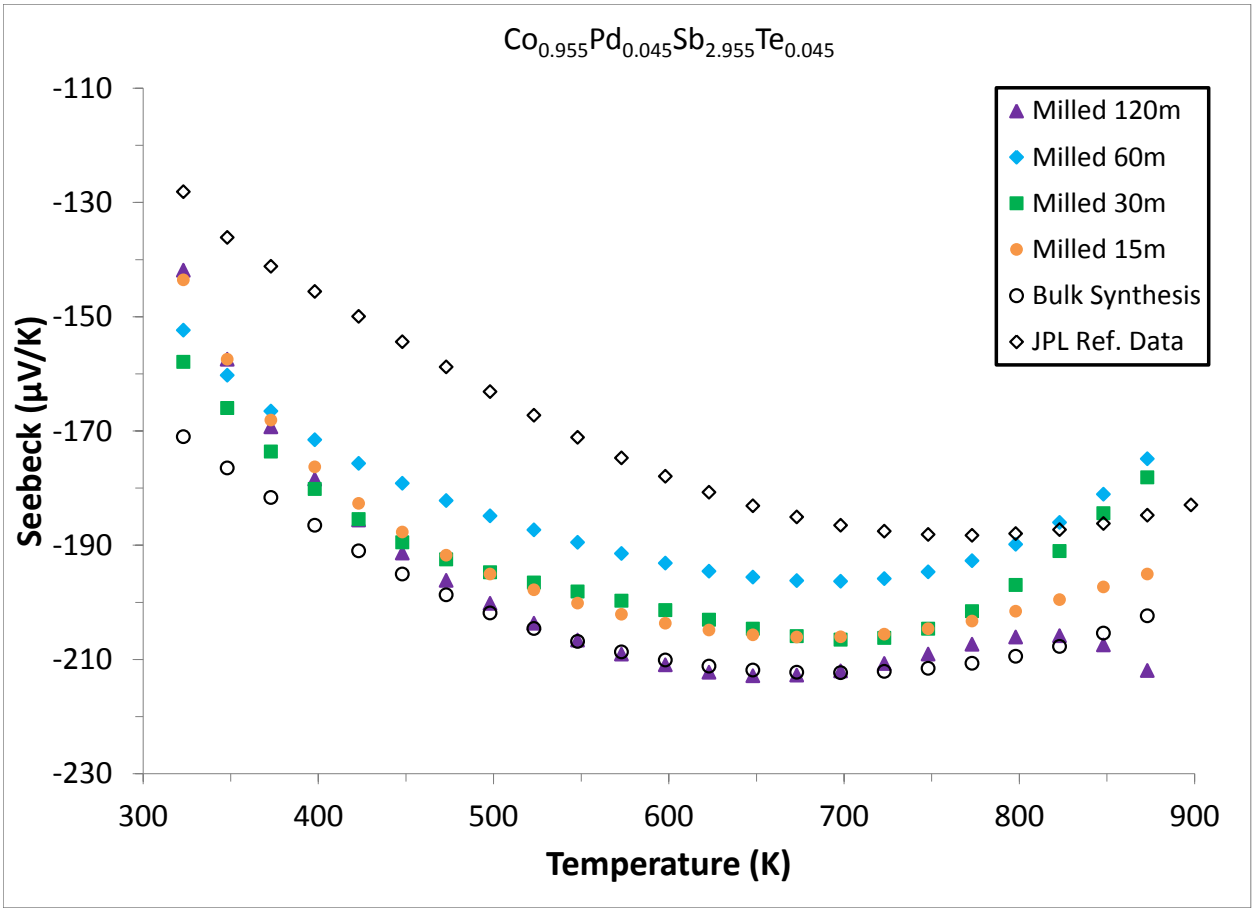

Figure 3.17. Temperature dependence of Seebeck coefficient in bulk and ball milled $Co_{0.955}Pd_{0.045}Sb_{2.955}Te_{0.045}$ skutterudite samples. The Seebeck coefficient was measured using a high temperature light pulse technique.[35] The error of the Seebeck coefficient measurement was estimated to be less than ±3%.

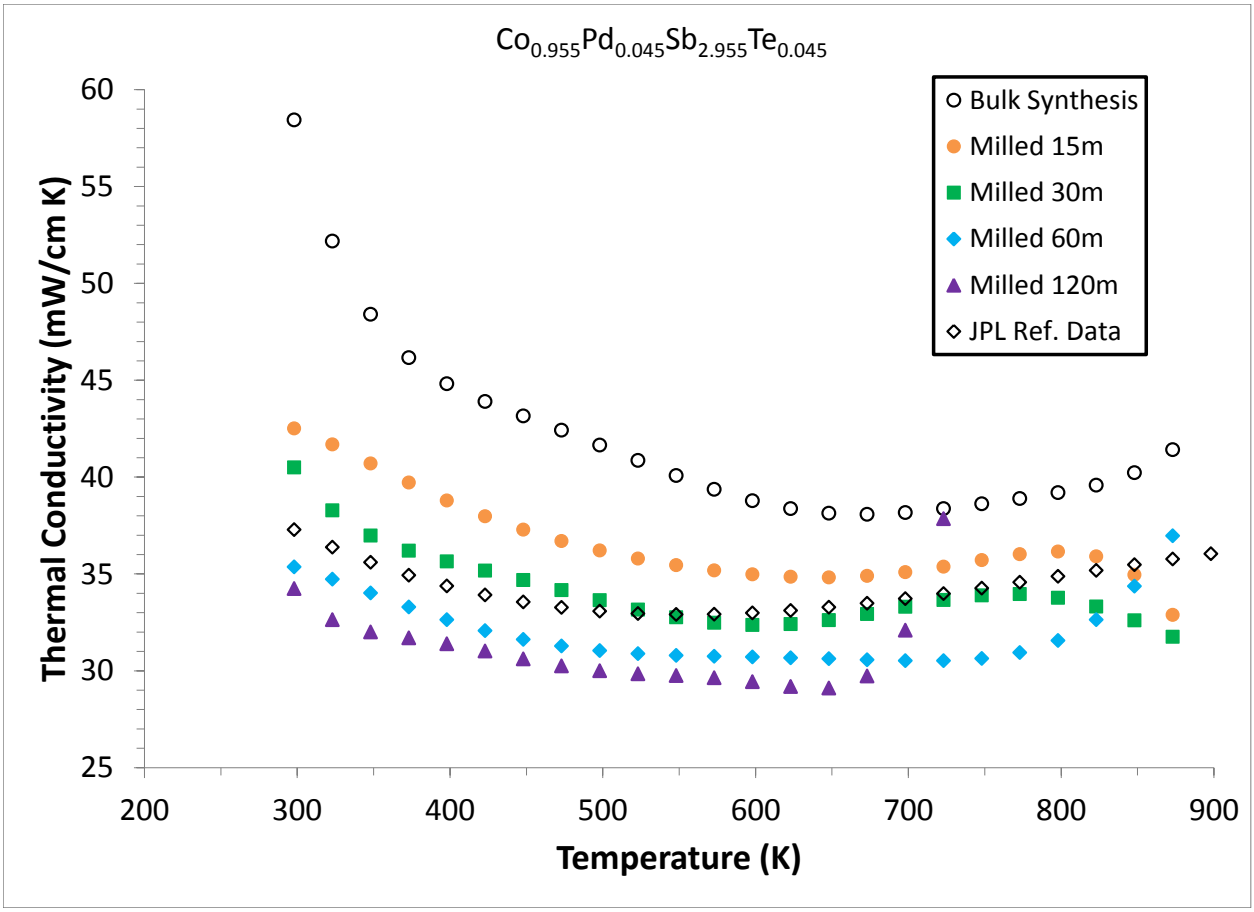

Figure 3.18. Temperature dependence of thermal conductivity (λ) in bulk and ball milled $Co_{0.955}Pd_{0.045}Sb_{2.955}Te_{0.045}$ skutterudite samples. The heat capacity and thermal diffusivity were measured using a flash diffusivity technique[33] and the overall error in the thermal conductivity measurements was estimated to be about ±10%. The thermal conductivity was calculated from the experimental mass, density, heat capacity, and thermal diffusivity values.

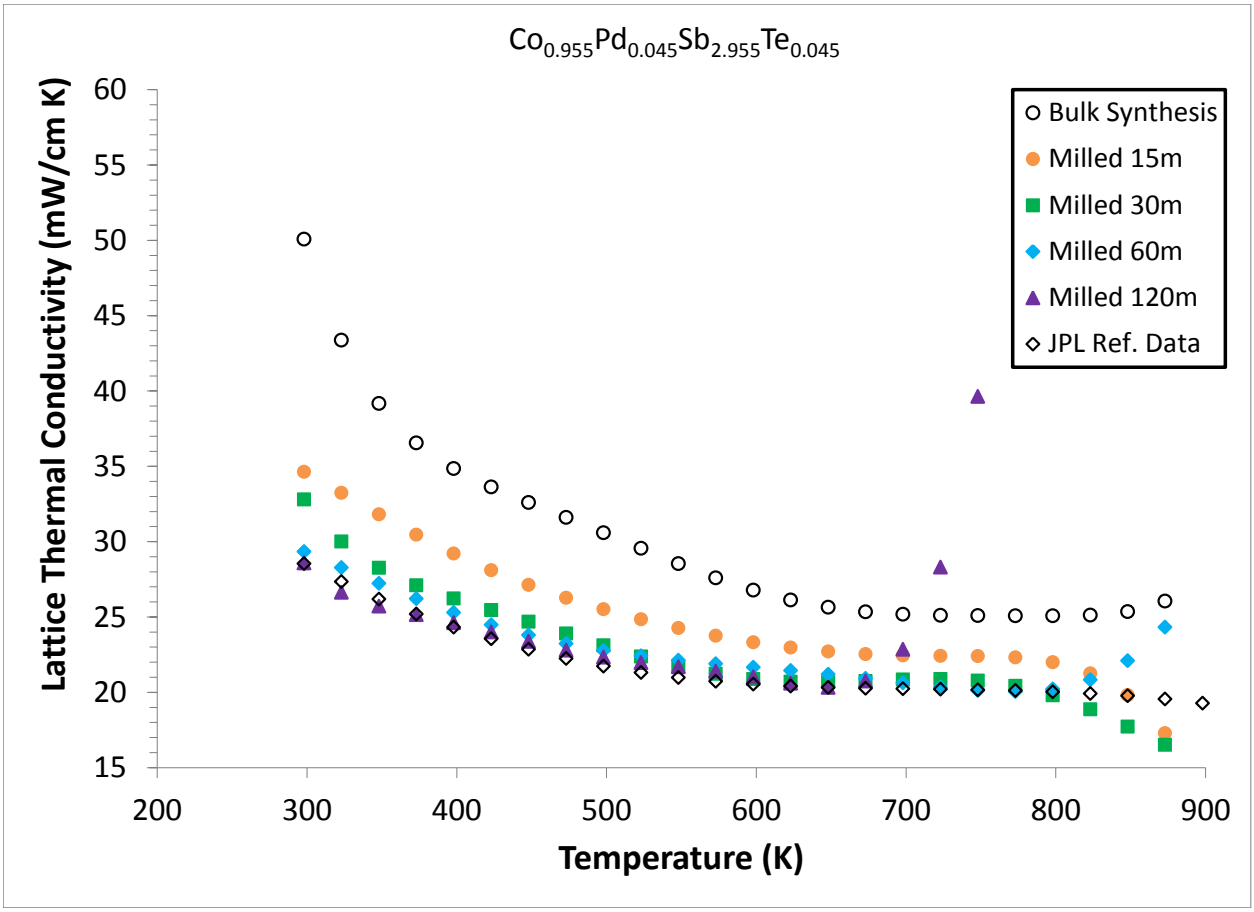

Figure 3.19. Temperature dependence of lattice thermal conductivity ($\lambda_{Lattice}$) in bulk and ball milled $Co_{0.955}Pd_{0.045}Sb_{2.955}Te_{0.045}$ skutterudite samples. The lattice thermal conductivity was obtained by subtracting the electronic thermal conductivity contribution from the total thermal conductivity. The electronic contribution was calculated from the resistivity and Lorenz number. The total thermal conductivity was calculated from the experimental mass, density, heat capacity, and thermal diffusivity values. The overall error in the thermal conductivity measurements was estimated to be about ±10%.

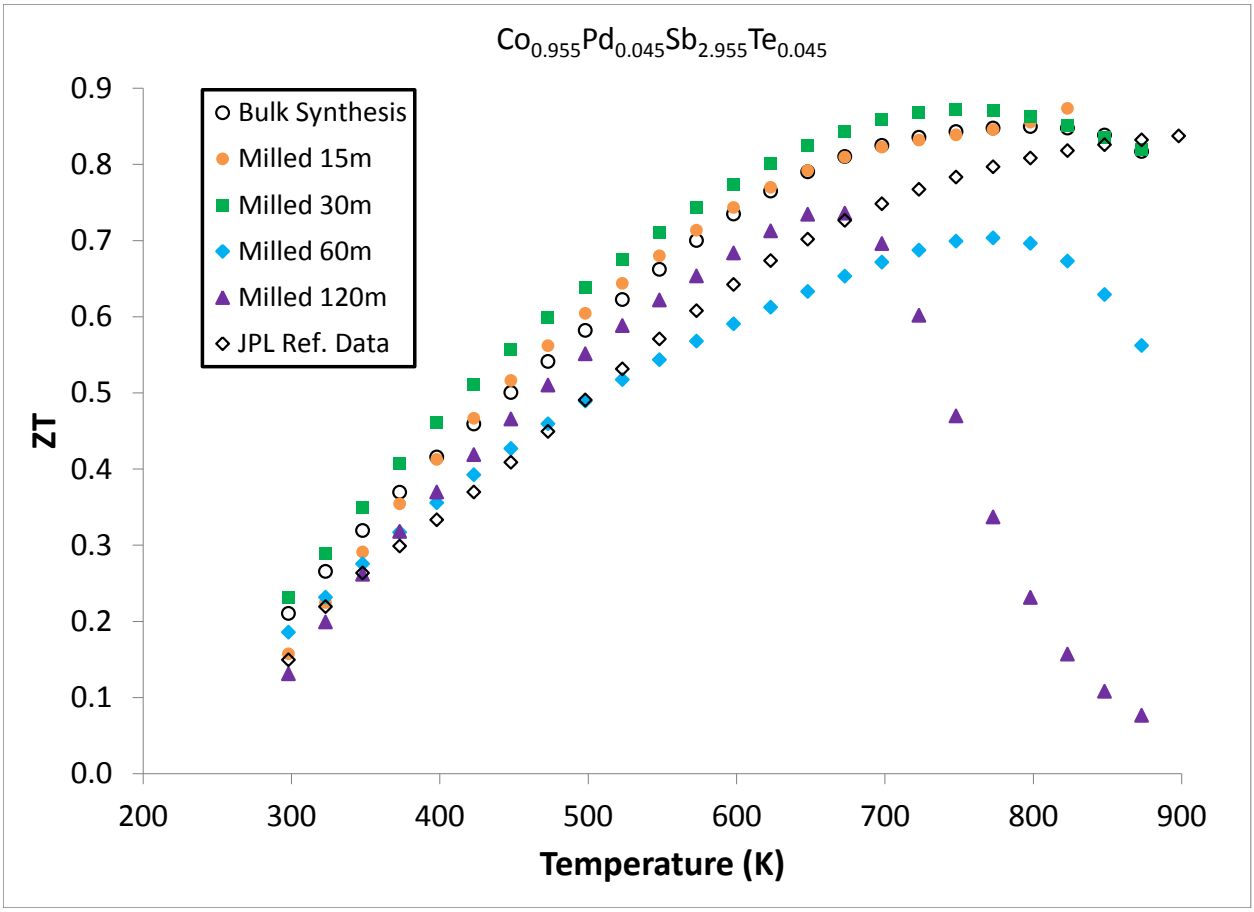

Figure 3.20. Temperature dependence of the thermoelectric figure of merit, ZT in bulk and ball milled $Co_{0.955}Pd_{0.045}Sb_{2.955}Te_{0.045}$ skutterudite samples. Combining the Seebeck coefficient, resistivity, and thermal conductivity measurements, the overall error in ZT was estimated to be about ±20%.

3.6.4 Milled, filled n-type $Ba_{0.05}Yb_{0.15}Co_4Sb_{12}$

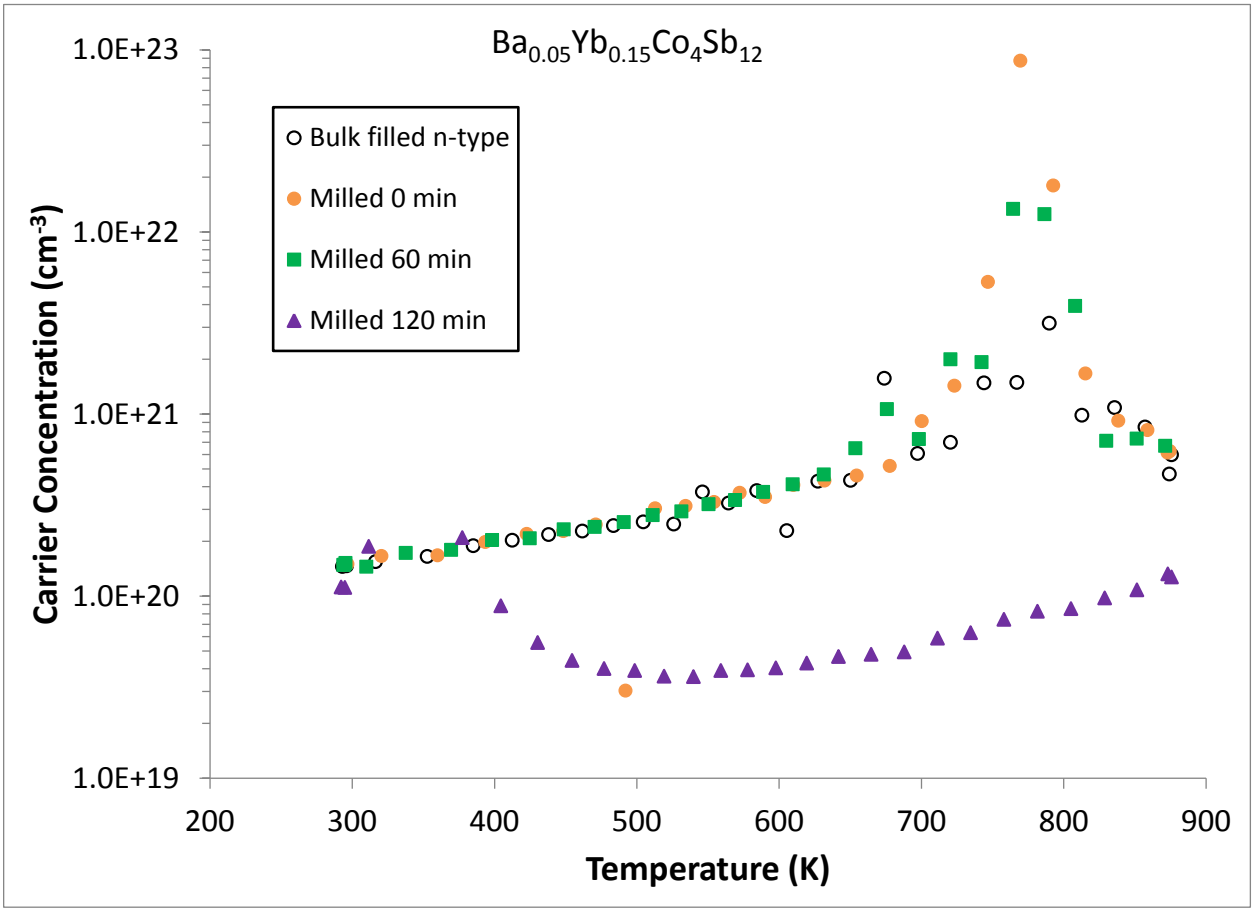

Figure 3.21. Temperature dependence of carrier concentration in bulk and ball milled $Ba_{0.05}Yb_{0.15}Co_4Sb_{12}$ skutterudite samples. A milled 0 minutes sample is included as a control sample because the bulk and milled samples were hot-pressed at different temperatures. The Hall coefficient was measured with a forward and reverse magnetic field value of ~8500 G. The carrier concentration was calculated from the Hall coefficient, assuming a scattering factor of 1 in a single carrier scheme, by $p/n = 1/R_H e$ where p and n are the densities of holes and electrons, respectively, and e is the electron charge. The measurement error was estimated to be ±2% for the Hall coefficient data.

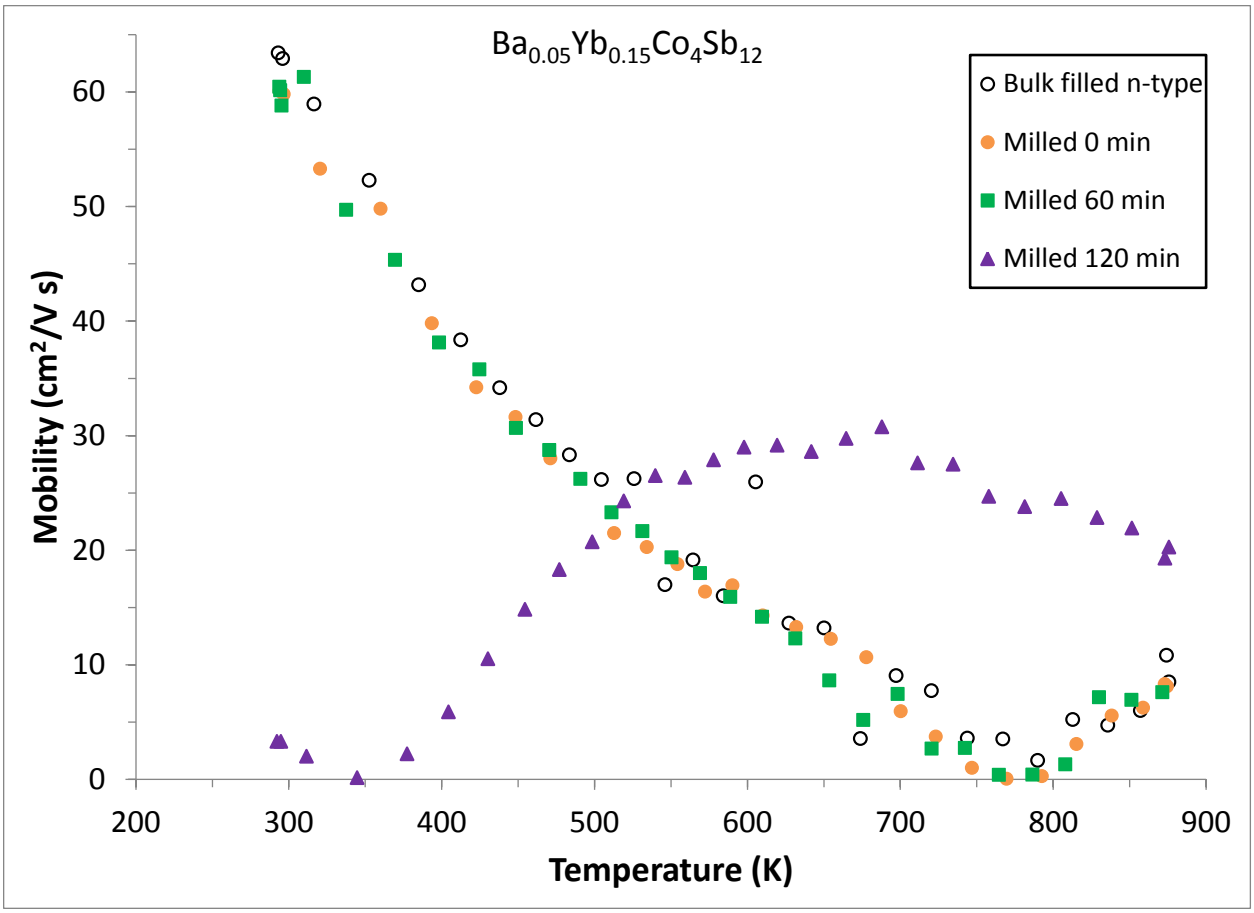

Figure 3.22. Temperature dependence of carrier mobility in bulk and ball milled $Ba_{0.05}Yb_{0.15}Co_4Sb_{12}$ skutterudite samples. A milled 0 minutes sample is included as a control because the bulk and milled samples were hot-pressed at different temperatures. The Hall coefficient was measured with a forward and reverse magnetic field value of ~8500 G and the Hall mobility was calculated from the Hall coefficient. The measurement error was estimated to be ±2% for the Hall coefficient data.

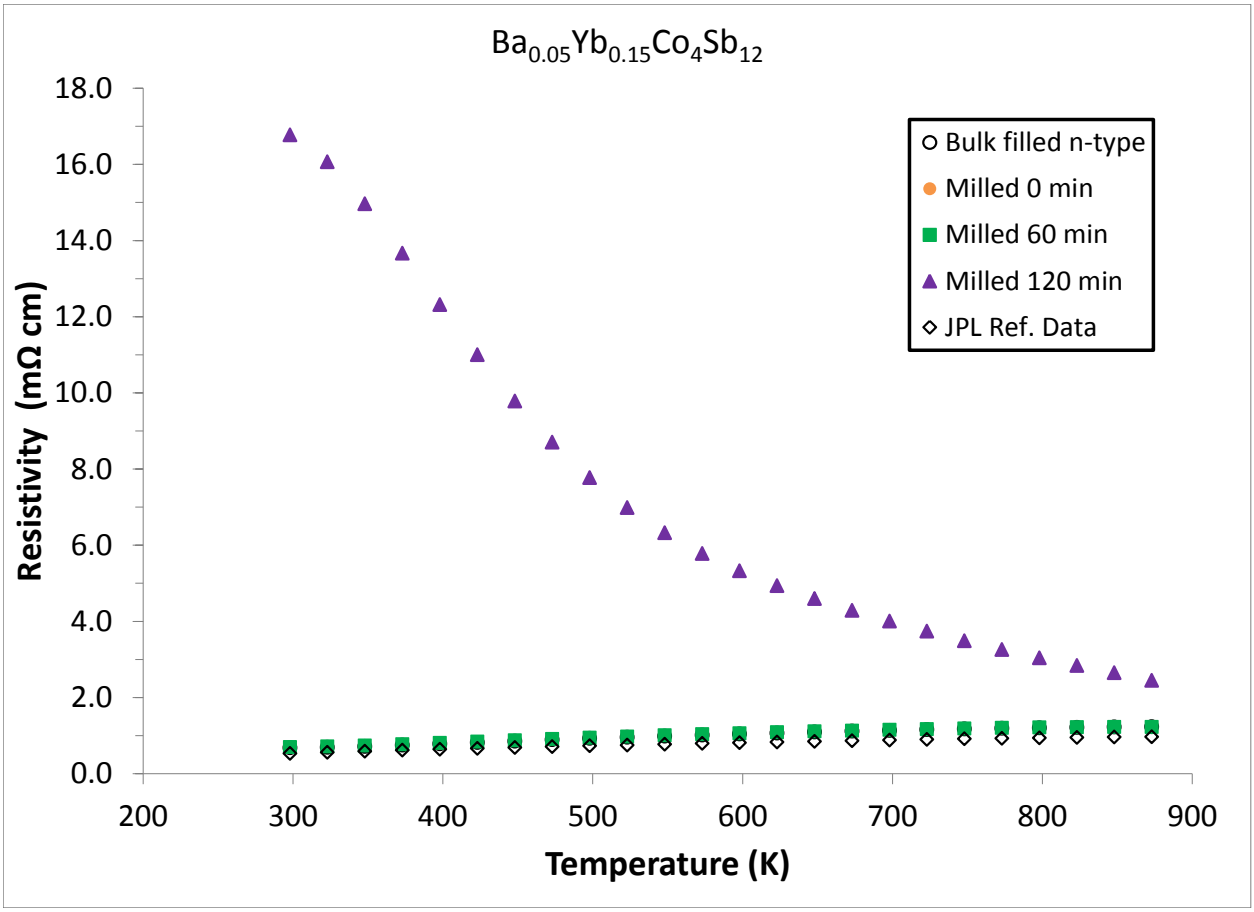

Figure 3.23. Temperature dependence of electrical resistivity in bulk and ball milled $Ba_{0.05}Yb_{0.15}Co_4Sb_{12}$ skutterudite samples. A milled 0 minutes sample is included as a control because the bulk and milled samples were hot-pressed at different temperatures. JPL Reference Data is averaged data from all qualified production batches of material with this composition. The electrical resistivity (ρ) was measured using the van der Pauw technique with a current of 100 mA. The measurement error was estimated to be ±0.5% for the resistivity data.

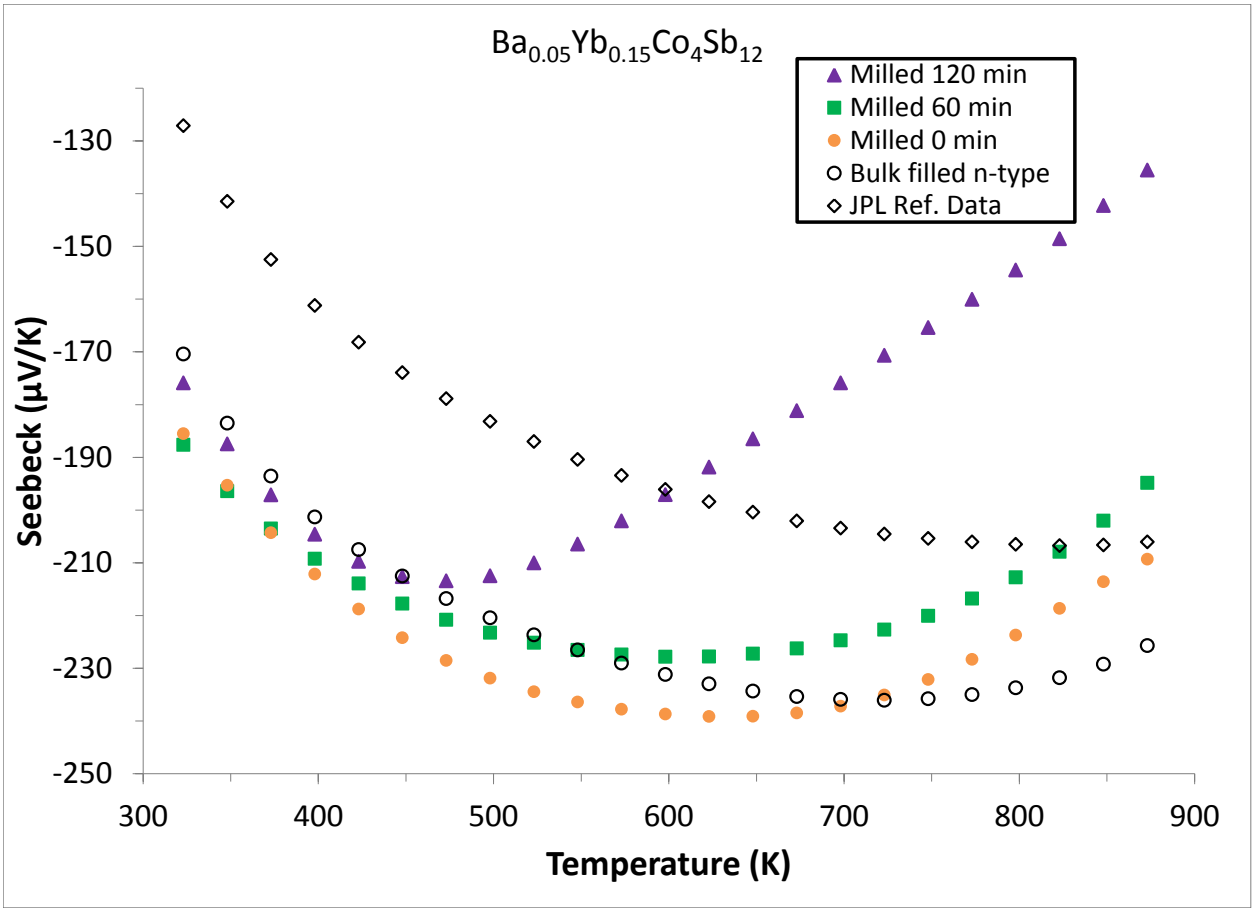

Figure 3.24. Temperature dependence of Seebeck coefficient in bulk and ball milled $Ba_{0.05}Yb_{0.15}Co_4Sb_{12}$ skutterudite samples. A milled 0 minutes sample is included as a control because the bulk and milled samples were hot-pressed at different temperatures. JPL Reference Data is averaged data from all qualified production batches of material with this composition. The Seebeck coefficient was measured using a high temperature light pulse technique.[35] The error of the Seebeck coefficient measurement was estimated to be less than ±3%.

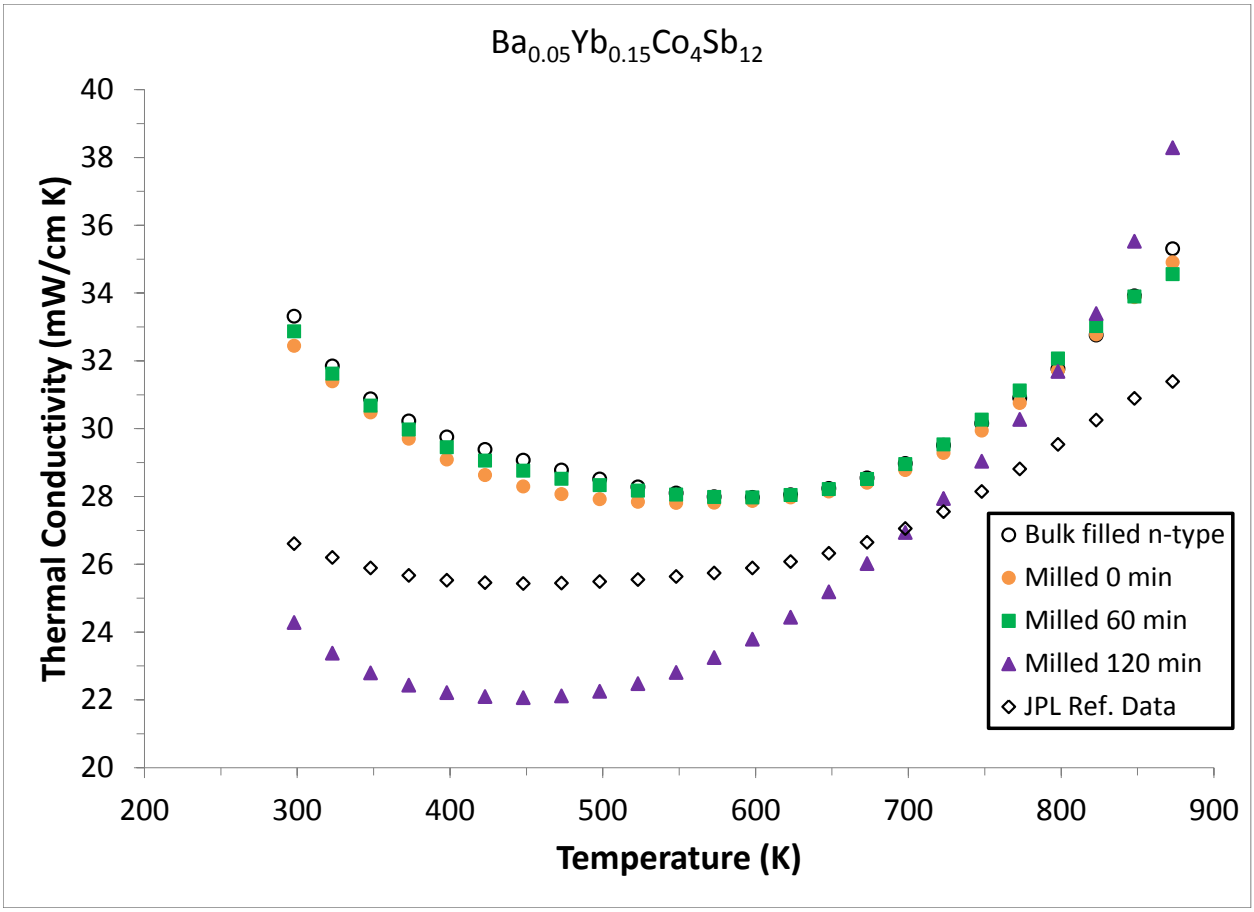

Figure 3.25. Temperature dependence of thermal conductivity (λ) in bulk and ball milled $Ba_{0.05}Yb_{0.15}Co_4Sb_{12}$ skutterudite samples. A milled 0 minutes sample is included as a control because the bulk and milled samples were hot-pressed at different temperatures. JPL Reference Data is averaged data from all qualified production batches of material with this composition. The heat capacity and thermal diffusivity were measured using a flash diffusivity technique[33] and the overall error in the thermal conductivity measurements was estimated to be about ±10%. The thermal conductivity was calculated from the experimental mass, density, heat capacity, and thermal diffusivity values.

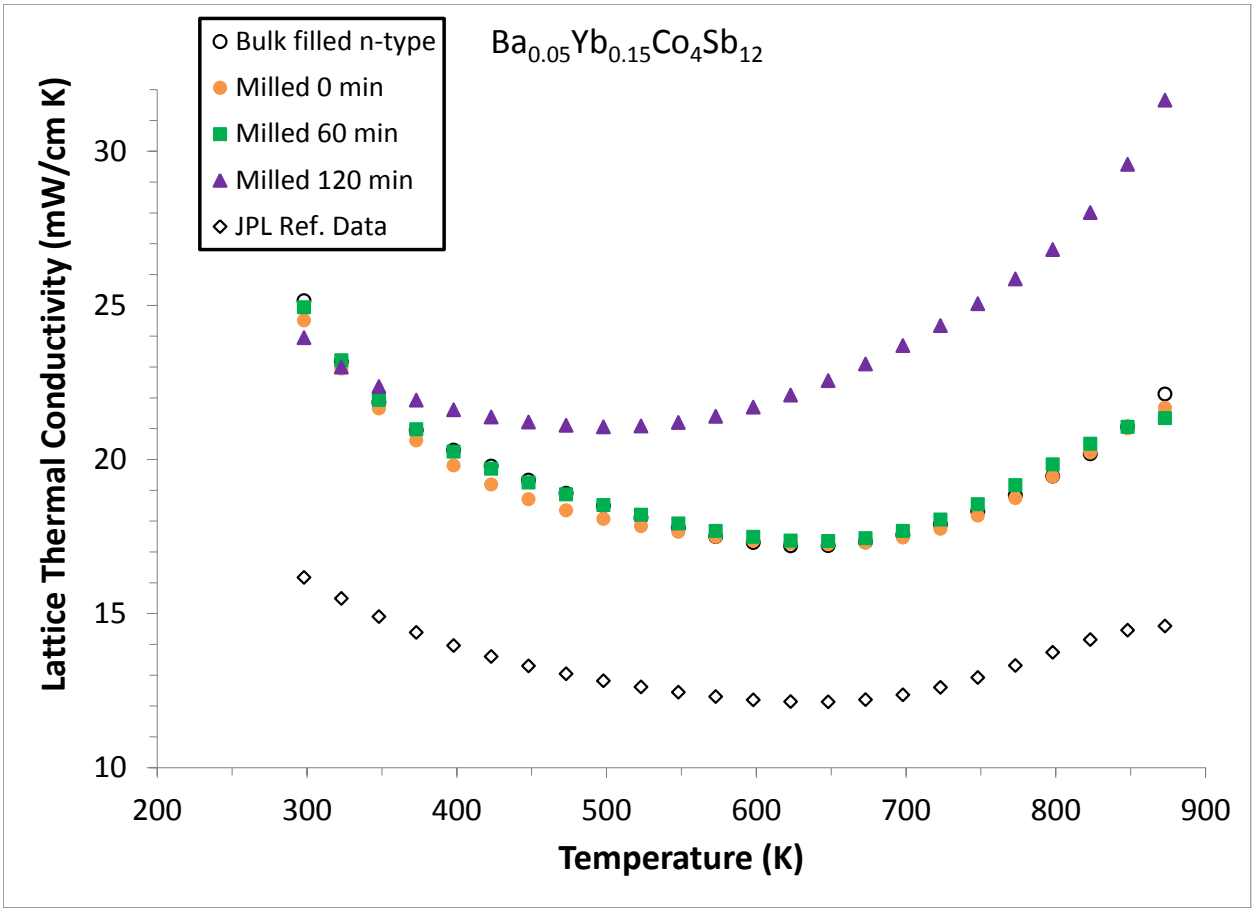

Figure 3.26. Temperature dependence of lattice thermal conductivity ($\lambda_{Lattice}$) in bulk and ball milled $Ba_{0.05}Yb_{0.15}Co_4Sb_{12}$ skutterudite samples. A milled 0 minutes sample is included as a control because the bulk and milled samples were hot-pressed at different temperatures. JPL Reference Data is averaged data from all qualified production batches of material with this composition. The lattice thermal conductivity was obtained by subtracting the electronic thermal conductivity contribution from the total thermal conductivity. The electronic contribution was calculated from the resistivity and Lorenz number. The total thermal conductivity was calculated from the experimental mass, density, heat capacity, and thermal diffusivity values. The overall error in the thermal conductivity measurements was estimated to be about ±10%.

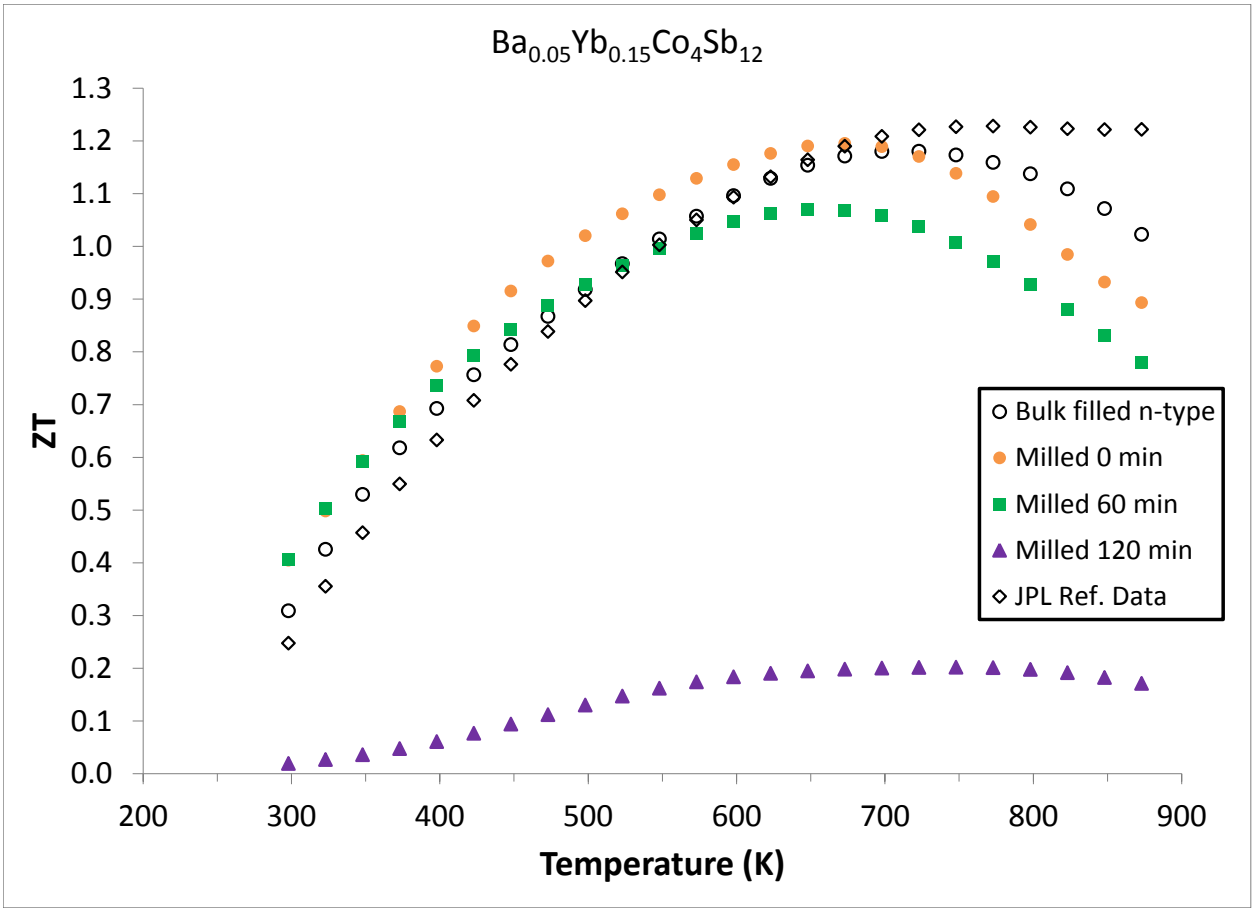

Figure 3.27. Temperature dependence of the thermoelectric figure of merit, ZT in bulk and ball milled $Ba_{0.05}Yb_{0.15}Co_4Sb_{12}$ skutterudite samples. A milled 0 minutes sample is included as a control because the bulk and milled samples were hot-pressed at different temperatures. JPL Reference Data is averaged data from all qualified production batches of material with this composition. Combining the Seebeck coefficient, resistivity, and thermal conductivity measurements, the overall error in ZT was estimated to be about ±20%.

3.6.5 Milled, filled p-type $Ce_{0.9}Fe_{3.5}Co_{0.5}Sb_{12}$

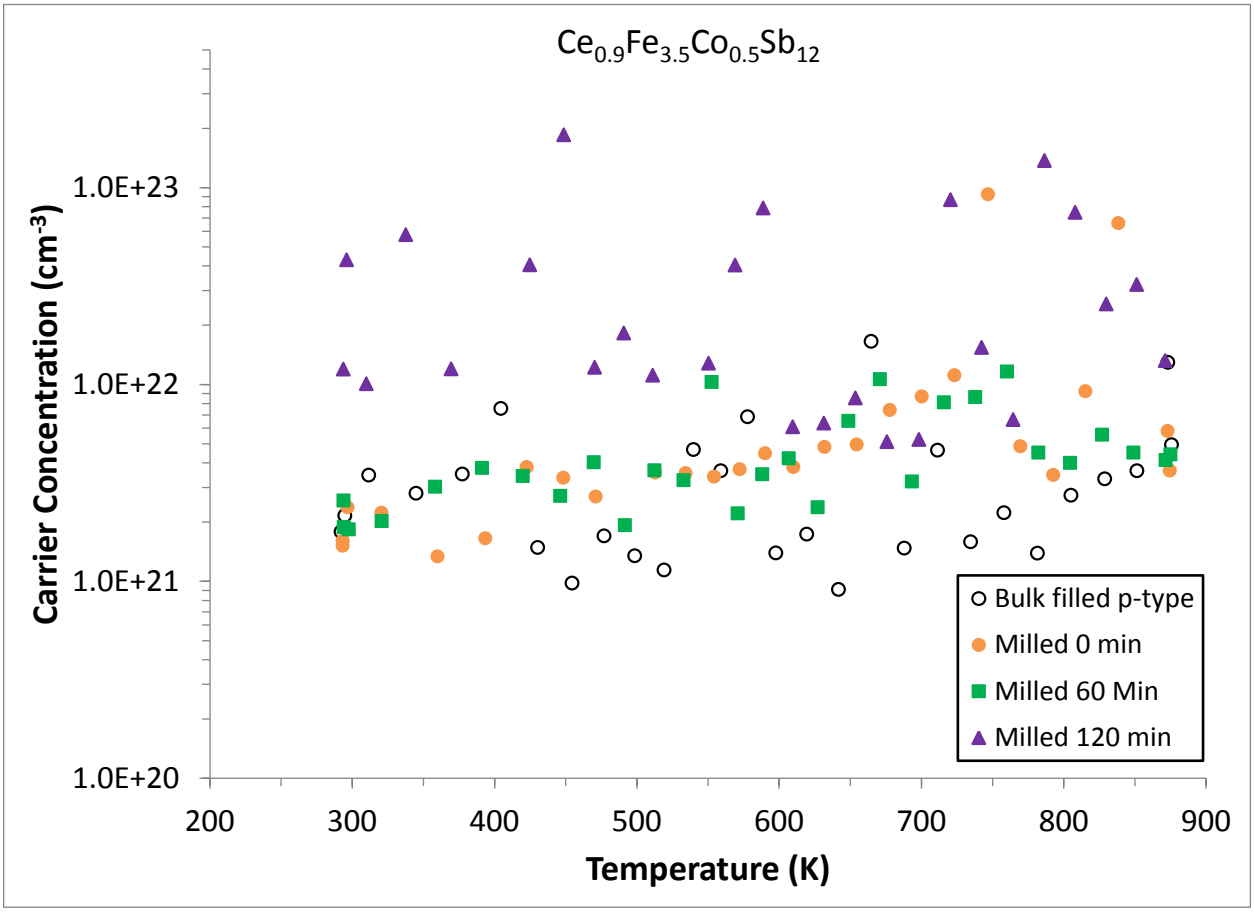

Figure 3.28. Temperature dependence of carrier concentration in bulk and ball milled $Ce_{0.9}Fe_{3.5}Co_{0.5}Sb_{12}$ skutterudite samples. A milled 0 minutes sample is included as a control because the bulk and milled samples were hot-pressed at different temperatures. The Hall coefficient was measured with a forward and reverse magnetic field value of ~8500 G. The carrier concentration was calculated from the Hall coefficient, assuming a scattering factor of 1 in a single carrier scheme, by $p/n = 1/R_H e$ where p and n are the densities of holes and electrons, respectively, and e is the electron charge. The measurement error was estimated to be ±2% for the Hall coefficient data.

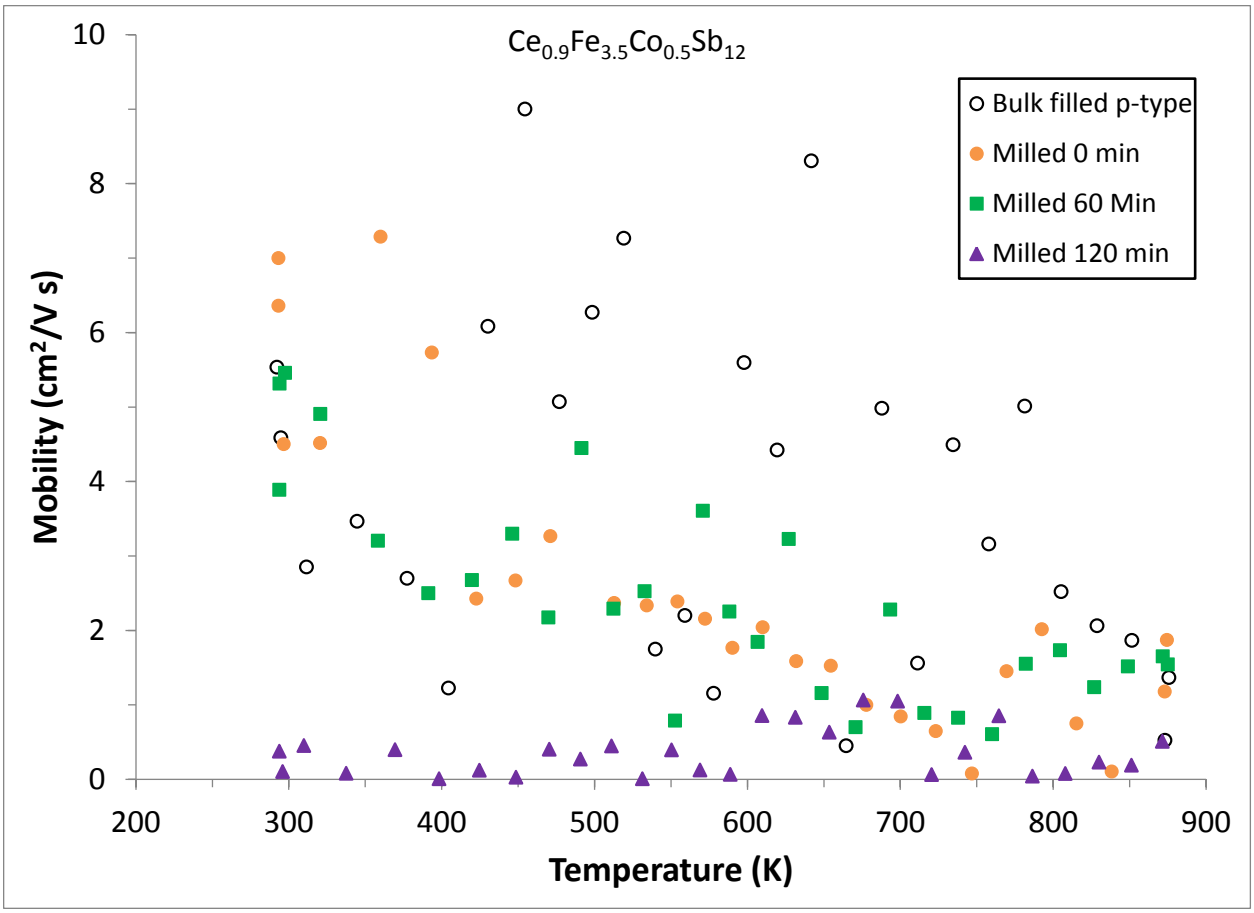

Figure 3.29. Temperature dependence of carrier mobility in bulk and ball milled $Ce_{0.9}Fe_{3.5}Co_{0.5}Sb_{12}$ skutterudite samples. A milled 0 minutes sample is included as a control because the bulk and milled samples were hot-pressed at different temperatures. The Hall coefficient was measured with a forward and reverse magnetic field value of ~8500 G and the Hall mobility was calculated from the Hall coefficient. The measurement error was estimated to be ±2% for the Hall coefficient data.

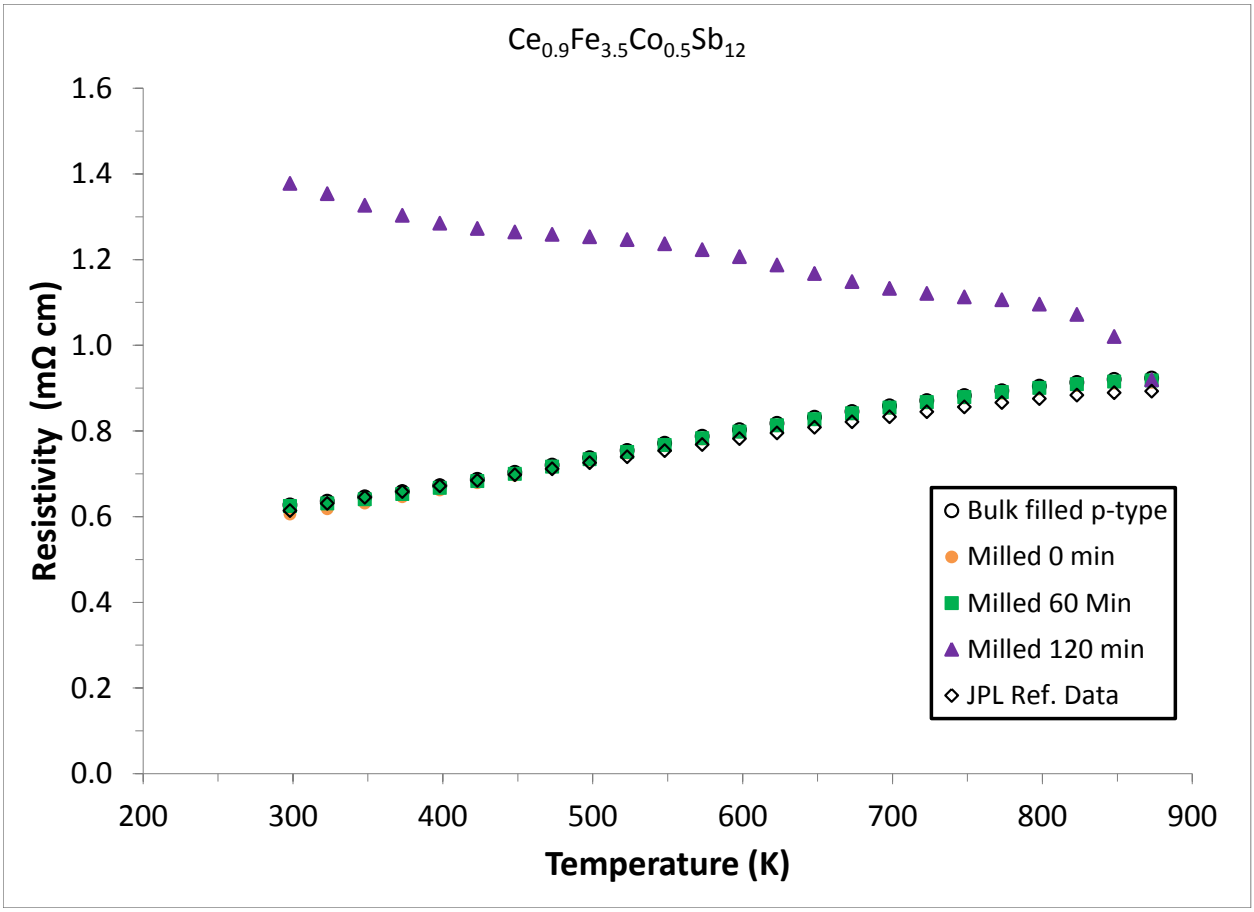

Figure 3.30. Temperature dependence of electrical resistivity in bulk and ball milled $Ce_{0.9}Fe_{3.5}Co_{0.5}Sb_{12}$ skutterudite samples. A milled 0 minutes sample is included as a control because the bulk and milled samples were hot-pressed at different temperatures. JPL Reference Data is averaged data from all qualified production batches of material with this composition. The electrical resistivity (ρ) was measured using the van der Pauw technique with a current of 100 mA. The measurement error was estimated to be ±0.5% for the resistivity data.

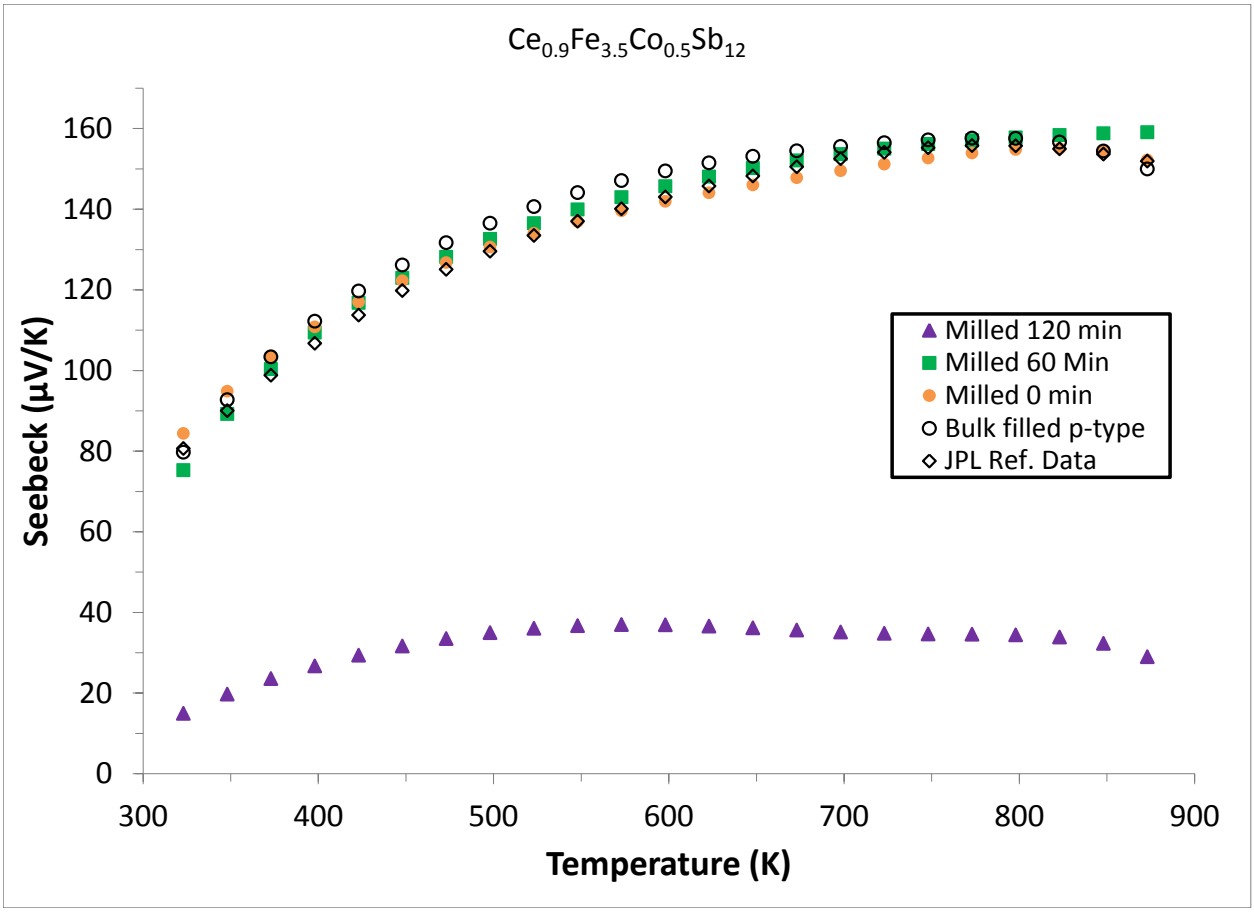

Figure 3.31. Temperature dependence of Seebeck coefficient in bulk and ball milled $Ce_{0.9}Fe_{3.5}Co_{0.5}Sb_{12}$ skutterudite samples. A milled 0 minutes sample is included as a control because the bulk and milled samples were hot-pressed at different temperatures. JPL Reference Data is averaged data from all qualified production batches of material with this composition. The Seebeck coefficient was measured using a high temperature light pulse technique.[35] The error of the Seebeck coefficient measurement was estimated to be less than ±3%.

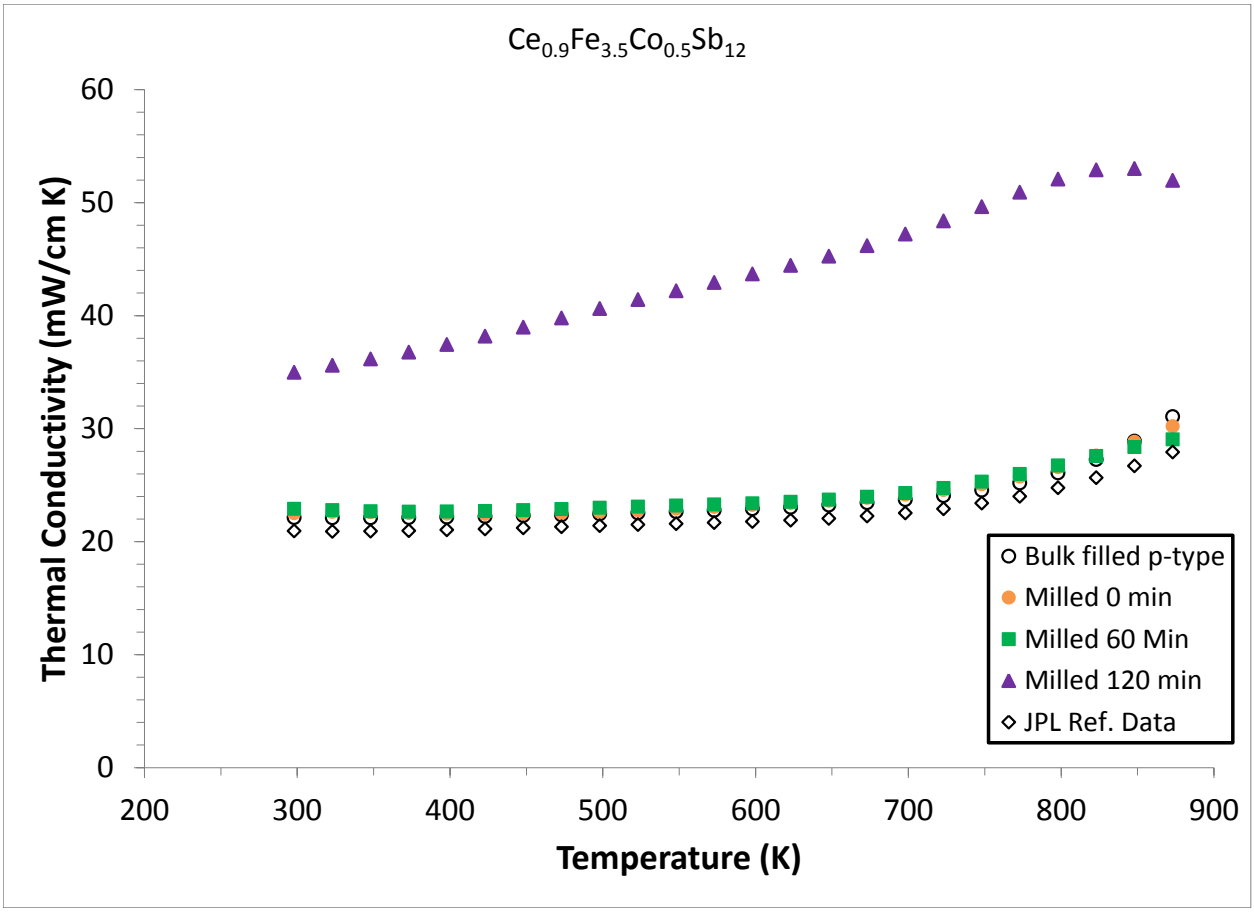

Figure 3.32. Temperature dependence of thermal conductivity (λ) in bulk and ball milled $Ce_{0.9}Fe_{3.5}Co_{0.5}Sb_{12}$ skutterudite samples. A milled 0 minutes sample is included as a control because the bulk and milled samples were hot-pressed at different temperatures. JPL Reference Data is averaged data from all qualified production batches of material with this composition. The heat capacity and thermal diffusivity were measured using a flash diffusivity technique[33] and the overall error in the thermal conductivity measurements was estimated to be about ±10%. The thermal conductivity was calculated from the experimental mass, density, heat capacity, and thermal diffusivity values.

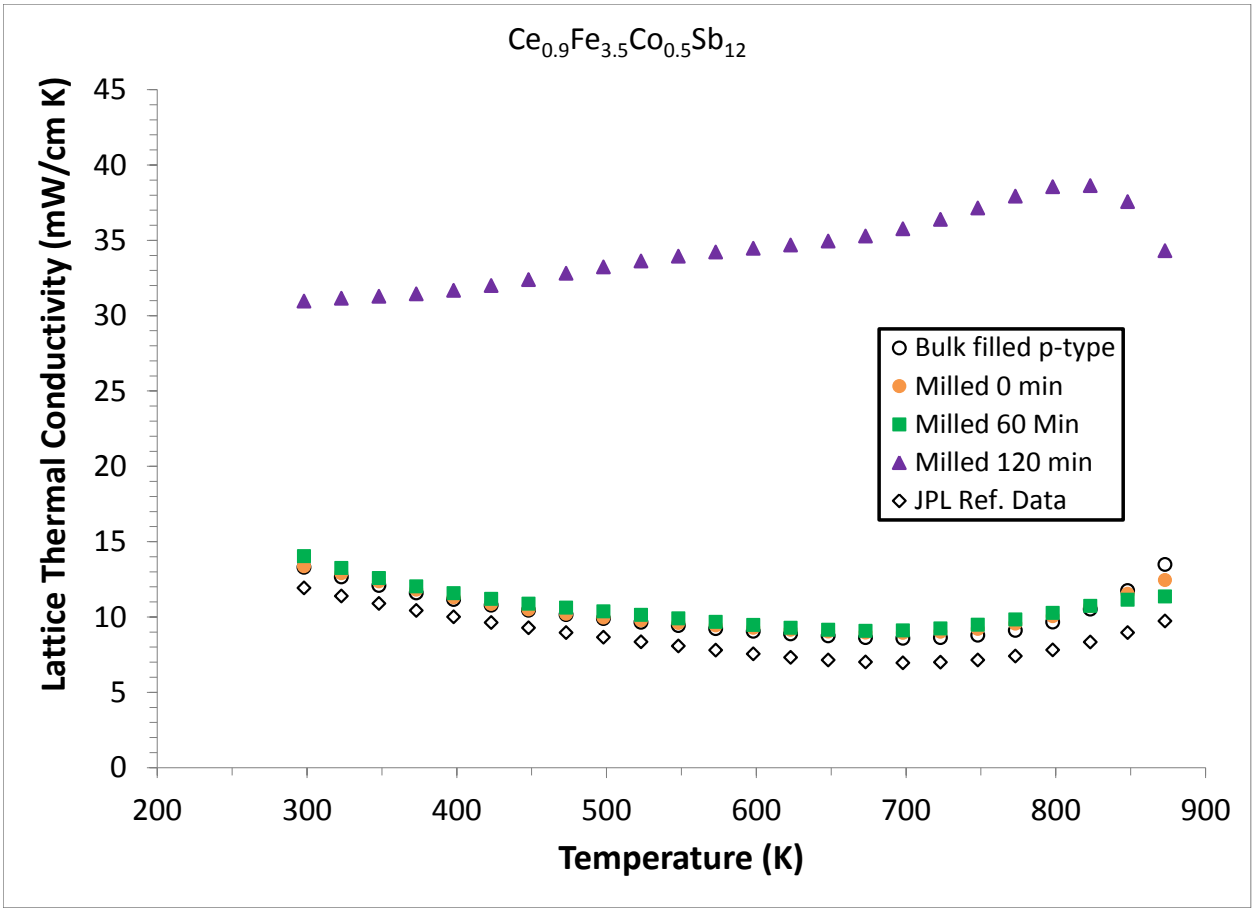

Figure 3.33. Temperature dependence of lattice thermal conductivity ($\lambda_{Lattice}$) in bulk and ball milled $Ce_{0.9}Fe_{3.5}Co_{0.5}Sb_{12}$ skutterudite samples. A milled 0 minutes sample is included as a sample because the bulk and milled samples were hot-pressed at different temperatures. JPL Reference Data is averaged data from all qualified production batches of material with this composition. The lattice thermal conductivity was obtained by subtracting the electronic thermal conductivity contribution from the total thermal conductivity. The electronic contribution was calculated from the resistivity and Lorenz number. The total thermal conductivity was calculated from the experimental mass, density, heat capacity, and thermal diffusivity values. The overall error in the thermal conductivity measurements was estimated to be about ±10%.

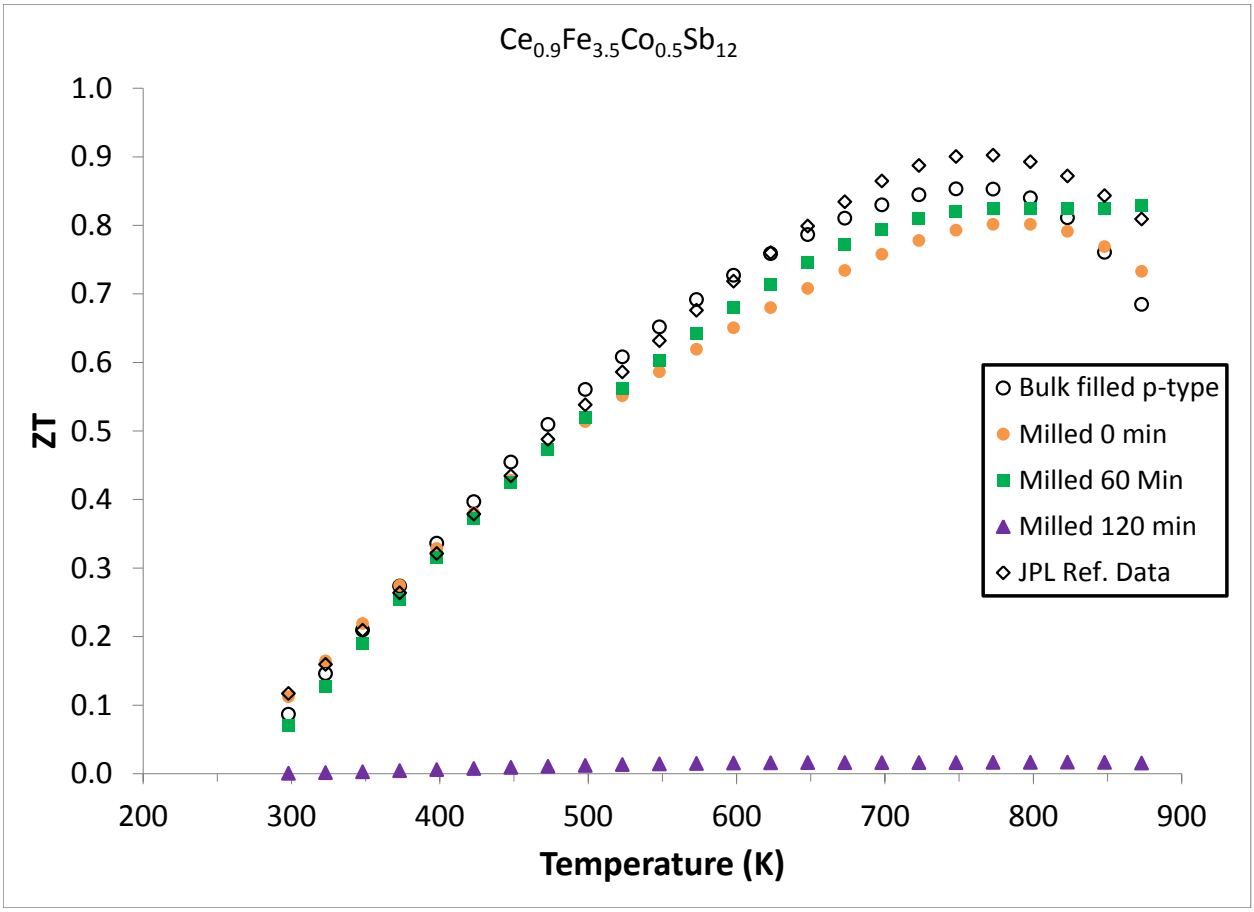

Figure 3.34. Temperature dependence of the thermoelectric figure of merit, ZT in bulk and ball milled $Ce_{0.9}Fe_{3.5}Co_{0.5}Sb_{12}$ skutterudite samples. A milled 0 minutes sample is included as a control because the bulk and milled samples were hot-pressed at different temperatures. JPL Reference Data is averaged data from all qualified production batches of material with this composition. Combining the Seebeck coefficient, resistivity, and thermal conductivity measurements, the overall error in ZT was estimated to be about ±20%.

3.7 References

(1) Yang, J. *ICT 2005. 24th Int. Conf. Thermoelectr. 2005.* **2005**, 170.

(2) Yang, J.; Caillat, T. *MRS Bull.* **2006**, *31*, 224.

(3) LaGrandeur, J.; Crane, D.; Hung, S.; Mazar, B.; Eder, a. *2006 25th Int. Conf. Thermoelectr.* **2006**, 343.

(4) Matsubara, K. In *21st International Conference on Thermoelectrics*; 2002; pp. 418–423.

(5) Fleurial, J.-P.; Caillat, T.; Borshchevsky, A. *Proc. 16th Int. Conf. Thermoelectr.* **1997**, 1.

(6) Rowe, D. M. *CRC Handbook of Thermoelectrics*; Rowe, D. M., Ed.; CRC Press, 1995.

(7) Hicks, L.; Dresselhaus, M. *Phys. Rev. B* **1993**, *47*, 727.

(8) Hicks, L.; Harman, T.; Sun, X.; Dresselhaus, M. *Phys. Rev. B. Condens. Matter* **1996**, *53*, R10493.

(9) Harman, T. C.; Taylor, P. J.; Walsh, M. P.; LaForge, B. E. *Sci.* **2002**, *297* , 2229.

(10) Venkatasubramanian, R.; Siivola, E.; Colpitts, T.; O'Quinn, B. *Nature* **2001**, *413*, 597.

(11) Bux, S. K.; Blair, R. G.; Gogna, P. K.; Lee, H.; Chen, G.; Dresselhaus, M. S.; Kaner, R. B.; Fleurial, J.-P. *Adv. Funct. Mater.* **2009**, *19*, 2445.

(12) Caillat, T. *J. Appl. Phys.* **1996**, *80*, 4442.

(13) Sales, B. C.; Mandrus, D.; Williams, R. K. *Science (80-.).* **1996**, *272*, 1325.

(14) Sales, B.; Mandrus, D.; Chakoumakos, B.; Keppens, V.; Thompson, J. *Phys. Rev. B* **1997**, *56*, 15081.

(15) Nolas, G.; Cohn, J.; Slack, G. *Phys. Rev. B* **1998**, *58*, 164.

(16) Chakoumakos, B. C.; Sales, B. C.; Mandrus, D.; Keppens, V. *Acta Crystallogr. Sect. B Struct. Sci.* **1999**, *55*, 341.

(17) Meisner, G.; Morelli, D.; Hu, S.; Yang, J.; Uher, C. *Phys. Rev. Lett.* **1998**, *80*, 3551.

(18) Lu, P.; Shen, Z.; Hu, X. *J. Mater. Res.* **2009**, *24*, 2873.

(19) Lu, P.-X.; Wu, F.; Han, H.-L.; Wang, Q.; Shen, Z.-G.; Hu, X. *J. Alloys Compd.* **2010**, *505*, 255.

(20) Alboni, P. N.; Ji, X.; He, J.; Gothard, N.; Hubbard, J.; Tritt, T. M. *J. Electron. Mater.* **2007**, *36*, 711.

(21) Wang, M.; Zhang, Y.; Muhammed, M. *Nanostructured Mater.* **1999**, *12*, 237.

(22) Bertini, L.; Billquist, K.; Christensen, M.; Gatti, C.; Palmqvist, A.; Platzek, D.; Rowe, D. M.; Saramat, A.; Stiewe, C.; Williams, S. G.; Golgi, V. C.; Division, M. C. In *22nd International Conference on Thermoelectrics*; 2003; pp. 48–51.

(23) Bertini, L.; Stiewe, C.; Toprak, M.; Williams, S.; Platzek, D.; Mrotzek, A.; Zhang, Y.; Gatti, C.; Müller, E.; Muhammed, M.; Rowe, M. *J. Appl. Phys.* **2003**, *93*, 438.

(24) Mi, J. L.; Zhao, X. B.; Zhu, T. J.; Tu, J. P. *Mater. Lett.* **2008**, *62*, 2363.

(25) Li, J. Q.; Feng, X. W.; Sun, W. a.; Ao, W. Q.; Liu, F. S.; Du, Y. *Mater. Chem. Phys.* **2008**, *112*, 57.

(26) Zhang, L.; Grytsiv, A.; Kerber, M.; Rogl, P.; Bauer, E.; Zehetbauer, M. J.; Wosik, J.; Nauer, G. E. *J. Alloys Compd.* **2009**, *481*, 106.

(27) Rogl, G.; Zehetbauer, M. J.; Kerber, M.; Rogl, P.; Bauer, E. *Mater. Sci. Forum* **2010**, *667-669*, 1089.

(28) Lan, Y.; Minnich, A. J.; Chen, G.; Ren, Z. *Adv. Funct. Mater.* **2010**, *20*, 357.

(29) Rogl, G.; Grytsiv, A.; Rogl, P.; Bauer, E.; Kerber, M. B.; Zehetbauer, M.; Puchegger, S. *Intermetallics* **2010**, *18*, 2435.

(30) Bux, S. K.; Fleurial, J.-P.; Kaner, R. B. *Chem. Commun. (Camb).* **2010**, *46*, 8311.

(31) Yang, J.; Chen, Y.; Peng, J.; Song, X.; Zhu, W.; Su, J.; Chen, R. *J. Alloys Compd.* **2004**, *375*, 229.

(32) Lee, H. W.; Lee, D. Y.; Kim, I. J.; Woo, B. C. In *Twenty-First International Conference on Thermoelectrics, 2002. Proceedings ICT '02.*; Ieee, 2002; pp. 17–20.

(33) Vandersande, J. W.; Wood, C.; Zoltan, A.; Whittenberger, D. *Therm. Conduct.* **1988**, *19*, 445.

(34) Mccormack, J. A.; Fleurial, J.-P. *MRS Proc.* **1991**, *234*, 135.

(35) Wood, C.; Zoltan, D.; Stapfer, G. *Rev. Sci. Instrum.* **1985**, *56*, 719.

Chapter 4: Solid solutions and nanoparticle composite skutterudite materials for thermoelectric power generation

4.1 Skutterudite Improvements

There are four general approaches to improving the thermoelectric properties of skutterudite materials. One approach that has already been discussed in a previous chapter is apopular thermoelectric material enhancement technique through nanostructuring.[1–4] Applying nanostructuring to skutterudite, ideally would reduce thermal conductivity with the assumption that the transport properties would remain relatively unchanged in the resulting nano material, thus increasing ZT. Extensive studies presented here for multiple skutterudite formulations have shown that this nanostructuring approach is not trivial for a material with a complex structure like that of skutterudite. A second approach to skutterudite improvement involves the filling of void spaces in the skutterudite lattice with large, "rattling" atoms. These "rattlers" not only benefit the material by scattering phonons,[5–9] but they also provide for better control over doping levels in the material as compared to substitutional doping methods.[10–13] They also have less detrimental effects on the electrical properties at the high doping levels that are necessary in skutterudite thermoelectric materials.

The other two approaches that have not yet been discussed in this work relate to alloying and nanocomposites, two types of mixtures whose names are occasionally interchanged based on the characteristics of the product of mixing two materials. The goal of both of these approaches is once again, to reduce the thermal conductivity of the final material to increase ZT. Alloying in this case refers to the mixing of two materials with similar structures, but different constituent elements, such that the two structures are miscible, creating a structure with point defects. These point defects scatter phonons because the substitution of atoms in the lattice for other atoms with

different masses and different bonding characteristics will cause electrical and thermal transport, across these substitutional sites, to differ from transport across unsubstituted regions. In the case of skutterudites, calculations of mixing enthalpies for $CoSb_3/IrSb_3$ alloys imply that these materials would have low internal strain and could have improved thermoelectric performance.[14]

4.2 Skutterudite Alloys

Mixtures of two similar materials that could possibly form alloys, because of their similar structures, are sometimes referred to as nanocomposites if the added phase is not uniformly dispersed throughout the sample. In this case, the added phase is visible as a second phase in the form of nanoscale or microscale inclusions. The distinction between an alloy and a composite is that an alloy will appear to be a single phase and have a given ratio of atoms at any given point in the sample, while a composite has discrete, visible domains of two separate phases of materials. When two materials are mixed with dissimilar, immiscible structures, this results in a composite material. For maximum efficacy, inclusions in a thermoelectric material must maximize the interfaces with the host material. Thus, the composite approach to reducing thermal conductivity in skutterudite is to form a nanocomposite.

Attempts to alloy small percentages of Ir in Co-based Ba-filled skutterudite[15] result in phase segregation of the $IrSb_3$ phase,[16] and our preliminary attempts at this exact type of alloy have confirmed this finding. However, our preliminary experiments have also shown that the reverse alloy where a small percentage of Co is substituted into Ir-based, Ba-filled skutterudite, results in a single phase material with even distribution of Co throughout. Optimization of filling and doping of this alloy should result in a measurable decrease in the lattice thermal conductivity with the point defect phonon scattering introduced by Co, and consequently an increase in ZT.

4.3 Nanocomposite Skutterudites

The nanocomposite approach for skutterudites is attractive in that there are many commercially available nanomaterials that are immiscible in the skutterudite structure. Nanoparticles have been mixed into all types of skutterudite, ranging from CeO_2 added to undoped $CoSb_3$,[17] to the *in situ* precipitation of InSb nanoparticles in the skutterudite structure.[18] We have conducted preliminary nanocomposite experiments of our own, attempting to fill $Ce_{0.9}Fe_{3.5}Co_{0.5}Sb_{12}$ p-type skutterudite with commercially available CeO_2 nanoparticles, but this resulted in lower ZTs. At first, we believed that the observed properties for our composite samples indicated that inclusion of CeO_2 in a skutterudite structure that is filled with a rare earth or alkaline earth metal may result in the filler atoms reacting with oxygen at high temperatures in the hot press and consequently no longer filling the voids of the skutterudite structure. However, there are a great deal of reports involving successful results with other oxide materials in skutterudite composites including ZrO_2,[19,20] Yb_2O_3,[21] and TiO_2 in unfilled[22] and filled[23] n-type skutteruidite all of which have been shown to increase ZT. However, the nanocomposite approach has also been tried with non-oxide materials in skutterudite such as TiN[24] and Bi,[25] which is not only promising because it avoids oxides in the structure, but the addition of a metal nanoinclusion could provide interfaces for scattering, while not hampering electrical conductivity as much as an inclusion that is an insulator.

Future work on both filled n-type $IrSb_3$ and filled n-type $CoSb_3$ will focus on nanoinclusions to form nanocomposites. The goal will first be to find a metal that is inert in the structure that can be made or purchased at a reasonable price. Recent, unpublished work at JPL indicates that nickel particles in lanthanum telluride can enhance the ZT of the material. If no

suitable metals can be found, the composite studies will shift to nitrides and oxides at very small sizes.

4.3 The Need for Band Structure Modeling

With the ever increasing complexities of reported skutterudite compositions,[26–34] it is abundantly clear that more accurate band modeling is needed for skutterudite materials. The modelling is first needed to better understand the effects of void filling in the structure with filler atoms. The differences in electrical and thermal properties exhibited in filled versus unfilled skutterudite suggests that filling leads to significant changes in the band structure. Additionally, as shown in the filled iridium skutterudite work presented earlier, different filler atoms result in drastically different Seebeck coefficients and electrical properties in spite of having similar measured filling fractions and similar electron counts. Most of the available modelling for skutterudite structures is insufficient to make meaningful pridictions.[35,36] The findings of this work serve to highlight the need for accurate band models for skutterudites order to better understand how composition changes in alloys and composites affect the band structure. Without a better model, time and resources will continue to be spent unnecessarily on a trial and error approach to finding new, better skutterudite compounds.

4.4 References

(1) Medlin, D. L.; Snyder, G. J. *Curr. Opin. Colloid Interface Sci.* **2009**, *14*, 226.

(2) Dresselhaus, M. S.; Chen, G.; Tang, M. Y.; Yang, R. G.; Lee, H.; Wang, D. Z.; Ren, Z. F.; Fleurial, J.-P.; Gogna, P. *Adv. Mater.* **2007**, *19*, 1043.

(3) Minnich, A. J.; Dresselhaus, M. S.; Ren, Z. F.; Chen, G. *Energy Environ. Sci.* **2009**, *2*, 466.

(4) Vineis, C. J.; Shakouri, A.; Majumdar, A.; Kanatzidis, M. G. *Adv. Mater.* **2010**, *22*, 3970.

(5) Sales, B. C.; Mandrus, D.; Williams, R. K. *Science (80-.).* **1996**, *272*, 1325.

(6) Sales, B.; Mandrus, D.; Chakoumakos, B.; Keppens, V.; Thompson, J. *Phys. Rev. B* **1997**, *56*, 15081.

(7) Nolas, G.; Cohn, J.; Slack, G. *Phys. Rev. B* **1998**, *58*, 164.

(8) Chakoumakos, B. C.; Sales, B. C.; Mandrus, D.; Keppens, V. *Acta Crystallogr. Sect. B Struct. Sci.* **1999**, *55*, 341.

(9) Meisner, G.; Morelli, D.; Hu, S.; Yang, J.; Uher, C. *Phys. Rev. Lett.* **1998**, *80*, 3551.

(10) Liu, W.-S.; Zhang, B.-P.; Li, J.-F.; Zhang, H.-L.; Zhao, L.-D. *J. Appl. Phys.* **2007**, *102*, 103717.

(11) Bertini, L.; Billquist, K.; Christensen, M.; Gatti, C.; Palmqvist, A.; Platzek, D.; Rowe, D. M.; Saramat, A.; Stiewe, C.; Williams, S. G.; Golgi, V. C.; Division, M. C. In *22nd International Conference on Thermoelectrics*; 2003; pp. 48–51.

(12) Chitroub, M.; Besse, F.; Scherrer, H. *J. Alloys Compd.* **2009**, *467*, 31.

(13) Bertini, L.; Stiewe, C.; Toprak, M.; Williams, S.; Platzek, D.; Mrotzek, A.; Zhang, Y.; Gatti, C.; Müller, E.; Muhammed, M.; Rowe, M. *J. Appl. Phys.* **2003**, *93*, 438.

(14) SHI, X.; ZHANG, W.; CHEN, L. D.; UHER, C. *Int. J. Mater. Res.* **2008**, *99*, 638.

(15) Uher, C.; Shi, X.; Kong, H. In *2007 International Conference on Thermoelectrics*; 2007; pp. 189–192.

(16) Xiong, Z.; Huang, X.; Chen, X.; Ding, J.; Chen, L. *Scr. Mater.* **2010**, *62*, 93.

(17) Alleno, E.; Chen, L.; Chubilleau, C.; Lenoir, B.; Rouleau, O.; Trichet, M. F.; Villeroy, B. *J. Electron. Mater.* **2009**, *39*, 1966.

(18) Li, H.; Tang, X.; Zhang, Q.; Uher, C. *Appl. Phys. Lett.* **2009**, *94*, 102114.

(19) He, Z.; Stiewe, C.; Platzek, D.; Karpinski, G.; Müller, E.; Li, S.; Toprak, M.; Muhammed, M. *J. Appl. Phys.* **2007**, *101*, 043707.

(20) Stiewe, C.; He, Z.; Platzek, D.; Karpinski, G.; Müller, E.; Li, S.; Toprak, M.; Muhammed, M. *Materwiss. Werksttech.* **2007**, *38*, 773.

(21) Ding, J.; Gu, H.; Qiu, P.; Chen, X.; Xiong, Z.; Zheng, Q.; Shi, X.; Chen, L. *J. Electron. Mater.* **2013**, *42*, 382.

(22) Zhu, Y.; Shen, H.; Chen, H. *Rare Met.* **2012**, *31*, 43.

(23) Xiong, Z.; Chen, X.; Zhao, X.; Bai, S.; Huang, X.; Chen, L. *Solid State Sci.* **2009**, *11*, 1612.

(24) Duan, B.; Zhai, P.; Wen, P.; Zhang, S.; Liu, L.; Zhang, Q. *Scr. Mater.* **2012**, *67*, 372.

(25) Mallik, R. C.; Anbalagan, R.; Raut, K. K.; Bali, a; Royanian, E.; Bauer, E.; Rogl, G.; Rogl, P. *J. Phys. Condens. Matter* **2013**, *25*, 105701.

(26) Ballikaya, S.; Wang, G.; Sun, K.; Uher, C. *J. Electron. Mater.* **2010**, *40*, 570.

(27) Ballikaya, S.; Uzar, N.; Yildirim, S.; Salvador, J. R.; Uher, C. *J. Solid State Chem.* **2012**, *193*, 31.

(28) Shi, X.; Yang, J.; Salvador, J. R.; Chi, M.; Cho, J. Y.; Wang, H.; Bai, S.; Yang, J.; Zhang, W.; Chen, L. *J. Am. Chem. Soc.* **2011**, *133*, 7837.

(29) Zhang, L.; Grytsiv, a; Rogl, P.; Bauer, E.; Zehetbauer, M. *J. Phys. D. Appl. Phys.* **2009**, *42*, 225405.

(30) Rogl, G.; Grytsiv, a; Melnychenko-Koblyuk, N.; Bauer, E.; Laumann, S.; Rogl, P. *J. Phys. Condens. Matter* **2011**, *23*, 275601.

(31) Graff, J.; Zhu, S.; Holgate, T.; Peng, J.; He, J.; Tritt, T. M. *J. Electron. Mater.* **2011**, *40*, 696.

(32) Bérardan, D.; Alleno, E.; Godart, C.; Puyet, M.; Lenoir, B.; Lackner, R.; Bauer, E.; Girard, L.; Ravot, D. *J. Appl. Phys.* **2005**, *98*, 033710.

(33) Ballikaya, S.; Uher, C. *J. Alloys Compd.* **2014**, *585*, 168.

(34) Eilertsen, J.; Berthelot, R.; Sleight, A. W.; Subramanian, M. a. *J. Solid State Chem.* **2012**, *190*, 238.

(35) Anno, H.; Nolas, G. S.; Akai, K.; Ashida, K.; Matsuura, M.; Matsubara, K. In *Proceedings of the 20th International Conference on Thermoelectrics*; 2001; Vol. 3, pp. 61–64.

(36) Lu, P.-X.; Ma, Q.-H.; Li, Y.; Hu, X. *J. Magn. Magn. Mater.* **2010**, *322*, 3080.